

NOTE TO USERS

This reproduction is the best copy available.

UMI[®]

ADAPTIVE SCHEDULING FOR AN INCREMENTAL
FLEXIBLE FORGING CELL

By

AMR MOHAMMED ELBADAN, BSC., MSC.

A Thesis Submitted
To The School of Graduate Studies
in Partial Fulfilment of The Requirements
for The Degree

Doctor of Philosophy

McMaster University

© Copyright by Amr Mohammed Elbadan, August 2004



Library and
Archives Canada

Bibliothèque et
Archives Canada

Published Heritage
Branch

Direction du
Patrimoine de l'édition

395 Wellington Street
Ottawa ON K1A 0N4
Canada

395, rue Wellington
Ottawa ON K1A 0N4
Canada

Your file *Votre référence*

ISBN: 0-494-04503-5

Our file *Notre référence*

ISBN: 0-494-04503-5

NOTICE:

The author has granted a non-exclusive license allowing Library and Archives Canada to reproduce, publish, archive, preserve, conserve, communicate to the public by telecommunication or on the Internet, loan, distribute and sell theses worldwide, for commercial or non-commercial purposes, in microform, paper, electronic and/or any other formats.

The author retains copyright ownership and moral rights in this thesis. Neither the thesis nor substantial extracts from it may be printed or otherwise reproduced without the author's permission.

AVIS:

L'auteur a accordé une licence non exclusive permettant à la Bibliothèque et Archives Canada de reproduire, publier, archiver, sauvegarder, conserver, transmettre au public par télécommunication ou par l'Internet, prêter, distribuer et vendre des thèses partout dans le monde, à des fins commerciales ou autres, sur support microforme, papier, électronique et/ou autres formats.

L'auteur conserve la propriété du droit d'auteur et des droits moraux qui protègent cette thèse. Ni la thèse ni des extraits substantiels de celle-ci ne doivent être imprimés ou autrement reproduits sans son autorisation.

In compliance with the Canadian Privacy Act some supporting forms may have been removed from this thesis.

Conformément à la loi canadienne sur la protection de la vie privée, quelques formulaires secondaires ont été enlevés de cette thèse.

While these forms may be included in the document page count, their removal does not represent any loss of content from the thesis.

Bien que ces formulaires aient inclus dans la pagination, il n'y aura aucun contenu manquant.


Canada

ADAPTIVE SCHEDULING FOR AN INCREMENTAL
FLEXIBLE FORGING CELL

DOCTOR OF PHILOSOPHY (2004)
Mechanical Engineering

McMaster University
Hamilton, Ontario

TITLE : Adaptive Scheduling for an Incremental Flexible Forging Cell

AUTHOR : Amr Mohammed Elbadan
BSc. (Alexandria University)
MSc. (Alexandria University)

SUPERVISORY COMMITTEE : Dr. Tim Nye (Principal Advisor)
Dr. Allan Spence
Dr. Don Metzger

NUMBER OF PAGES: xvii, 170

Abstract

An adaptive forging schedule procedure that targets forging simple 3-D external profiles on a flexible forging cell is presented. The cell is composed of a numerically controlled press, a robot for workpiece manipulation, a shape feedback system and a main supervisory computer. The scheduling procedure utilizes the shape error, computed from the required and the initial workpiece shapes, to plan and execute a set of forging steps. The feedback system is then used to capture the deformed shape of the workpiece and update the shape error to adaptively plan the next set of forging steps. This adaptive control loop iterates until the workpiece shape is forged within a preset tolerance. The reduction in height and the bite values used in the schedule are limited by a set of technological bounds. Several of those bounds were identified and modelled as constraints on the adaptive scheduling procedure.

Illustrative case studies showed that the adaptive scheduling procedure successfully forged external profiles (given an arbitrarily set tolerance limit) when *a-priori* approaches failed. The studies also showed that the new scheduling procedure could forge 2-D and 3-D profiles as easily (in terms of programming effort) as forging a uniform billet.

Three new spread prediction models are developed, of which the newly developed Incrementally Updated Upper Bound model proved to provide the most accurate spread estimate compared to other developed and traditional spread prediction models. This model was then chosen to be integrated with the adaptive scheduling procedure to form an intelligent forging schedule procedure. The integration provided predictive capabilities to the adaptive scheduling module and enabled the generation of better quality forging schedules. In a typical example the number of forging steps in the forging schedule were reduced from six (using the adaptive scheduling procedure) to two (using the intelligent scheduling one).

Acknowledgments

I received help from many individuals in the course of performing the research described in this thesis. First and foremost, I sincerely thank my supervisor, Dr. Tim Nye, for his unfailing help, guidance, patience and other assistance. I am grateful for having had the opportunity of being his student, and for the extensive knowledge I have acquired from him.

I would like also to extend heartfelt thanks to my thesis committee, Dr. Don Metzger and Dr. Allan Spence, whose discussions and comments helped me profoundly in developing this thesis and steering it to its final format. Dr. Don Metzger in particular has provided me with the H3DMAP finite element software and continuous support and valuable direction in the development phase of the finite element model.

And last but not least, I would like to thank my family, especially my wife, for their support and understanding during the many stressful hours I spent bringing this thesis to a successful conclusion.

Nomenclature

B : Bite = The value of the tool feed after each squeezing operation.

h_i : Initial workpiece height.

h_f : Final workpiece height.

Δh : Reduction in workpiece height = $h_i - h_f$.

w_i : Initial workpiece width.

w_f : Final workpiece width.

Δw : Increase in workpiece width = $w_f - w_i$.

L_i : Workpiece initial length.

L_f : Workpiece final length.

ΔL : Increase in workpiece length = $L_f - L_i$.

ϵ_w : Width strain = $\ln \frac{w_f}{w_i}$.

ϵ_h : Height strain = $\ln \frac{h_f}{h_i}$.

s : Spread coefficient = $-\frac{\text{width strain}}{\text{height strain}} = -\frac{\epsilon_w}{\epsilon_h}$.

θ : Bite Ratio = $\frac{B}{w_i}$.

ϕ : Shape Factor = $\frac{h_i}{w_i}$.

R : Squeeze Ratio = $\frac{\Delta h}{h_i}$.

DWR : Die Width Ratio = $\frac{B}{h_i}$.

x : Feed direction.

y : Width direction.

z : Squeezing direction.

Process Plan : is the aggregate schedule comprising a sequence of operations used to generate multiple features on the workpiece.

Operation : is a series of forging steps required to forge a single feature on the workpiece.

Forging Schedule : is the detailed-schedule for forging each operation. It specifies the tool paths and their sequence to perform an operation.

Forging Path : is a sequence of squeezing actions along a specified forging feed direction.

Contents

Abstract	iii
Acknowledgments	iv
Nomenclature	v
List of Tables	xi
List of Figures	xiii
List of Algorithms	xvii
1 Introduction	1
1.1 Background	1
1.2 Research Motivation	3
1.3 Objective and Scope	4
1.4 Thesis Outline	4
2 Literature review	6
2.1 Introduction	6
2.2 Flexible Forging Cell Configuration	7
2.3 Classification of Incremental Forging Operations	14
2.3.1 Cogging Operations	14
2.3.2 Ring Forging	15
2.3.3 Rotary Forging	15
2.3.4 Bend Forging	17
2.3.5 Internal Profiling	17
2.4 Scheduling Forging Operations	21
2.4.1 Cogging Schedules	21
2.4.2 Enhancing Internal Material Structure	22
2.5 Predicting Material Spread and Elongation in Forging	29
2.5.1 Empirical Models	30

2.5.2	Analytical Models (<i>Upper Bound Models</i>)	32
2.5.3	Finite Element Models	35
2.5.4	Neural Network Models	37
2.5.5	Closure	38
2.6	Technological Bounds on the Forging Schedule	39
2.7	Feedback Systems in Metal Forming	42
2.8	Summary	43
3	General Structure of the Incremental Forging Cell	44
3.1	Incremental Forging Cell Hardware Configuration	45
3.2	Structured Light Vision Feedback System	46
3.3	Incremental Forging Operation Plan	50
3.3.1	Process Plan (A1) and Operation Selection (A2)	50
3.3.2	Tool Selection (A3)	52
3.3.3	Forging Cell Shape Feedback Control (A6)	52
3.3.4	Error Computation Algorithm	53
3.3.5	Forging Schedule (A4)	59
3.4	Virtual Forging Cell (A42)	67
3.4.1	Die Modelling	67
3.4.2	Workpiece Modelling	69
3.4.3	The Scheduling Strategy	72
3.5	Summary	72
4	Case Studies	74
4.1	Simulated Case Studies on the Virtual Forging Cell	74
4.1.1	Forging a 2 nd Degree Polynomial Surface	74
4.1.2	Forging a Wedge	79
4.1.3	3-D Geometries Forged on the Virtual Cell	87
4.2	Wedge Forging on the Forging Cell (an Experimental Case Study)	89
4.2.1	Procedure	89
4.2.2	Results	89
4.3	Summary	93
5	Spread Prediction by the Upper Bound Method (B1)	94
5.1	Introduction	94
5.2	Formulation of the Upper Bound Method	95
5.2.1	Assumptions	97
5.2.2	The Deformation Power	97
5.2.3	The Shear Power	98
5.2.4	The Friction Power	98
5.2.5	Upper Bound Solution Procedure	99
5.3	Metal Flow Analysis for Cogging Operation	99

5.3.1	Homogeneous Pattern of Deformation - Center Indentation Case	101
5.3.2	Fish-Bone Pattern of Deformation - Continuous Cogging Case	109
5.3.3	Incrementally Updated Upper Bound Method	116
5.4	Summary	118
6	Experimental Analysis of Side Material Spreading	119
6.1	Introduction	119
6.2	Online Spread Assessment for Cogging Operation	119
6.2.1	Instrumentation and Equipment	119
6.2.2	Experimental Setup and Procedure	120
6.2.3	Assessment of the Forged Width	121
6.2.4	Results	123
6.2.5	Analysis of the Results	125
6.2.6	Comparison to Theoretical Spread Predicting Models	129
6.3	Summary	135
7	Intelligent Forging Schedule Procedure	137
7.1	Optimum Schedule of Overhead Cycles	139
7.2	Illustrative Example	141
8	Conclusions and Recommendations	144
8.1	Summary of Achievements and Conclusions	144
8.1.1	Adaptive Scheduling for the Incremental Forging Cell	144
8.1.2	Spread Prediction Models	146
8.1.3	Intelligent Forging Schedule Procedure	146
8.1.4	Incremental Forging Limitations	147
8.1.5	Programming Environment of the Virtual Forging Cell	148
8.2	Recommendations for Future Work	148
	Bibliography	150
A	Comparison Between Machining, Open Die Forging and Adaptive Forging of a Typical Product	159
A.1	Machining	160
A.2	Forging	161
B	Ring Compression Test	164
C	Regression Analysis of Spread Measurements	165

D Analytical Proof for Tarnowski's (1950) Empirical Spread Prediction Formula

169

List of Tables

2.1	The Baraya and Johnson (1964) Material Dependent Spread Coefficient Values	33
2.2	Spread Predicting Formulae	39
2.3	Technological Bounds due to Shutt (1963)	42
3.1	Coordinate Assignment for the Workpiece Outer Surfaces	57
3.2	Workpiece Model Attributes	58
3.3	Implemented Technological Bounds due to Shutt (1963)	64
3.4	Simulated Die Material Properties, (Mild Steel Material) (Wong et al. 1996)	69
3.5	Simulated Workpiece Material Properties, (Mild Steel Material) (Wong et al. 1996)	70
3.6	Simulated Workpiece Material Properties, (Pure Aluminum Material (Al1100)) (Wong et al. 1996)	71
3.7	Simulated Workpiece Material Properties, (Pure Lead Material) (Wong et al. 1996)	71
4.1	Forging Schedule for 2 nd Degree Surface	76
4.2	Wedge Forging Steps	80
4.3	The Forging Schedule Implementing the Tarnowski (1950) Formula for Spread Prediction	82
4.4	Scheduling Using the Tomlinson and Stringer (1959) Formula for Spread Prediction	84
4.5	Error Plots Based on the Tarnowski (1950) Formula Schedule	84
4.6	Error Plots Based on the Tomlinson and Stringer (1959) Formula Schedule	85
4.7	3-D Shapes Forged in the Virtual Forging Cell	88
4.8	Forging Schedule of Sample Workpiece	91
6.1	Average Forged Width Estimation Error Using Different Formulae	133
7.1	Feedback Control Forging Schedule	142
7.2	Intelligent Forging Schedule	142
A.1	Milling Cutter Specifications	160
A.2	Forging Schedule for the Sample Product	163
A.3	Forging vs Machining of the Sample Product	163

B.4	Ring Initial Dimension	164
B.5	Deformed Ring Diameters, Height=2 mm	164
B.6	Friction Factor m	164

List of Figures

1.1	Schematic of Closed Die Forging Process	2
1.2	Schematic of Open Die Forging Process	2
2.1	Integrated Flexible Closed Die Forging Cell (Tsujimura and Gen 1999)	8
2.2	Flexible Forging Die (Nielsen et al. 1997)	9
2.3	Hasenclever Radial Forming Machine, (as presented in Nye (1988))	9
2.4	Radial Forging Machine (Nieschwitz et al. 1988)	10
2.5	Schey and Abramowitz (1973) Incremental Forging Operation	11
2.6	Melligeri and Lilly (1994) Cell Configuration	12
2.7	Melligeri and Lilly (1994) Cell Control Schematic	12
2.8	Ferreira and Osman (1999) Cell configuration	13
2.9	Osman and Ferreira (1999) Incremental Forging Cell Operation	13
2.10	Basic Cogging Operation	15
2.11	Cogging Die Shapes (Kiefer and Shah 1990)	15
2.12	Cogging Die Arrangements (Kiefer and Shah 1990)	16
2.13	Principle of Ring Forging (Welchhof and Kopp 1989)	16
2.14	Principle of Rotary Die Forging (Standring et al. 1980)	16
2.15	Bend Forging (Kopp and Bechmann 1996)	17
2.16	Basic Internal Incremental Forging Operations (a and b) Without Restraining Side Spread, (c and d) Restraining Side Spread (Welchhof and Kopp 1989)	18
2.17	Lead Specimen Produced by Incremental Forging Operations a) Without Restraining Side Spread, b) Restraining Side Spread (Welchhof and Kopp 1989)	18
2.18	Deformed Lead Specimen Without the Use of Side Restricting Dies (Schey and Abramowitz 1973)	18
2.19	Stretch Forging Die (Kopp et al. 1982)	19
2.20	Lead Specimen Produced by Stretch Forging (Kopp et al. 1982)	19
2.21	Main Landing Gear Support for the Boeing 747 (Kopp et al. 1982)	19
2.22	Simulation of a Step in the Stretch Forging Operation (Kopp et al. 1982)	20

2.23	Metal Flow With and Without Restricting Dies (Welchhof and Kopp 1989)	20
2.24	Restricting Die Design (Welchhof and Kopp 1989)	20
2.25	Formation of Suckback and Laps (Welchhof and Kopp 1989)	21
2.26	Die Configuration for Preventing Suckback (Welchhof and Kopp 1989)	21
2.27	Alternative Forging Sequences (Appleton et al. 1979)	23
2.28	Operating Regions for Open Die Forging (Aksakal et al. 1993), IAR:Initial aspect ratio, CRAR:Compressed rotated aspect ratio	23
2.29	Equivalent Core Strain Distribution at the Centreline After 8 Forging Passes a)Without Bite Offset b)With Bite Offset (Siemer et al. 1986)	24
2.30	Distribution of Local Elongation Rate Over the Length of Stepped Forging Bar With and Without Bite Offset (Siemer et al. 1986)	25
2.31	Schematic Diagram of the Deformation Zone for the Free from Mannesmann Cogging Method (Wang and Cao 1995)	26
2.32	Plastic Strain Distribution Forging Lead Specimen a) Without Turnover b) With 180° Turnover (Wang and Cao 1994b)	26
2.33	Effective Strain Distribution Forging Lead a) With Die Stag- gering b)Without Die Staggering (Wang and Cao 1994b)	27
2.34	Schematic Diagram of the Deflection of the Center Line With 180° Turnover and Half Die Staggering Procedure (Wang and Cao 1994b)	27
2.35	Illustration of Different Patterns of Material Spread	30
2.36	Different Die Arrangements for Open-Die Forging (Kiefer and Shah 1990)	36
2.37	Die Configurations (Hung and Kobayashi 1992)	37
2.38	Performance Comparison Between Functional Neural Network and Back-Propagation Network, (Kim et al. 2002)	38
2.39	Forging Defects	41
3.1	Flexible Manufacturing Cell Layout for Forged Metal Parts	45
3.2	Structured Light Vision System Principle (Park et al. 2001)	46
3.3	Vision System Calibration Image	49
3.4	Scatter Error Assessment Using Blockgauges	49
3.5	Incremental Forging Operation Plan (<i>Shaded Areas are the Fo- cus of This Research</i>)	51
3.6	Control Schematic of the Forging Cell	53
3.7	Forging Cell Coordinates	54
3.8	Types of Operations that Can Be Performed on the Cell	54
3.9	Instantaneous vs Required Forged Shapes of a Sample Workpiece	56
3.10	Workpiece Modelling	57
3.11	Projection Area for Sample Case	59

3.12	Error in Height Computation Method	59
3.13	Forging Schedule Module (A4) (<i>Shaded Areas are the Focus of This Research</i>)	62
3.14	Improper Die Width Ratio	65
3.15	Virtual Forging Cell Procedure	68
4.1	Workpiece With a 2 nd Surface (all dimensions in mm)	75
4.2	Wedge Workpiece (all dimensions in mm)	79
4.3	Adaptive Schedule Convergence Rate	80
4.4	Control Schematic of the Forging Cell Based on Spread Prediction Models	81
4.5	Maximum Allowable Slope	85
4.6	Wedge Workpiece (width=38.1 mm)	90
4.7	Experimental Setup for Forging a Wedge	90
4.8	Inspection Procedure With Template	91
4.9	Measurements Results	92
5.1	Flat Tool Indentation vs Cogging	101
5.2	Homogeneous Deformation Pattern	102
5.3	Integration Bounds of the Friction Work on the Interface Surface for (Cartesian And Polar Representations)	105
5.4	Sliding Area for Uniform Deformation Pattern	107
5.5	Development of Fish-Bone Deformation Pattern	110
5.6	Typically Observed Fish-Bone Deformation Pattern in a Cogging Operation	111
5.7	Fish-Bone Deformation Pattern	111
6.1	Experimental Setup Showing Press and Robot (Nye et al. 2001)	120
6.2	Experimental Setup Showing End-Effector, Tooling and Gauges (Nye et al. 2001)	121
6.3	Displaced Volume for Center Indentation.	122
6.4	Manual vs Online Measurement Readings	124
6.5	Elongation in Length vs Reduction in Height for Experimental Set 1	126
6.6	Increase in Width vs Reduction in Height for Experimental Set	1126
6.7	Elongation in Length vs Reduction in Height for Experimental Set 2	126
6.8	Increase in Width vs Reduction in Height for Experimental Set	2126
6.9	Elongation in Length vs Reduction in Height for Experimental Set 3	127
6.10	Increase in Width vs Reduction in Height for Experimental Set	3127
6.11	Forged Spread vs Reduction in Height for Experimental Set 1	127
6.12	Forged Spread vs Reduction in Height for Experimental Set 2	128
6.13	Forged Spread vs Reduction in Height for Experimental Set 3	128

6.14	Variation of Spread Coefficient With the Reduction in Height	129
6.15	Estimated vs Measured Average Forged Width Using Wang and Cao (1995) Spread Predicting Formula Set 1	131
6.16	Estimated vs Measured Average Forged Width According to Various Spread Predicting Formulae Set 1	131
6.17	Estimated vs Measured Average Forged Width According to Various Spread Predicting Formulae Set 2	132
6.18	Estimated vs Measured Average Forged Width According to Various Spread Predicting Formulae Set 3	132
6.19	Theoretical Models Estimating the Spread Coefficient vs Actual Spread Coefficient for Experimental Set 3	134
7.1	Intelligent Forging Cell Procedure	138
7.2	Optimum Overhead Cycle Schedule	140
7.3	Intelligent Forging Schedule Illustrative Example	142
A.1	Sample Workpiece	159
A.2	Machining Operation Process Plan	161
A.3	Forging Schedule for Sample Product	162
C.4	Regression Analysis of Average Deformed Width Set 1 Data .	166
C.5	Regression Analysis of Average Deformed Width Set 2 Data .	167
C.6	Regression Analysis of Average Deformed Width Set 3 Data .	168

List of Algorithms

3.1	Error Algorithm (z Direction)	60
3.2	Path Generation Algorithm for Generating External Profiles Defined by Monotonically Decreasing Functions.	63
4.1	Forging Schedule Generation Algorithm Using Spread Coefficient Predicting Formulae	83
5.1	Homogeneous Pattern of Deformation Upper Bound Algorithm	108
5.2	Fish-Bone Pattern of Deformation Upper Bound Algorithm . .	115
5.3	Incrementally Updated Upper Bound Algorithm	117
7.1	Optimum Overhead Scheduling Algorithm	141

Chapter 1

Introduction

1.1 Background

Forging is a bulk forming process in which dies, mounted on a hammer or a press, are used to apply an external pressure on the workpiece in order to alter its shape and/or enhance its internal structure. The process is normally (but not always) performed hot. It is generally classified, based on the degree the material flow is constrained by the dies, into open die forging and closed die forging processes.

In closed die forging¹ the die set, composed of two or more dies, has the impression of the product engraved in them (Fig. 1.1). As the dies are closed, they encapsulate the material, constraining and forcing it to take the shape of the impression. A single blow by the press forges complex multi-featured products with high precision. It is typically used in the production of medium to small sized products where high strength, reliability and precision are required. Compared to machining, closed die forging can forge products in shorter time while maintaining higher material utilization and lower energy consumption (European Powder Metallurgy Association 2004).

In contrast, open die forging does not require special tooling for each product (Fig. 1.2). Universal dies of simple shapes are used to incrementally forge the product. During the forging operation they partly constrain the flow of the material resulting in shape errors and requiring finishing operations. Material feeding, as practised in the industry, can either be: linear, to produce beams, as in cogging operations²; or circular, to produce rings, as in ring forging. The process is used in the production of massive simply-shaped products such as ships transmission and propeller shafts. Open die forging improves the

¹Closed die forging is also known as impression die forging.

²Cogging is a 2-D forming operation where bars are incrementally forged to reduce their cross-section and increase their length.

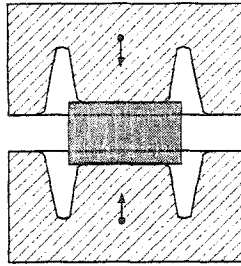


Figure 1.1: Schematic of Closed Die Forging Process

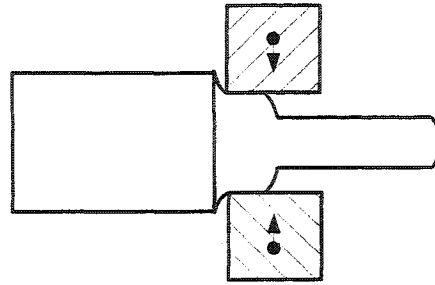


Figure 1.2: Schematic of Open Die Forging Process

mechanical properties of the material by closing any present internal voids or gaps and by reducing the grain size. Geometrical and dimensional accuracies are often considered of secondary importance as the product is subsequently finished by other operations.

The major limitations on the closed die forging processes are the high cost and long production delay associated with manufacturing and setting the dies (if the product shape or dimensions are changed). These limitations render the process inadequate to operate in a flexible production environment characterized by frequent product changes and small lot sizes.

In contrast, open die forging can be easily adapted to frequent changes in the product's design. Manufacturing products by open die forging, however, requires the development of a forging schedule comprising the squeezing and feeding sequence, directions and magnitudes. Such schedules are typically manually generated rendering the process highly dependent on the skill and experience of the forgemaster.

The Forging Industry Association Technology Roadmap (Barnett 2000) credits forged components as generally desired for their high quality, reliability and long life cycle but notes that forged products are associated with high manufacturing costs and long lead-time. The competition to the forging industry comes mainly from investment casting, machining and powder metallurgy. The ability of the industry to compete and satisfy current demand for affordable, low volume, quality parts is dependent on its ability to change over from rigid mass production systems to flexible manufacturing systems. This transition will improve forging plants competitiveness and help them to achieve economic growth.

The development of a flexible forging cell based on an open die forging architecture will have the potential advantage of significantly reducing the production lead-time, rendering the forging process competitive with other processes such as machining. In an illustrative example the total production time of a sample product was reduced from 30 min 14 s to 2 min 7 s by

switching from machining to open die forging (Appendix A).

1.2 Research Motivation

The forging process provides a number of advantages compared to alternative manufacturing processes where it can reduce the production time significantly while at the same time increases the material utilization.

The use of forging is typically limited by lack of flexibility in closed die forging and by high labour cost and the difficulty of creating forging schedules in open die forging. A Flexible Forging System³ has the potential to overcome these difficulties. Although this concept has been investigated for a number of years (Kopp et al. 1982; Pahnke 1983; Siemer et al. 1986; Kopp 1986; Welchof and Kopp 1989; Aksakal et al. 1993; Kopp and Bechmann 1996; Aksakal et al. 1997; Ferreira and Osman 2000) it has so far met with little success because of the challenge of generating the forging schedule.

Research on forging schedule generation focused on predicting the instantaneous shape of the material as it is being forged by using spread prediction models⁴. Current spread prediction models are limited to predicting the spread in cogging operations with flat or radiused dies (in which the models only consider 2-D material spread). Nye et al. (2001) compared several spread prediction models with actual spread measurements and reported that current models produce low quality estimates that are not capable of directly generating acceptable incremental forging schedules.

Researchers have recommended online measurement of the deformed workpiece shape to overcome the low estimation quality of the spread prediction models (Appleton et al. 1979; Lilly and Melligeri 1996; Aksakal et al. 1997; Ferreira and Osman 2000; Nye et al. 2001). This is the main motivation for this research; to explore the concept of generating adaptive forging schedules based on the online measurement of the deformed workpiece shape. The key to the operation of such system is that the instantaneous shape of the workpiece is captured by a vision feedback system and the shape difference between the captured instantaneous and current shapes of the workpiece is computed. This difference is then used to drive the forging schedule.

³A Flexible Forging System, roughly speaking is an automated open die forging system that can automatically forge parts of different shapes with a short setup time and without the need for skilled operators.

⁴Spread prediction models are developed to estimate how the workpiece material flows during deformation.

1.3 Objective and Scope

The main objective of the thesis is to explore the concept of implementing online shape feedback to adaptively generate the forging schedule for a flexible forging cell. Current forging schedule generation procedures depend on accurate prediction of the deformed workpiece shape using spread prediction models. Such models are utilized for single step forging operations and their estimation error accumulates to an unacceptable limit if used in a complex forging schedule composed of multiple consecutive forging steps. For this reason forging schedules based on spread prediction models are limited to generating beams with uniform cross-sections. A secondary objective of this research is to develop accurate spread prediction models and to integrate them with the adaptive forging schedule generation procedure to enhance the quality of the generated schedule.

The original scope of this research was intended to study external and internal profiling operations. Experiments on internal profiling showed that the lapping defect can not be avoided in such operations. For this reason the scope was limited to external profile generation with convex shaped dies that extend beyond the workpiece (the fundamental forging operation in such case is a cogging one).

This work aims to study generating 3-D profiles of moderate complexity to within a preset tolerance limit. The workpieces are of small to medium sizes that are forged from a defect-free billet. For this reason studying the change in the material internal structure was not included in this work. The press used is assumed to have excess capacity and as such force prediction was not included in the work scope. Forging is a bulk deformation process and as such no bending operations are included in this work.

1.4 Thesis Outline

A review of flexible forging cells potentials and anticipated limitations is presented in Chapter 2, in which Section 2.2 presents possible forging cell configurations with an emphasize on configurations based on open die forging architecture. Section 2.5 presents available spread prediction models and their limitations (these models forms the backbone of current forging schedule generation models). Experiments were carried out to compare actually measured spread with the prediction of current spread prediction models and the results indicated that those models are of poor quality, those findings were published in the *Journal of Engineering Materials and Technology* (Nye et al. 2001). Technological bounds on the forging operation (these bounds are the scheduling constraints) are presented in Section 2.6. Relevant applications of the

adaptive feedback procedure in other metal forming operations are presented in Section 2.7.

The general structure of the forging cell is presented in Chapter 3 in which suggested cell hardware and operation plan are presented. The adaptive scheduling algorithm was used to produce 2-D and 3-D profiles (Chapter 4). A paper describing the adaptive schedule used to generate 2-D and 2- $\frac{1}{2}$ -D profiles was submitted for publication in *the International Journal of Machine Tools and Manufacture* (Elbadan and Nye 2003) and a paper describing the adaptive schedules used to generate 3-D profiles is currently under preparation (Elbadan and Nye 2004a).

Chapter 5 presents three newly derived spread prediction models that are used to enhance the convergence rate of the adaptive forging schedule procedure. The Incrementally Updated Upper Bound solution (Section 5.3.3) in particular proved to provide the best spread estimate compared to other spread prediction models (the comparison is presented in Section 6.2.6). This model was then used in an enhanced adaptive schedule generation model presented in Chapter 7. A paper is currently under preparation on the developed Incrementally Updated Upper Bound spread prediction model and its implementation in the enhanced adaptive schedule generation model (Elbadan and Nye 2004b). Finally conclusions are drawn and future research recommendations are presented in Chapter 8.

Chapter 2

Literature review

2.1 Introduction

The literature review that pertains to the potentials, possible limitations and operational control of flexible forging cells is presented in this chapter. Possible cell configurations are presented in Section 2.2 of which the open die forging configuration offers the highest degree of flexibility. Flexible forging cells based on an open die forging architecture are generally composed of a numerically controlled press, a robot for workpiece manipulation and a supervisory computer.

A review of literature on incremental forging operations that could be executed on the forging cell is presented in Section 2.3; classified based on the direction of feed and generated profile class. Products are forged incrementally on the forging cell where the operations' execution sequence is specified in the forging schedule. Such schedules were mainly derived to enhance the internal structure of the material (especially void closure) while very few addressed the geometrical and dimensional aspects of the forged products. Spread prediction models (Section 2.5) were used to predict the workpiece forged dimensions in order to generate cogging schedules for forging beams and bars. A classification of forging schedules based on the scheduling objective is presented in Section 2.4.

Incremental forging is a process where one must control the flow of the forged material by proper design of the forging tool and by proper selection of the forging parameters. The forging schedule (comprising the sequence of squeezing actions) is developed such that the material will flow in a preferable manner. As the dies only constrain part of the deforming material, one can never have full control of the process. It often occurs that the material will deform in a way that can never be subsequently corrected, resulting in the generation of a forging defect. Though forging defects can not be rectified by

forging, their generation can be avoided by selecting proper operation parameters. The range in which an operation parameter can be used is defined by the technological bounds of the process (Section 2.6). Unfortunately there is a narrow range within which the process can work successfully and not all technological bounds have been identified. Finally the use of feedback process control as applied in sheet metal forming processes is presented in Section 2.7.

2.2 Flexible Forging Cell Configuration

There have been four major research approaches to develop a flexible forging cell. Three based on closed die forging architecture and intended to reduce the die setup and changing time and one based on automating open die forging cells.

- Developing an integrated closed die forging cell was the first approach to develop a flexible forging system (Tsujimura and Gen 1999). The cell was composed of a press to provide the forming load, a tool-magazine where several dedicated dies are stored, and a robot for handling raw material and finished products (Fig. 2.1). The system had the advantage of cutting down the setup times for the dies. It also created an integrated workplace for closed die forging where the dies are stored and rapidly assembled when needed. This system triggered efforts to standardize die heights in order to maintain rapid tool changing and facilitate the automatic change of the dies. The major limitation of the system was that each product had to have its own die set. New products had to wait for appropriate dies to be designed and manufactured which worked well for systems with small product variety and high production volume.

Park et al. (1999) reported an interesting implementation of a flexible forging system in the industry. Progressive stamping dies were used to attain flexibility in mass production of electronic parts. A separate die is used to forge each feature, allowing features to be altered or deleted by modifying the respective die.

- Developing reconfigurable dies¹ was another attempt to reduce the die setup time. A compound die (Nielsen et al. 1997) is used to perform multi operations on the same workpiece without the need to change the

¹Remarkable achievements in developing reconfigurable dies (that are able to forge more than one product with minor modification) for sheet metal forming process has been reported in the literature (Walczyk et al. 1998; Walczyk and Im 2000; Cai and Li 2002; Walczyk et al. 2003). The dies are composed of a matrix of pins whose heights can be re-adjusted for each specific product shape.

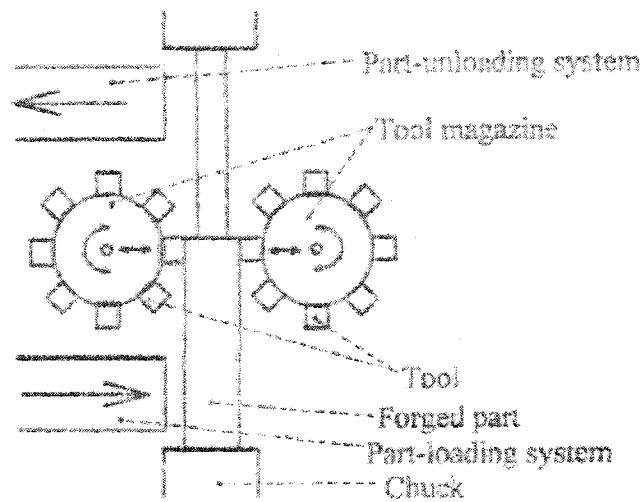


Figure 2.1: Integrated Flexible Closed Die Forging Cell (Tsujimura and Gen 1999)

dies. It has the advantage of having single setup for multi operations but is intended for the production of a single product. It is rigid in terms of changes to product specification (dimension wise or geometrical wise) (Fig. 2.2).

- Developing radial forging (Swaging) machines (Wright et al. 1982; Nieschwitz et al. 1988; Nye 1988) (Figs. 2.3 and 2.4) on which multiple rams are arranged circumferentially working synchronously or individually on a single cross-section of the workpiece. Such design provided enough support to perform multi external profiling operations such as bending and swaging.
- Automating the open die forging process promises the highest flexibility to changes in product design. The automation was achieved by coordinating the press and the manipulator motions and numerically controlling the squeezing motion of the press (Appleton et al. 1979; Kopp et al. 1982; Pahnke 1983; Welchof and Kopp 1989; Aksakal et al. 1993; Lilly and Jablow 1995; Kopp and Bechmann 1996; Teti et al. 1999; Ferreira and Osman 2000; Nye et al. 2001; Kim et al. 2002).

In this research it will be shown that automating the open die forging process forms the base to developing an intelligent incremental forging cell suitable for the production of medium to small sized workpieces with moderate shape complexity. The process can be implemented as a preliminary operation

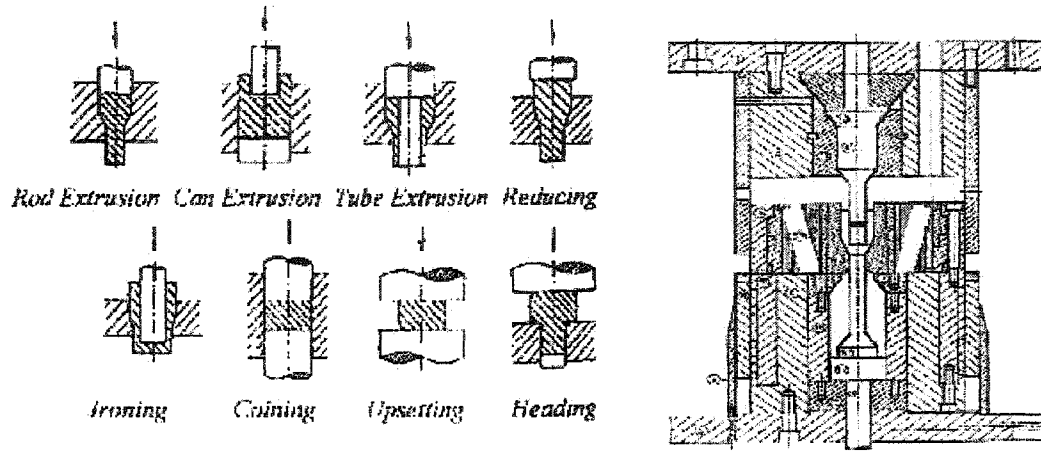


Figure 2.2: Flexible Forging Die (Nielsen et al. 1997)

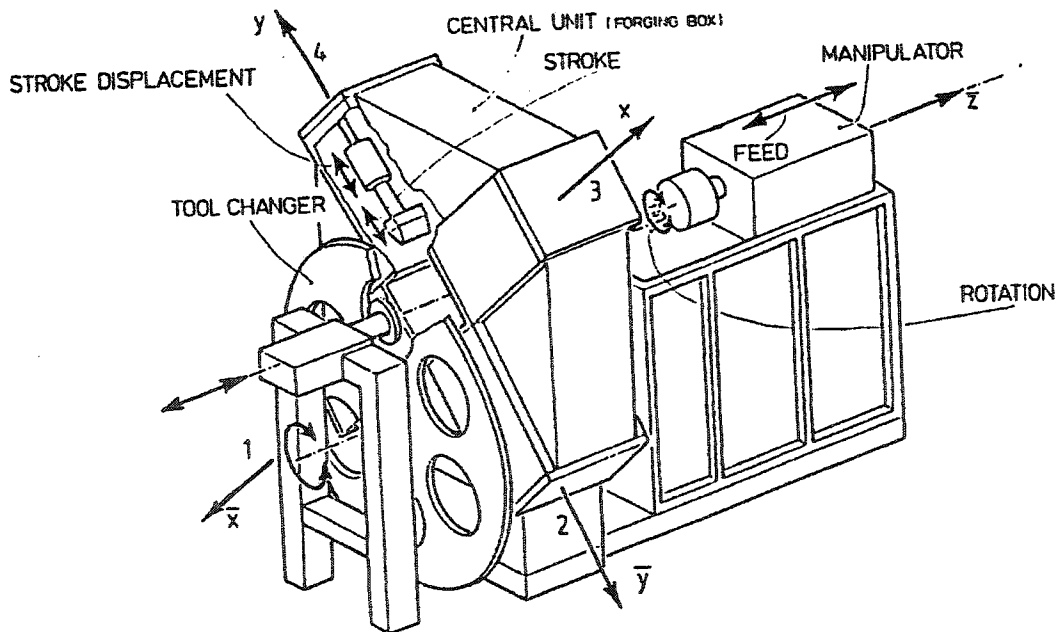


Figure 2.3: Hasenclever Radial Forming Machine, (as presented in Nye (1988))

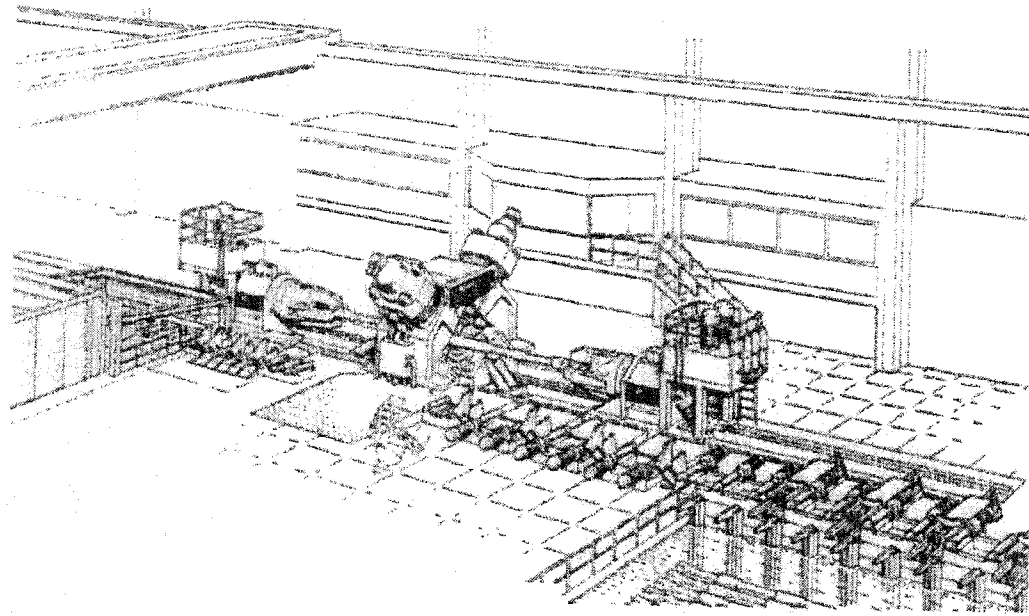


Figure 2.4: Radial Forging Machine (Nieschwitz et al. 1988)

to achieve a high shape transformation that can be then followed by finishing operations. Several researchers studied the development of such system and their work will be presented in what follows.

Schey and Abramowitz (1973) studied incrementally forming complex shapes of typical airframe components incorporating thin webs and narrow tall ribs and stiffening cross-ribs which are typically machined, to improve material utilization. The original configuration of their cell consisted of a main press that provided the main forging load and a workpiece manipulator. Experimental results showed that sequenced indentation with only one pair of dies was unsatisfactory as the material was pushed back and forth during the forging process. From this they concluded that the unpredictable nature of material spread necessitates the use of auxiliary dies to control spreading. They subsequently used a sub press with side rams to simultaneously forge the material with two pairs of dies (Fig. 2.5). The procedure proved to provide better workpiece shapes and prevented nonhomogeneous side material spreading and maintained better geometrical accuracy, however, it was highly sensitive to the bite and reduction ratios. Their main conclusion was that internal complex profiles can not be forged incrementally as material displacement cannot be controlled. The entire web had to be forged in a single step with the aid of auxiliary dies to prevent undesired side material spreading.

The Appleton et al. (1979) cell configuration was composed of a 750 000 KN hydraulic press, a Versatran D301 robot (point to point cylindrical coor-

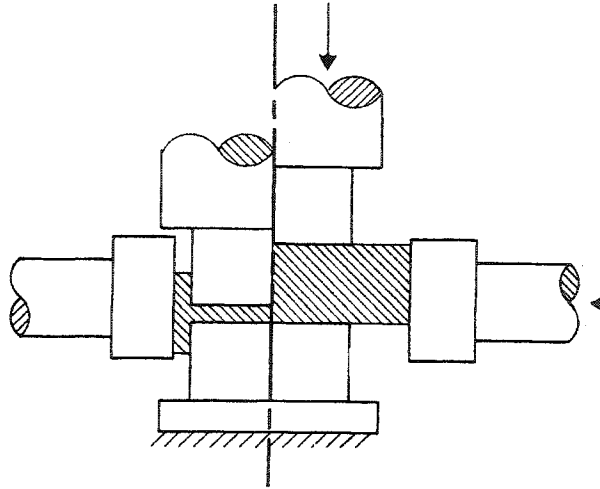


Figure 2.5: Schey and Abramowitz (1973) Incremental Forging Operation

dinate robot), a controller and a specially designed gripper. As the workpiece is deformed it elongates toward its free surface direction. The gripper was designed to comply with such elongation and to return the gripper to the datum position after the die releases the workpiece, thus, preserving the workpiece datum. It is interesting to note that the gripper designed by Appleton et al. (1979) did not compensate for the vertical displacement of the centreline of the workpiece (the press used was a single acting press for which the workpiece centreline is displaced in the squeezing direction during the forging operation). They overcame this problem by keeping the deformation low in order to allow the robot structural compliance to accommodate this displacement.

Melligeri and Lilly (1994) proposed applying a neural network for compliance control of robot manipulators used in an incremental forging cell (Fig. 2.6). As the workpiece is deformed its locating surface is displaced requiring the robot gripper to comply with such a displacement in order to avoid overstressing the gripper and the robot. The proposed model used neural networks to control the robot in order to comply with such workpiece displacement. A set of experiments was generated first through simulating the forging process and the resultant displacement of the locating surface is used to train the neural network. The output of the network was then utilized by a reverse kinematic transform and appropriate motion was generated by the controller to adaptively comply with the displacement in the locating surface (Fig. 2.7).

Aksakal et al. (1993, 1997) proposed a forging cell consisting of a numerically controlled press, a robot for workpiece manipulation and a supervisory computer where forging schedules were generated. They concluded that workpiece handling and positioning is a potential problem in designing the

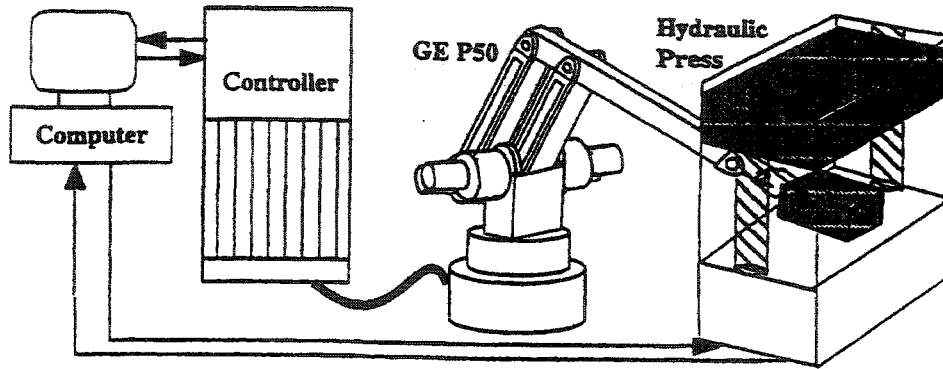


Figure 2.6: Melligeri and Lilly (1994) Cell Configuration

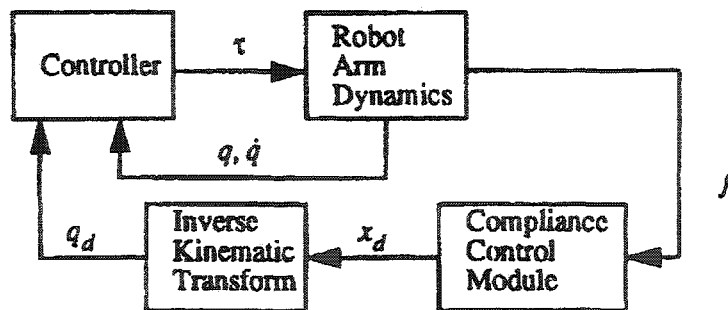


Figure 2.7: Melligeri and Lilly (1994) Cell Control Schematic

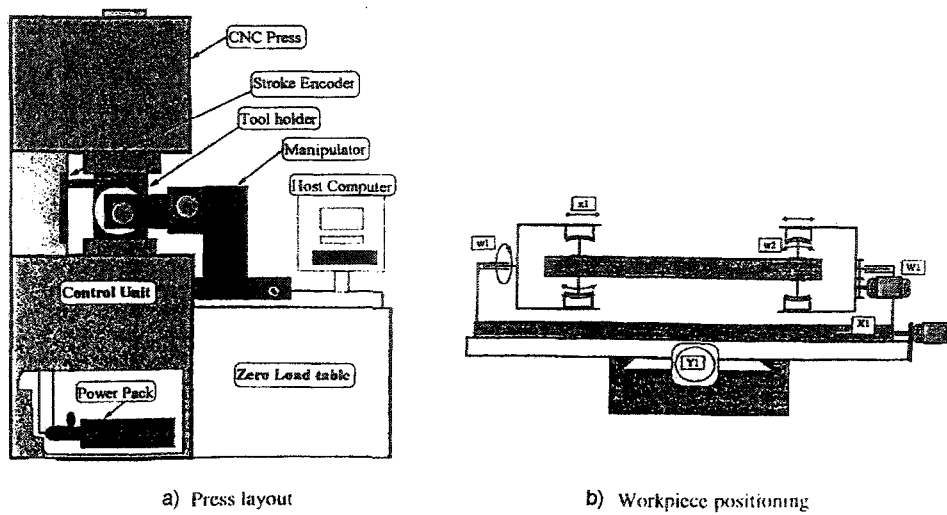


Figure 2.8: Ferreira and Osman (1999) Cell configuration

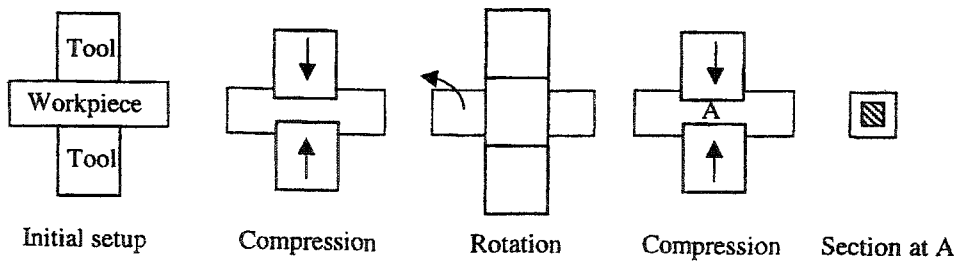


Figure 2.9: Osman and Ferreira (1999) Incremental Forging Cell Operation

workpiece manipulator. During forging the workpiece material spreads in all directions and the workpiece's reference surfaces are displaced. The manipulator must be designed to accommodate and compensate for such displacement while at the same time prevent material spreading in undesirable directions.

Ferreira and Osman (1999); Osman and Ferreira (1999) developed a workpiece manipulator to be integrated with a numerically controlled press for incremental forging operations (Fig. 2.8). The manipulator had enough flexibility to comply with workpiece elongation and vertical displacement. It has three linear and one rotational degrees of freedom for positioning the workpiece under the dies. The cell is intended for cogging operations in which radiused or flat dies can be used (Fig. 2.9).

Most of these researchers agreed in their conclusion that feedback control is necessary for compliance control of the robot positioning to compensate for accumulated positioning errors and unpredictability of workpiece spread (Appleton et al. 1979; Lilly and Melligeri 1996; Aksakal et al. 1997; Ferreira

and Osman 2000).

2.3 Classification of Incremental Forging Operations

Incremental forging operations can be generally classified into external and internal profiling. The majority of the incremental forging operations research pertains to external profiling, especially for cogging operations. In external profiling the dies clear the workpiece cross-section as it is forged. As a result only convex shaped cross-sections can be forged by such an operation. External profiling is classified based on the forging feed direction into cogging, ring forging, rotary forging and bend forging.

In internal profiling the die indents the workpiece material and does not clear the workpiece cross-section as it forges it. The cross-section during the forging operation has a non-convex shape. The operation is typically implemented in incremental rib forging of large beams.

2.3.1 Cogging Operations

Research on external profiling focused on cogging, which can be regarded as the fundamental open die forging operation. In cogging (Fig. 2.10), dies of simple shapes incrementally squeeze segments of the workpiece. A manipulator holds the workpiece and is used to rotate and feed the material into the working zone between the dies. Cogging is used to *draw out* bars and billets (i.e, reduce their cross-section and increase their length), occasionally changing their cross-sectional shape. Simple longitudinal profiles², such as stepped shafts, are forged in open dies while more complex profiles are harder to generate and are commonly produced by other processes.

A cogging die might be flat, V shaped, or round, and the die set is composed of two dies having any of the previously mentioned shapes (Fig. 2.11). Conventionally a cogging die set is symmetric where both dies act together to forge local zones on the workpiece. The locally forged area has a length equal to the forging bite and a width equal to the workpiece width (Fig. 2.12 a). In Free from Mannesmann (FM) (Kiefer and Shah 1990; Wang and Cao 1994a) forging the upper die applies the forging pressure and the lower die is used to support the workpiece (Fig. 2.12 b). There is another form of Free from Mannesmann forging where the upper die dimensions are smaller than the

²Longitudinal profiles are 2-D profile in which the thickness varies with the longitudinal direction (*forging feed direction*) and are generated by varying the squeeze value along the feed direction.

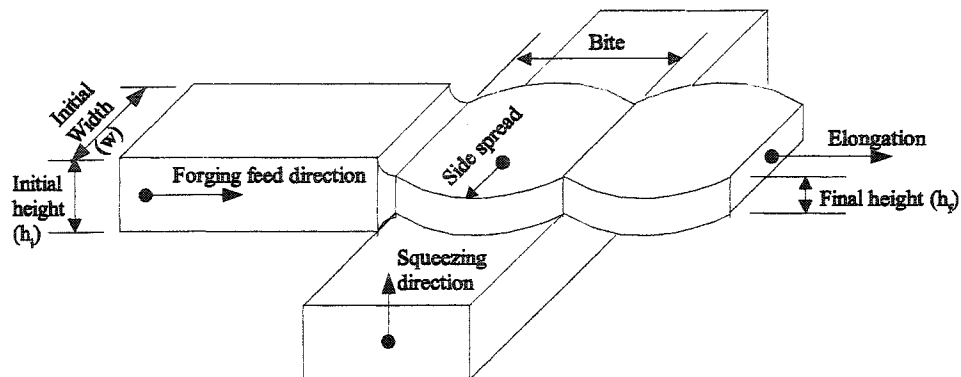


Figure 2.10: Basic Cogging Operation

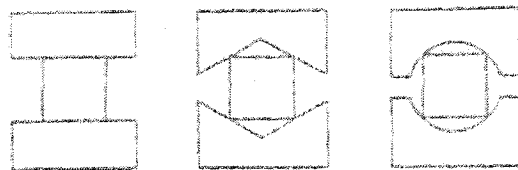


Figure 2.11: Cogging Die Shapes (Kiefer and Shah 1990)

workpiece dimensions and as such it indents in the forged material forming a rectangular impression on it (Fig. 2.12 c).

2.3.2 Ring Forging

Ring forging can be considered as a special type of cogging operations where the forging feed direction is angular (Welchhof and Kopp 1989). The process is used to produce seamless rings by incrementally upsetting an initial ring to increase its diameter and reduce its height (Fig. 2.13).

2.3.3 Rotary Forging

Figure 2.14 shows the principle of rotary forging (Standring et al. 1980). A conical die rotates and oscillates incrementally indenting the surface of the workpiece. The process is mainly used for upsetting hard material.

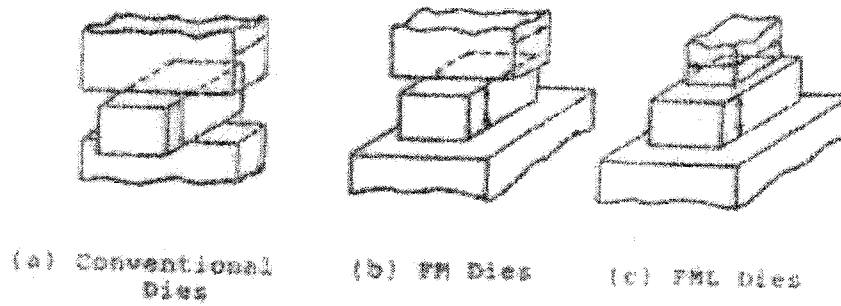


Figure 2.12: Cogging Die Arrangements (Kiefer and Shah 1990)

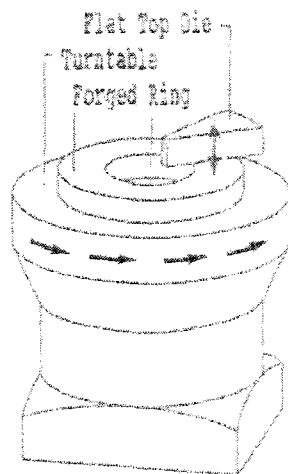


Figure 2.13: Principle of Ring Forging (Welch and Kopp 1989)

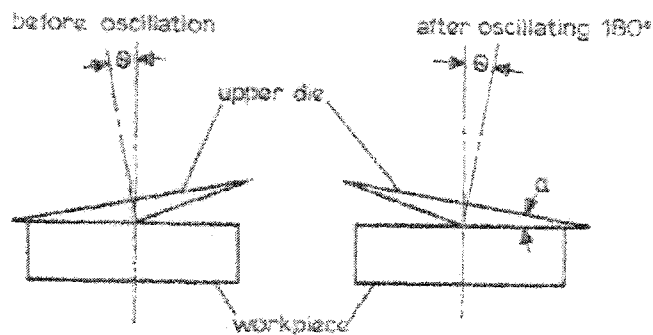


Figure 2.14: Principle of Rotary Die Forging (Standring et al. 1980)

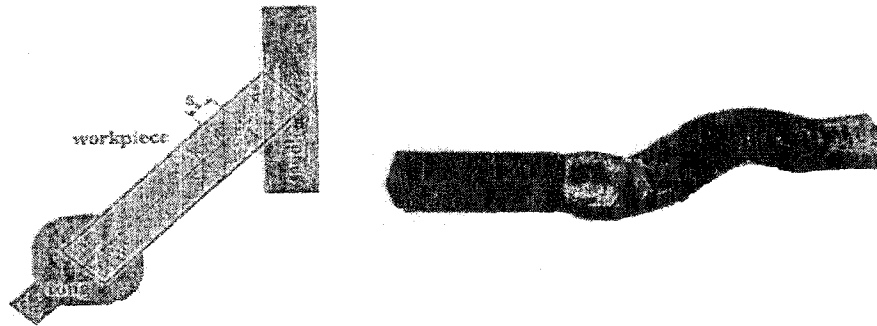


Figure 2.15: Bend Forging (Kopp and Bechmann 1996)

2.3.4 Bend Forging

Bend forging is based on controlling the transverse stretching of the material as it is being upset by the dies (Kopp and Bechmann 1996). The workpiece is aligned with a setting angle to the direction of the feed and the axis of the forging dies (Fig. 2.15). As the die upsets the workpiece it spreads the material unevenly causing its axis to bend. By adjusting the setting angle and the feed through a trial and error procedure the shape of the bend can be controlled.

2.3.5 Internal Profiling

Restrained internal profiling is an intermediate process between closed die forging and open die forging. In such a process side material spread is controlled either through the use of side auxiliary dies (Schey and Abramowitz 1973) or by incrementally forging the profile in a closed die, as applied in stretch forging³ (Kopp et al. 1982). In contrast unrestrained internal profiling is a more flexible process where the material is forged by incremental indentation of simple dies. The die design is much simpler in this type of process but the produced profile generally is of lower shape quality (Figs. 2.16 a and b, Fig. 2.17 a, and Fig. 2.18).

Kopp et al. (1982) presented a general review of work done on incremental forging processes. They presented stretch forging as a competitive process that reduces the cost and investment in the die while at the same time requiring a lower press capacity to do the job. A part is forged incrementally in a die set (Fig. 2.19) which partly restrains the spreading of the forged material to maintain a good tolerance. A lead specimen has been forged (Fig. 2.20) by these dies simulating the forging of an aircraft landing gear component

³A class of incremental forging operations where a part is incrementally forged in semi closed dies.

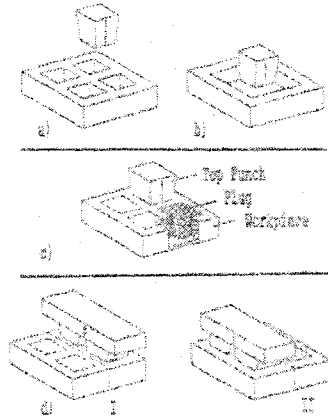


Figure 2.16: Basic Internal Incremental Forging Operations (a and b) Without Restraining Side Spread, (c and d) Restraining Side Spread (Welchhof and Kopp 1989)

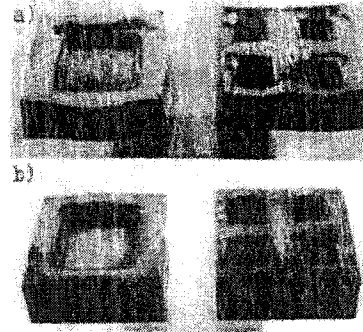


Figure 2.17: Lead Specimen Produced by Incremental Forging Operations a) Without Restraining Side Spread, b) Restraining Side Spread (Welchhof and Kopp 1989)

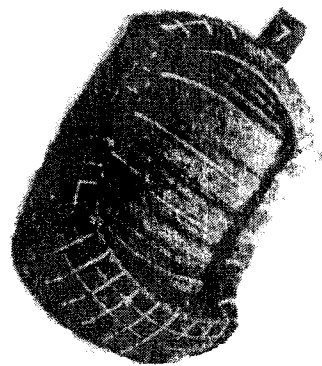


Figure 2.18: Deformed Lead Specimen Without the Use of Side Restricting Dies (Schey and Abramowitz 1973)

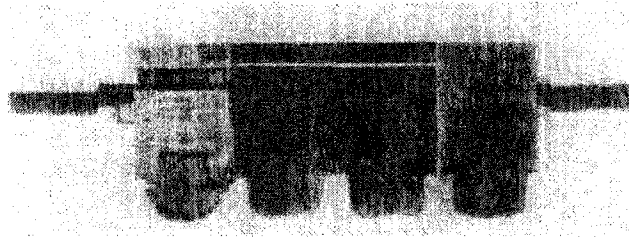


Figure 2.19: Stretch Forging Die (Kopp et al. 1982)



Figure 2.20: Lead Specimen Produced by Stretch Forging (Kopp et al. 1982)

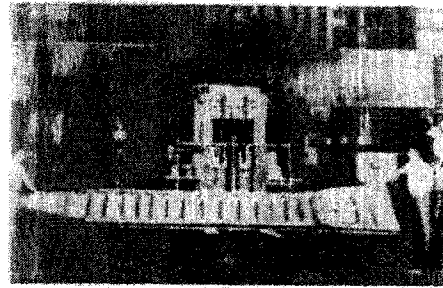


Figure 2.21: Main Landing Gear Support for the Boeing 747 (Kopp et al. 1982)

(Fig. 2.21). Figure 2.22 shows a simulation of a single step in the forging operation for this type of forging process.

Welchhof and Kopp (1989) presented an overview of the incremental forging processes, prospective capabilities and limitations for internal incremental forging processes and ring forging. They generally classify internal forging processes to unrestrained (Figs. 2.16 a and b and Fig. 2.23 a) and restrained processes (Figs. 2.16 c and d and Fig. 2.23 b).

They recommended a specially designed die set for the internal incremental forging operation. The die set is composed of a restraining die to prevent side material spread (Fig. 2.24) a modified bottom die to prevent suckback (Figs. 2.25 and 2.26) and an upper indenting die. Figure 2.17 shows lead specimens produced with and without the restricting die.

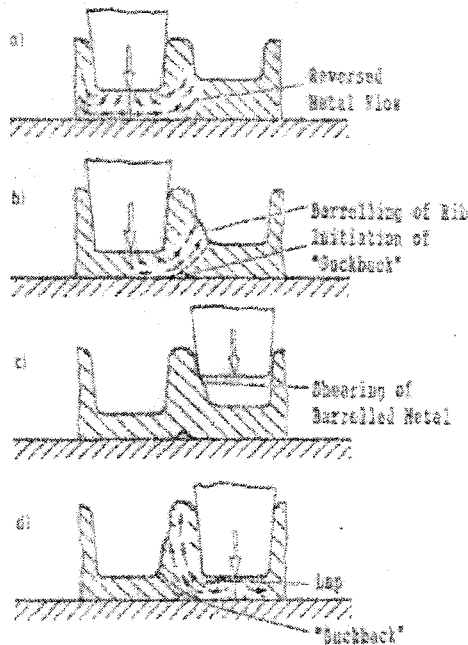


Figure 2.25: Formation of Suckback and Laps (Welchof and Kopp 1989)

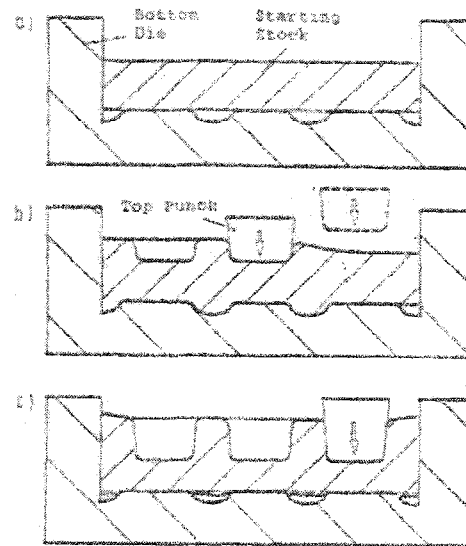


Figure 2.26: Die Configuration for Preventing Suckback (Welchof and Kopp 1989)

2.4 Scheduling Forging Operations

Forging⁴ schedules targeted either cogging or enhancing the internal structure of forged workpieces. The values of the forging parameters in the schedule (such as the reduction in height and the bite) are typically constrained by various technological bounds such as material spreading, thermal effects, press capacity and internal structure changes (Berger et al. 1982). Several forging schedule generation procedures that are used for cogging workpieces or in enhancing the internal structure of the workpiece are presented in what follows.

2.4.1 Cogging Schedules

There are virtually an infinite number of possible cogging schedules to forge a given part. A billet starting with an original cross-sectional shape, say rectangular, can be forged into another shape, say hexagonal, through a series of intermittent transformations to any arbitrary intermediate (transient) shapes such as circular, rectangular, square, or any other arbitrary shape, before being finally forged to the desired hexagonal shape. Research on generating cogging

⁴Refer to Section 2.3.1.

schedules for simple intermediate shapes is presented below.

Wisterich and Shutt (1959) used the Tarnowski⁵ spread formula and assumed linear constraints to represent the forging technological bounds to develop nonlinear mathematical models to optimize cogging schedules. Optimum bite ratio for cogging of square bars where the cross-sectional shape alternates between square / rectangular shapes were derived to minimize the total forging time, or, if a cost function can be developed, to minimize the total forging cost.

Appleton et al. (1979) compared four different sequences (Fig. 2.27) for cogging steel using lead as a simulating material and concluded that the forging sequence can be utilized to minimize the distortions of the deformed workpiece shape. In addition, the experiments showed that it is hard to predict the elongation of the workpiece and thus adjust the feed of the material. As such they recommended the use of online measurement of the elongation to adjust the feed.

Aksakal et al. (1993) used the upper bound method to predict spread for cogging rectangular bars with flat dies. In their experiments they simulated cogging operations by single step indentation. Using their spread estimate they assumed that the optimum cogging schedule is the one that alternates between rectangular / square cross sections and developed, experimentally, an operating figure (Fig. 2.28) to assist in generating cogging schedules. The figure shows the feasible and infeasible working zones and the optimum operating line (which corresponds to the feasible region for infinite number of rotational cycles). Their main conclusion is that the stable working region depends on the workpiece aspect ratio⁶.

Berger et al. (1982); Belova et al. (1987) presented a framework for forging schedules for open die forging. The procedure is intended for cogging operations without taking into consideration geometrical and dimensional errors. It targets generating schedules to optimize the forging time in order to prevent the workpiece temperature from falling below a preset limit at which the material is too hard to be forged. In a typical example presented by Belova et al. (1987) the total manufacturing time was reduced from 171 hr and 48 min to 136 hr and 35 min.

2.4.2 Enhancing Internal Material Structure

Siemer et al. (1986) developed cogging schedules that establish a homogeneous plastic strain distribution in the core of the material for cogging square bars with flat tools. In their experiments they measured the internal plastic strain

⁵As reported in Tomlinson and Stringer (1959).

⁶Aspect ratio is the ratio between the width and height of the workpiece.

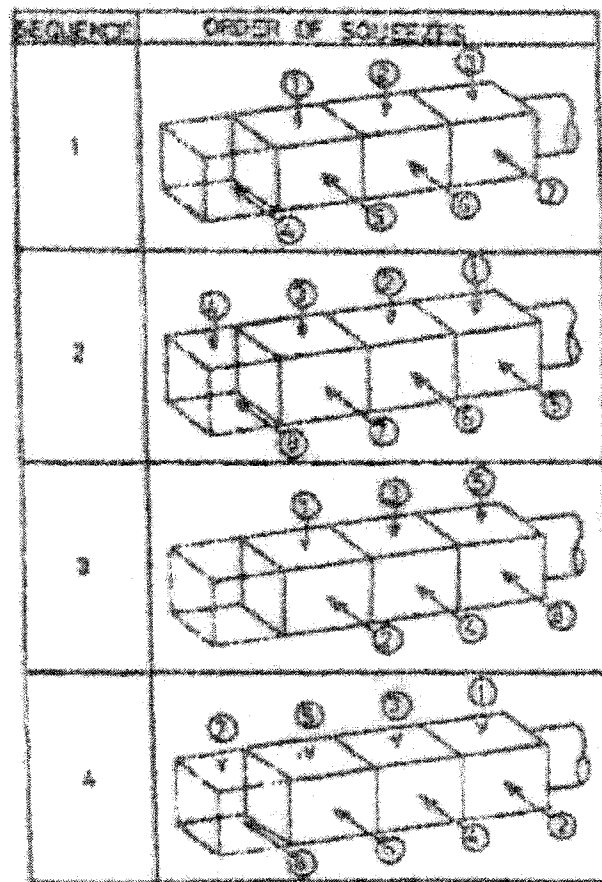


Figure 2.27: Alternative Forging Sequences (Appleton et al. 1979)

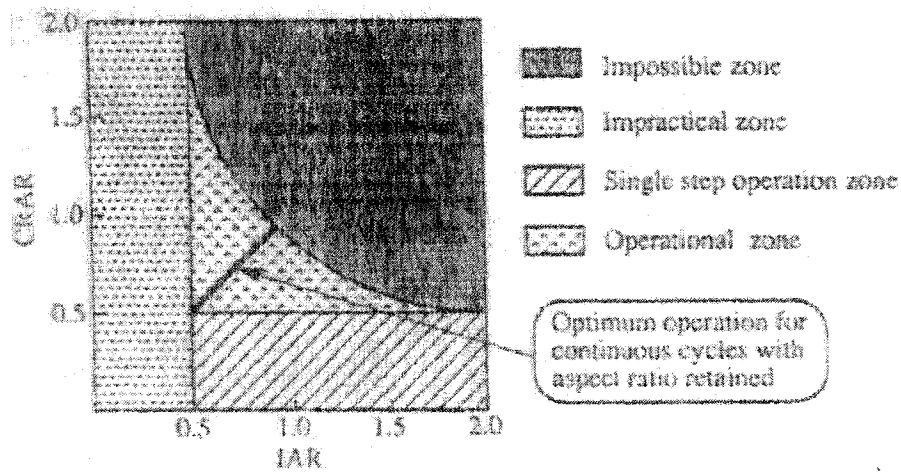


Figure 2.28: Operating Regions for Open Die Forging (Aksakal et al. 1993), IAR:Initial aspect ratio, CRAR:Compressed rotated aspect ratio

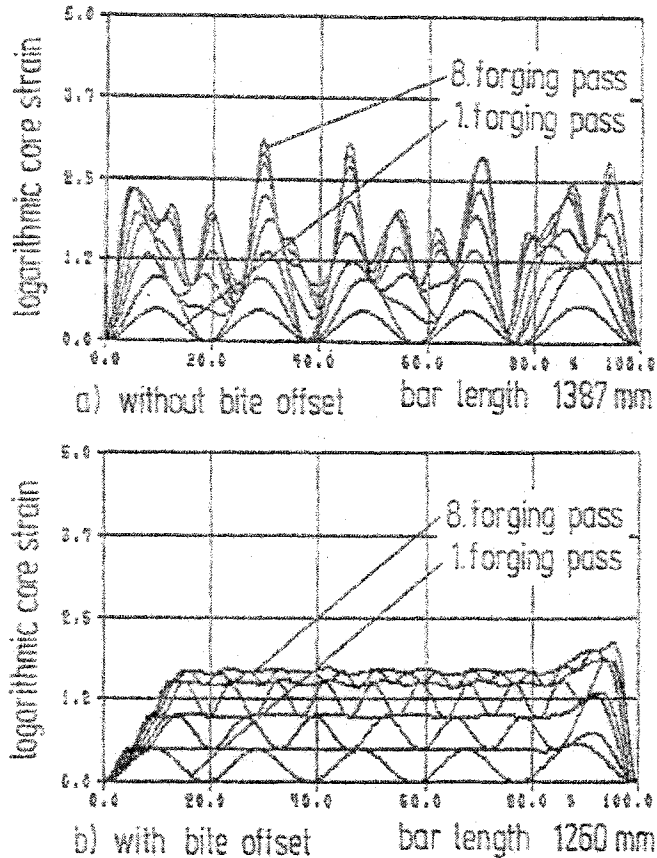


Figure 2.29: Equivalent Core Strain Distribution at the Centreline After 8 Forging Passes a) Without Bite Offset b) With Bite Offset (Siemer et al. 1986)

at the centreline of the material and found that offsetting the bite between cogging steps results in more uniform strain distribution in the material core (Fig. 2.29) and at the same time reduced the probability of surface crack formation which is proportional to the elongation rate λ_r , (Fig. 2.30).

Szyndler and Klimkiewicz (1992) developed a nonlinear mathematical model for cogging ingots in order to maintain uniform effective strain distribution inside the material. The schedule alternates between simple upsetting and cogging in order to have a uniform distribution of the plastic strain. It is designed for three classes of cogging schedules where the material alternates between:

- Rectangular / Square or Rectangular / Rectangular
- Round / Square
- Square / Round

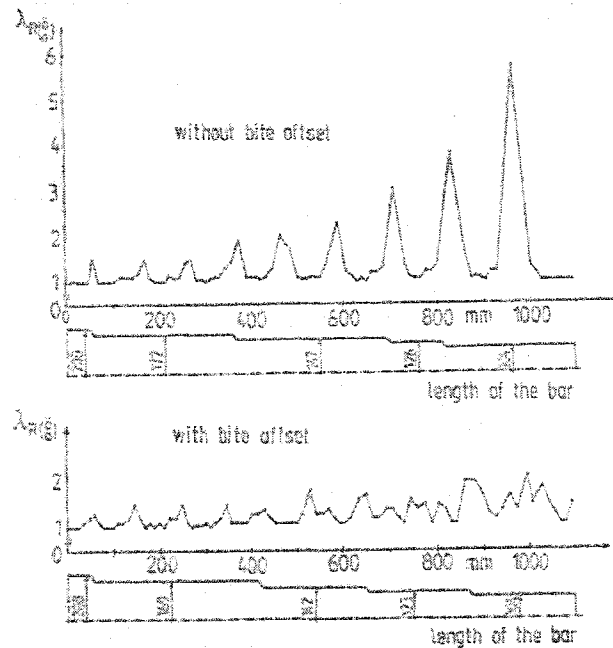


Figure 2.30: Distribution of Local Elongation Rate Over the Length of Stepped Forging Bar With and Without Bite Offset (Siemer et al. 1986)

The model optimizes the required ingot diameter given an upper limit on the allowable reduction to be used (dictated by the capacity limit, and the allowable forging temperature range). The decision parameters were the choice of the forging operation (upsetting or cogging) and the amount of reduction to be applied. The model did not take into account the effect of material spreading.

Wang and Cao (1994b, 1995) used the Moire method to measure the plastic strain in the material after it is being cogged by the Free from Mannesmann Method (Fig. 2.31). They performed several experiments and recommended the following strategies for cogging any given part:

- It is recommended to use symmetric dies to maintain more homogeneous plastic strain distribution. If the Free from Mannesmann method is used it is recommended to turn over the workpiece 180° and divide the total reduction such that half of the reduction is forged while the workpiece lies on one side then turn it 180° and forge the second half of the reduction (Fig. 2.32)
- Die staggering⁷ reduces the fluctuation in the plastic strain distribution

⁷Die staggering: is a procedure where the starting position of the dies for forging the part is shifted between passes.

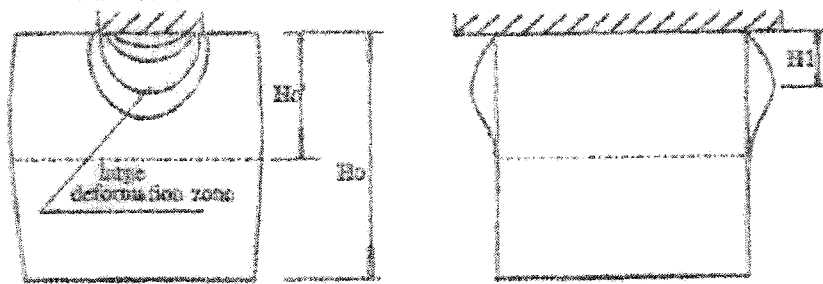


Figure 2.31: Schematic Diagram of the Deformation Zone for the Free from Mannesmann Cogging Method (Wang and Cao 1995)

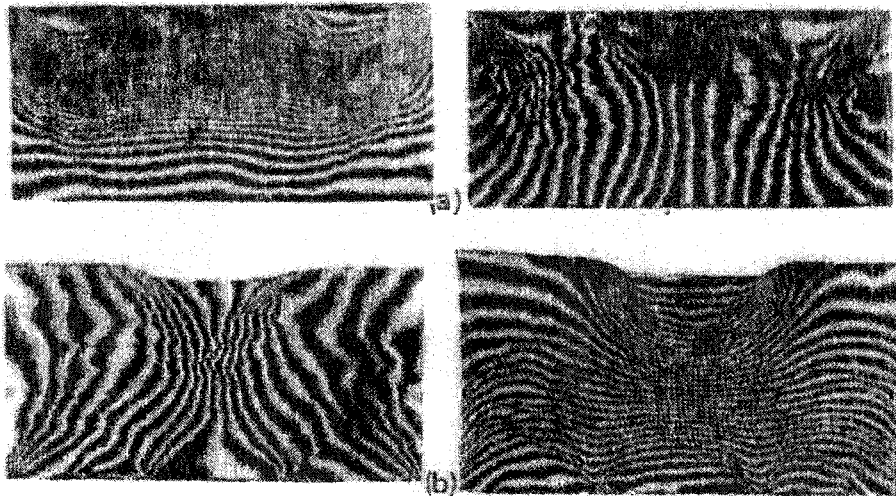


Figure 2.32: Plastic Strain Distribution Forging Lead Specimen a) Without Turnover b) With 180° Turnover (Wang and Cao 1994b)

and increases the chance of closing all internal cavities (Fig. 2.33).

- Using the optimum die width ratio⁸, DWR , of 0.6, 180° turnover and half die staggering the center line deflection is shown experimentally to be about 3.5% (Fig. 2.34).

Kim et al. (2002) used an artificial neural network to generate cogging schedules for forging square and rectangular bars. The neural network gathers forging parameter inputs such as ram position, pressure, temperature and

⁸Although the term Bite to Height Ratio is more precise, it was decided that the original terminology will be used as presented in Wang and Cao (1994a,b, 1995) papers. Only the first word was changed from their original term “Anvil Width Ratio (AWR)” to “Die Width Ratio (DWR)” to be consistent with the terminology used in this work.

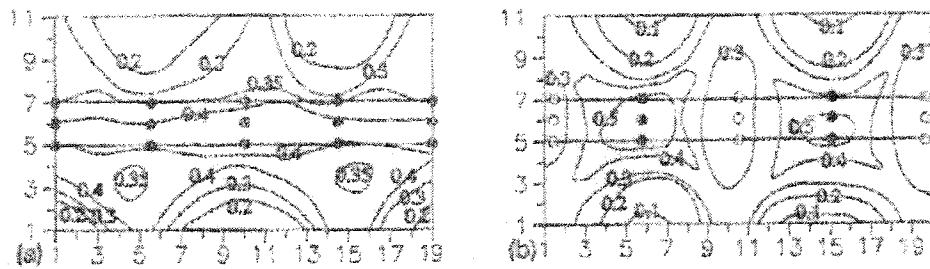


Figure 2.33: Effective Strain Distribution Forging Lead a) With Die Staggering b) Without Die Staggering (Wang and Cao 1994b)

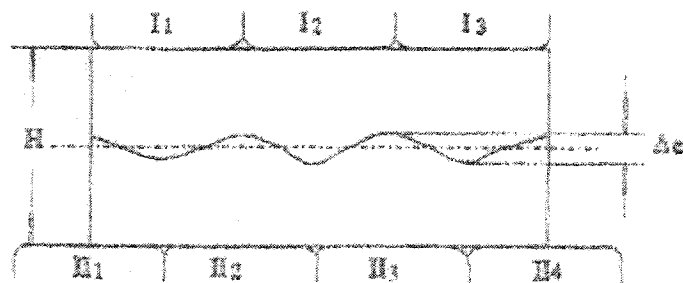


Figure 2.34: Schematic Diagram of the Deflection of the Center Line With 180° Turnover and Half Die Staggering Procedure (Wang and Cao 1994b)

manipulator position and is trained (through a training set) to predict the spread of the material, deformation resistance, and temperature as the material is being forged. The results of the training network showed that an absolute average error of 0.28 mm is to be expected in predicting spread ranging from 6 to 28 mm. They also executed finite element studies to investigate the forging conditions required for closing voids of about 10 mm radius inside the material.

Although their experiments did not have sufficient data to investigate the effect of the forging bite they concluded that the reduction ratio and the number of forging passes are the main controlling parameters in void closure (contradicting the majority of researchers (Siemer et al. 1986; Kiefer and Shah 1990; Dudra and Im 1990a; Wang and Cao 1994b,a, 1995) who concluded that the forging bite is the main controlling parameter for void closure). An issue with their work is that they cited few papers in their literature review on void closure in open die forging, in particular those mentioned above, which led them to miss the main controlling factor in void closure (forging bite and specifically the die width to height ratio (*DWR*)).

They then developed a scheduling algorithm that targets closing voids. The algorithm first calculates the maximum allowable reduction ratio that can be achieved on the press then from their finite element analysis study calculates the required number of paths to close the voids. Their scheduling algorithm distributes the reduction in height (known from the initial and required workpiece dimensions) on the number of paths. The neural network is then used to predict the forging parameters such as material spread and forging pressure for each forging pass. Their approach though novel is time consuming. A regression model will be much more precise than the neural network and will not require a large number of training sets as needed by the neural network. Regression models also give the scheduler more control on the shape of the function to be expected in estimating any of the forging parameters. Thus over training (a problem commonly encountered when using neural networks) could be avoided.

Dudra and Im (1990a,b) conducted physical and finite element experiments on void closure in cogging operations and found that V-shaped dies produce higher compressive strain in the center of the workpiece compared to flat ones. Tamura and Tajima (2003) used finite element analysis to study the effect of die radius on plastic strain distribution for a rough cogging operation. They concluded that flat dies with a small edge radius result in high strain at the center of the workpiece necessary to reduce any internal defect.

2.5 Predicting Material Spread and Elongation in Forging

Predicting spread has been perceived to be the key to developing a forging schedule. Spread is the result of conservation of matter. As the workpiece is squeezed along one dimension, it expands in other dimensions (Fig. 2.10). The effect of spread on a forging schedule is better explained by comparing the process to machining.

In machining the final workpiece geometry can be accurately predicted by subtracting the tool swept volume⁹ (Voelcker and Requicha 1977) from the workpiece geometry. Thus the final workpiece shape after each machining operation can be accurately predicted to be used by the schedule generation procedure.

In forging, determining the final workpiece geometry after a forging operation is not so straightforward. The tool indents the workpiece squeezing the material and forcing it to disperse in other directions. The material spreads in a manner that will minimize the total dissipated energy/work. The total dissipated work is the sum of the deformation work, work against friction and work dissipated in internal shearing. While a forging step sets a dimension in one direction, spread distorts the shape and alters the dimensions in other directions often resulting in the necessity to rework previously forged surfaces. Predicting part shape after each forging operation is thus far more difficult than in other operations like machining. This fact is aggravated when executing a forging schedule that necessitates frequent accurate updating¹⁰ of the workpiece shape between forging passes.

Spread is of random unpredictable nature, being controlled by a number of unknown factors such as friction, shearing on slip planes inside the material, temperature distribution, etc. It often happens that material piles in zones already forged by the die necessitating rework (e.g., (Fig. 2.35 a)). The deformation can have different shapes. It can have single (e.g., (Fig. 2.35 c)), double (e.g., (Fig. 2.35 b)) or multiple bulges¹¹. The shape of deformation depends on the depth of penetration of the plastic strain, which is controlled by the bite ratio, squeeze ratio, die width ratio, workpiece material and other forging parameters.

At the start of the forging operation the plastic strain propagates through the surface layers and the free surface of the material develops a

⁹Tool swept volume is defined by the intersection of the tool profile in the direction of the tool path with the workpiece.

¹⁰The updating of the workpiece shape in this case is performed by the spread prediction model.

¹¹Multiple bulges are commonly known as hourglass shape defect.

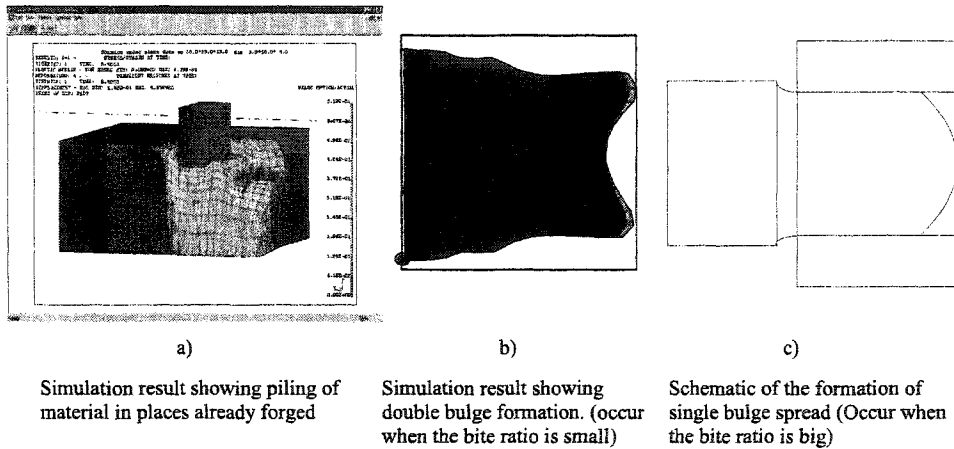


Figure 2.35: Illustration of Different Patterns of Material Spread

bulge at each contact surface between the die and the workpiece. The number of bulges is thus equivalent to the number of forging dies, which for the special case of cogging has double bulges. The center of the bulge location from the interfacial surface depends on the friction factors between the die and the workpiece (the lower the friction the closer the bulge to the contact surface) and the forging bite (the higher the bite the greater the penetration of the plastic strain and the longer the distance of the bulge center from the interfacial surface). As the die indents further into the workpiece the bulges move further toward the center of the workpiece and finally double bulges merge together into a single bulge.

Predicting spread in forging operations is still a task that needs more research. Current spread prediction formulae only apply to the simple case of flat tool cogging. Empirical, analytical, neural network and finite element models for spread prediction will be presented in what follows.

2.5.1 Empirical Models

Tomlinson and Stringer (1959), the most cited study on spreading in flat tool cogging, presented the *spread coefficient*, s , (ratio between the width to height strains), Eq. (2.1), as a valuable parameter to measure spreading. Knowing the initial and final workpiece heights, h_i and h_f , the spread coefficient is used to predict the final workpiece length, l_f , and the final workpiece width, w_f :

$$s = - \frac{\epsilon_w}{\epsilon_h} \quad (2.1)$$

$$l_f = \left(\frac{h_i}{h_f} \right)^{1-s} l_i \quad (2.2)$$

$$w_f = \left(\frac{h_i}{h_f} \right)^s w_i \quad (2.3)$$

In their study, empirical formulae for spread prediction were presented and the *bite ratio*, θ , (ratio between the bite and workpiece width) was identified as the main parameter affecting spread:

$$s = 0.29 - 0.16 \frac{h_f}{h_i} + 0.343 \theta - 0.048 \theta^2 \quad (2.4)$$

Tarnowski¹² presented one of the simplest yet effective empirical formula for predicting spread coefficient in upsetting and cogging operations, Eq. (2.5). Wisterich and Shutt (1959) used the Tarnowski formula for spread prediction in their analytical model to produce optimum cogging schedules for producing rectangular bars with flat tools:

$$s = \frac{\theta}{1 + \theta} \quad (2.5)$$

Shutt (1960) used plasticine to simulate hot forging of steel between rough flat dies. From his results he developed an empirical formula for spread coefficient prediction in such an operation:

$$s = \frac{\theta(1.789 - 0.321\phi)}{1 + \theta(1.789 - 0.321\phi)} \quad (2.6)$$

where $\phi = \frac{h_i}{w_i}$ is the shape factor.

Pahnke (1983) used the Forslund formula, Eq. (2.7), to predict side spread in flat tool cogging.

$$s = 1 - e^{C_1 \left(\frac{h_i}{w} \right)^{C_2}} \quad (2.7)$$

where C_1 and C_2 are material dependent constants that can be determined experimentally.

Wang and Cao (1995) argued that the Die Width Ratio, *DWR* (ratio between the bite and the original height of the workpiece) is the main parameter that controls the spread and that affect the deformation pattern. They tested 40 mm square test pieces with 60 mm length under different *DWRs* from which they developed an empirical formula for the spread:

¹²As reported in Tomlinson and Stringer (1959).

$$\beta = 0.5 + 0.3DWR \quad (2.8)$$

$$\alpha = 1 - \beta + 2\beta R(1 - 2R)(1 + 2\beta R) \quad (2.9)$$

where α is the spread rate $= \frac{\Delta w}{w_i} / \frac{\Delta h}{h_i}$, β is the elongation rate $= \frac{\Delta L}{L_i} / \frac{\Delta h}{h_i}$, Δw and Δh are the increase in width and reduction in height, R is the Squeeze Ratio $= \frac{\Delta h}{h_i}$

2.5.2 Analytical Models (*Upper Bound Models*)

There are essentially two analytical procedures of converging approximation in plastic deformation analysis: namely, the separate relaxation (in whole or in part) of either the kinematic or the statical boundary conditions and field equations. For elastic plastic solids with identical yield function and flow potential the relaxation of the statical boundary condition gives an upper bound solution for the deformation work while the relaxation of the kinematic boundary condition gives a lower bound of the deformation work (Hill 1963).

In forging a major concern is to determine the required press capacity to perform a given forging operation and as such the upper bound method was used to calculate an upper limit for the forging load needed. This mathematically attractive procedure is subject to the following restrictions (Hill 1963):

- The yield function must be convex and identical with the flow potential.
- The instantaneous shape of the considered body, together with the local yield functions at all points must be known in advance. This rules out many steady state forming processes that do not completely pre-determine the final dimensions, such as cogging.
- In the presence of any type of friction the method fails at least when the direction of relative sliding is not fixed by symmetry, and fails universally for Coulomb friction.
- The associated functional is often awkward to handle. In practice the method relies on rather artificial velocity fields giving a crude representation of the actual flow pattern.

Models based on the classical upper bound method for predicting spread simplified the modelling process by relaxing the statical equilibrium constraint. An arbitrary kinematically admissible velocity field is constructed in the deformation zone and is then used to calculate the dissipated work during deformation. This work is composed of the deformation work, work dissipated in internal shearing and work against friction.

Table 2.1: The Baraya and Johnson (1964) Material Dependent Spread Coefficient Values

Material	D	E	F	G
Annealed Lead	0.064	0.61	-0.37	0.079
Annealed Aluminum	-0.0060	0.75	-0.43	0.084
Half Hard Aluminum	0.136	0.18	-0.07	0.020

The chosen velocity field normally has some free parameter(s) describing its distribution. Those free parameter(s) can be assessed by minimizing the total work function. As the upper bound solution gives an upper bound for the work for any given velocity field the minimization of the work ensures that the solution is closer to the true solution.

Baraya and Johnson (1964) used an analytical velocity field and the concept of rigid sliding blocks for calculating theoretical upper bounds to the loads in flat-tool forging. They reported the specific forging pressure, coefficient of sideways spread, bulge profile, elongation and maximum amount of spread for various forging geometries from experimental work under the condition of sticking friction. They suggested empirical formulae for predicting spread for lead and aluminum, Eq. (2.10) with coefficient values given in Table 2.1. A special formula for cogging half hard aluminum, Eq. (2.11), was also presented.

$$s = D + E\theta + F\theta^2 + G\theta^3 \quad (2.10)$$

where D, E, F and G are material dependent spread coefficients.

$$s = 0.74 + 0.095\theta + 0.029\frac{B}{h_i} - 0.72\frac{h_f}{h_i} \quad (2.11)$$

Sagar and Juneja (1979) used the upper bound method to calculate the forging load required for flat tool indentation in a rectangular bar. Their model incorporated bulging of sides. A sinusoidal velocity field was assumed for both the length and width direction and a linear velocity field was assumed in the vertical direction. Their analysis included studying the effect of the friction factor where they found an increase in the required load with the increase of friction.

Li and Zhou (1989) proposed the upper bound element technique (UBET)¹³ and upper bound strip technique (UBST) for three dimensional plastic flow analysis. The deformation region is divided into a number of smaller strip elements where parallel linear velocity field is used within each element. Velocity discontinuity was assumed to occur only at the surfaces or interfaces between adjacent elements. Their model can be regarded as a special class of finite element analysis where a simple velocity field is assumed within each element and the overall response is computed by assembling all the elements together. All velocity components are taken as optimization parameters that are computed by minimizing the rate of energy dissipation (i.e., the classical upper bound approach).

The newly developed model was applied to study spread in flat tool cogging operations. The strip element's main axis was aligned to the side spread direction. The assembled response of the elements is then used to calculate the dissipated work. They performed several numerical experiments using the new technique which compared well with other published results and their main observation was that the shape factor ϕ controls the change from single bulge to double-bulge and noted that this generalization was contradicted by some of their experimental results¹⁴.

Aksakal et al. (1993, 1997) compared three classes of velocity fields for computing the side spread in flat tool center indentation in rectangular bars. In their analysis they assumed symmetric deformation in the three major axes of deformation thus only an octant of the deformation zone was analyzed. They compared a homogeneous pattern of deformation (uniform, rectangular deformation pattern) corresponding to a linear velocity field in the major deformation directions, a triangular deformation pattern, corresponding to a 2nd degree polynomial velocity field, and a parabolic deformation pattern corresponding to a 3rd degree polynomial velocity field, and found that the parabolic velocity field is the one that best represents the deformation pattern observed from experiments. They then recommended the use of the spread prediction corresponding to the parabolic deformation pattern in automatic generation of cogging schedules of rectangular bars.

Sagar and Juneja (1991) used the upper bound method to predict spread in upsetting a four sided irregular disc. They divided the irregular disc into three deformation zones composed of twelve triangles each of which deforms independently. They assumed sinusoidal velocity distribution in each

¹³UBET is used for preform design in closed die forging (Bramley 2001).

¹⁴Their experimental data was re-examined in this research using the die width ratio (introduced by Wang and Cao (1994a)), and it was found that as Wang and Cao (1994a) have concluded a *DWR* of 0.5 marks the transition from single to double bulge. This explained the instances of double bulge occurrence in their data that contradicted their shape factor theory.

triangle and developed an upper bound solution to define the deformation and calculate the required forging pressure.

Nye (1999) and, Osman and Ferreira (1999) used the upper bound method to predict side material spread in cogging rectangular bars with cylindrical dies. The main observation was that side material spread is much lower when using cylindrical dies than when using flat dies. This agrees with the observations of Ferreira and Osman (1997) who performed experimental studies using semi-circular dies for cogging operations and observed that the mode of deformation with such dies is predominantly in the longitudinal direction and that side spread is of minor value.

Hill (1963) proposed a variant of the upper bound solution, where one selects an arbitrary class of velocity fields satisfying all the kinematic conditions and then chooses from the considered class of velocity field that one that most nearly satisfies the statical conditions. Hill developed a formula, Eq. (2.12), for predicting the spread coefficient for cogging rectangular bars with flat dies. The model is applicable when the coefficient of friction is small and the cross section of the forged bar is nearly a square (shape factor $\phi \approx 1$).

$$s = \frac{1}{2} \left\{ 1 - \frac{1}{2\sqrt{3} \times \theta} \tanh(2\sqrt{3} \times \theta) \right\} \quad (2.12)$$

Lahoti and Kobayashi (1974) modified Hill's formula for spread prediction to accommodate for friction. The predictions of spread, elongation and bulge compared well with experiments with small to medium bites for nearly square bars. However, for large bites and for bar shapes far from square the correlation between theory and experiments was unsatisfactory.

Braun-Angott and Berger (1982) modified Hill's formula for spread prediction to be applied for situations with sticking friction and for cogging rectangular bars with shape factor far from unity. They used a simple velocity field to calculate the spread. The admissible velocity field varied linearly with the width and polynomially in the length and height directions to accommodate for bulging and barrelling. They used nonlinear programming to search for the value of the free parameters of the velocity fields that minimize the work function and concluded that the effect of friction can be neglected for the range of parameters valid for forging presses.

2.5.3 Finite Element Models

Finite element models are not limited by specific forging operations and generally provide accurate results. For example Sun et al. (1983) developed finite element models, based on a rigid plastic material model, to study flat tool indentation and flat bar cogging. Their results showed excellent agreement

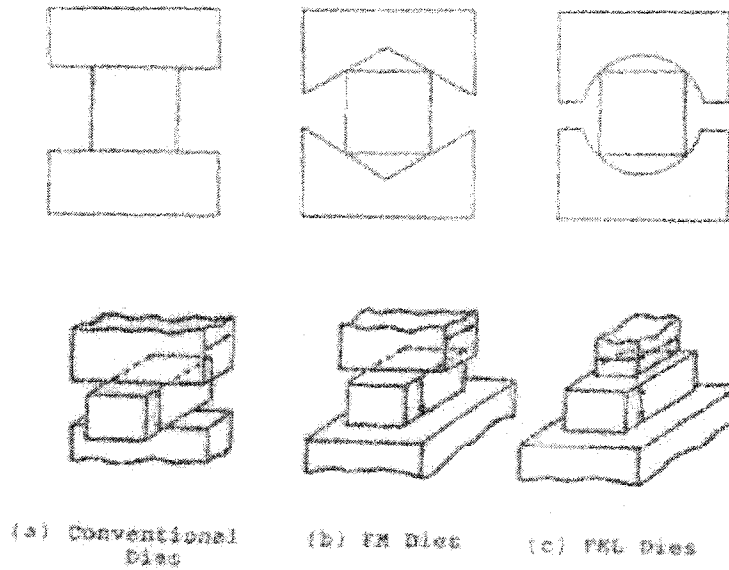


Figure 2.36: Different Die Arrangements for Open-Die Forging (Kiefer and Shah 1990)

between finite element results and experimental observations. Nevertheless, finite element models are unsuitable for online adaptive scheduling of forging processes due to the long time required to build and execute the model. A typical simulation run for a single flat tool cogging operation took 15 min to simulate on a 1.3 GHz AMD processor (Elbadan and Nye 2003).

Kiefer and Shah (1990) developed finite element models, based on a rigid plastic material model, to study cogging of rectangular bars with conventional dies (flat, V-shaped and circular-shaped) and Free from Mannesmann dies (Fig. 2.36). The simulation results showed that for conventional forging with flat dies the stress state changes from tension in one direction and bi-axial compression in the other two to triaxial compression for DWR s greater than 0.654. It was also observed that the maximum longitudinal strain was associated with a DWR of 0.654. FM and FML dies are used to provide better center line consolidation than conventional ones. This fact was not clearly shown by the simulation results while the width strain (side spread) was higher for FML dies than conventional ones.

Hung and Kobayashi (1992) developed finite element models, based on a rigid plastic material model, to study the effect of cogging with flat and V shaped dies working individually or combined on longitudinal and side spread for cylindrical bars (Fig. 2.37). Their study showed that using double V dies

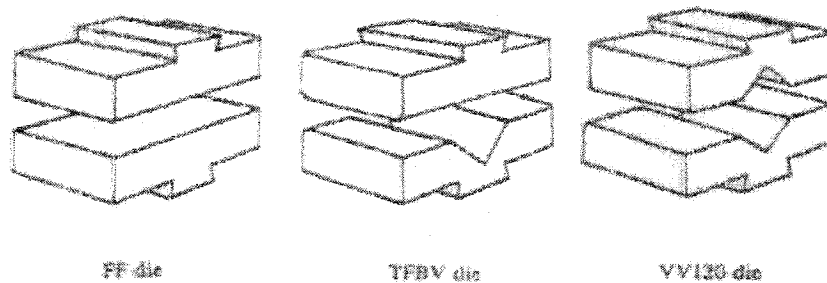


Figure 2.37: Die Configurations (Hung and Kobayashi 1992)

with large included angle provide high centreline deformation and the highest longitudinal spread. A flat top and V bottom die configuration resulted in the best homogeneity and smallest longitudinal spread. This configuration is thus recommended for shaping the cross-sectional shape of the workpiece rather than drawing it out. The conventional top flat bottom flat dies configuration required the smallest forging force and is thus recommended for working with limited press capacity.

Other general purpose forming simulation packages were presented in the literature. Rodrigues et al. (1994) presented the Plast3 package for simulating open die forging processes. The finite element models, based on a rigid plastic material model was used to simulate FM forging of aluminum alloy. The results compared well to physical experiments and the package was used to predict the required load to perform the forging operation along with the strain and stress distributions and an estimate of the bending of the workpiece under different reduction ratios. Wu et al. (1994) presented DEFORM as a general purpose package capable of performing 3D analysis of open die forging processes. It was also capable of interfacing with other pre and post processor packages.

2.5.4 Neural Network Models

Melligeri and Lilly (1994) and Lilly and Melligeri (1996) proposed using neural networks for closed loop compliance control for an automated open die forging cell. The automated open die forging cell is composed of a forging press, a robot for workpiece handling and force sensors and a compliance controller for the robot. The control circuit (Fig. 2.7) utilizes force measurement at the robot gripper. The neural network is used to compute the gripper displacement associated with those forces. An inverse kinematic transformation is then used to calculate the required joint movements to compensate for the displacement

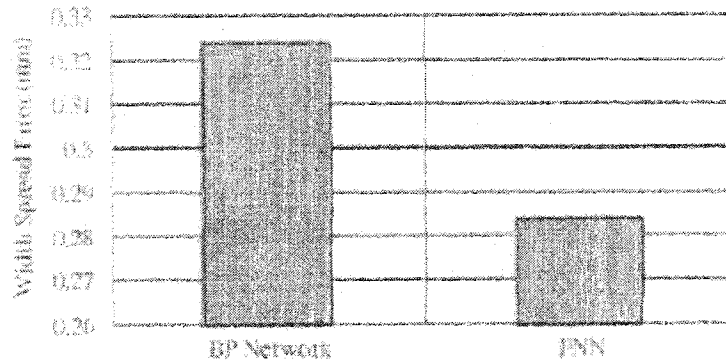


Figure 2.38: Performance Comparison Between Functional Neural Network and Back-Propagation Network, (Kim et al. 2002)

at the gripper end. They conducted numerical studies to test the performance of their proposed control cell using back-propagation neural networks with two hidden layers composed of 30 and 20 neurons. Their simulation studies showed that the control circuit can be effectively used for robotic compliance control and the reduction of reaction forces at the end gripper of the robot.

Kim et al. (2002) used functional neural network (FNN) to predict the width spread in billet to bar forging. The network input variables were the height, width, squeeze ratio, bite and temperature and was then trained to predict the spread value. Functional neural network has the advantage of adding higher order terms without adding joint activations in the design phase of the network. This enables the network to predict the spread with higher accuracy compared to other networks such as the back-propagation network (BPN) (Fig. 2.38).

2.5.5 Closure

Empirical, analytical, finite element and neural network models has been developed to predict side material spread in cogging operations. Table 2.2 summarises most of the closed form spread prediction formulae. The majority of the developed models are used for flat tool cogging. Experimental and finite element models suggest that side material spread can be reduced by: reducing the bite, or using V shaped or radiused dies. A *DWR* greater than 0.6 is required to eliminate the hourglass defect.

Nye et al. (2001) compared several analytical and empirical formulae with online measurement of the spread for flat tool cogging, and concluded

Table 2.2: Spread Predicting Formulae

Source	Type	Model
Tarnowski (1950)	Empirical	$s = \frac{\theta}{1+\theta}$
Tomlinson and Stringer (1959)	Empirical	$s = 0.29 - 0.16\left(\frac{h_f}{h_i}\right) + 0.343\theta - 0.048\theta^2$
Shutt (1960)	Empirical	$s = \frac{\theta(1.789-0.321\phi)}{1+\theta(1.789-0.321\phi)}$
Hill (1963)	Analytical	$s = \frac{1}{2} \left\{ 1 - \frac{1}{2\sqrt{3}\times\theta} \tanh(2\sqrt{3} \times \theta) \right\}$
Baraya and Johnson (1964)	Empirical	$s = D + E\theta + F\theta^2 + G\theta^3$ <i>For half-hard Aluminum</i> $s = 0.74 + 0.095\theta + 0.029\frac{E}{h_i} - 0.72\frac{h_f}{h_i}$
Forslund formula (Pahnke 1983)	Empirical	$s = 1 - e^{C_1 \left(\frac{h_f}{w}\right)^{C_2}}$ C_1 and C_2 are material constants
Wang and Cao (1995)	Empirical	$\alpha = 1 - \beta + 2\beta R(1 - 2R)(1 + 2\beta R)$ where $\beta = 0.5 + 0.3DWR$

that spread prediction formulae are imprecise with limited scope of application (flat tool cogging), rendering them inadequate for forging schedule generation. They recommended online spread measurement when forging parts.

Neither finite element models nor neural networks models are suitable as spread prediction models to be used in online adaptive schedule generation for flexible forging cells. Finite element models are custom built for specific forging operations, and require considerable time to build, run and analyze. Much the same, neural network models are custom built for specific forging operations. They also require an extensive set of data, collected from experimental or finite element studies, to train them. In addition, they can not easily include prior knowledge¹⁵ of the expected shape or type of relation between the dependent (spread parameter) and independent (bite, reduction, etc.) variables in the neural network model.

2.6 Technological Bounds on the Forging Schedule

Technological bounds set an upper or lower limit on the quantitative values of the scheduling parameters. The most common technological bound is the press capacity. The open die forging industry is typically working with large-scale products; higher capacity is always appreciated. Other technological bounds are simple constraints to prevent defect formation, such as: central bursts; suck-backs; overlaps, buckling and other geometric distortions

¹⁵Such knowledge could be based on experience or from published research in the subject area. In contrast, such knowledge can be easily incorporated in a regression model.

(Fig. 2.39). Those defects are by far more pronounced in internal profiling than in external profiling.

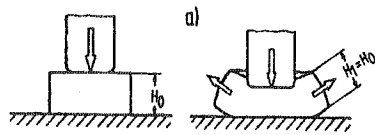
The most influential forging parameters are the bite ratio, θ , and the die width ratio, DWR (the ratio between the bite and the height of the workpiece). The bite ratio has a direct effect on the spreading of the material and on lap formation. Generally, the smaller the bite the lower the spread but the more likely a lap will be formed, and vice versa. The DWR , however, affects the penetration of the plastic strain to the center of the material. A large DWR results in better penetration of the plastic strain and elimination of internal defects with a single bulge formation. On the other hand, a small DWR results in lower depth of penetration of the plastic strain and the formation of double bulge on the free surface of the workpiece.

Shutt (1963) studied different stability operating regions for the forging operation. His study included making physical models of plasticine and steel. Table 2.3 summarizes his results for safe working zones. He also studied the effect of flat die edge-radius, edge-chamfer and the use of bevelled dies on lap formation. He concluded that lap formation can be significantly reduced using either edge-radiused or chamfered dies. This facilitates the use of lower bite ratios (necessary to forge minute details), as the probability of lap formation is inversely proportion to the bite ratio (the lower the bite ratio the more likely a lap will form).

Wang and Cao (1994b), contrary to Shutt (1963), attributed the hour-glass effect to the DWR . They experimentally found that a DWR of 0.5 marks the transition from tensile to compressive stress at the center of the workpiece. They recommended a DWR of 0.6 to avoid the hourglass effect and maintain better penetration of the plastic strain. Their conclusion was confirmed by re-examining Li and Zhou (1989) results, who, like Shutt (1963), attributed the transition to the effect of the shape factor, contradicting some of their own observations. Ettouney and Stelson (1990) developed a model to predict foldover for simple upsetting of cylindrical workpieces, while Narayanasamy and Pandey (2000) studied barrelling of the sides.

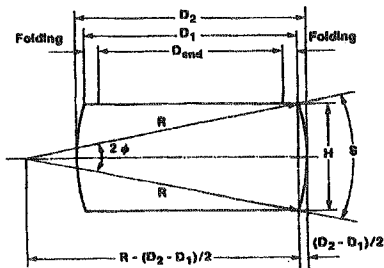
Teti et al. (1999) used a neural network to test the feasibility of forging schedules for a stepped shaft forging operation. A schedule is examined by the neural network and if feasible is chosen for implementation. The ability of the developed neural network to successfully identify feasible schedules was demonstrated for a case of forging a stepped shaft having five different diameters. Three forging operations could be applied on the workpiece: upsetting, cogging, and closed die forging.

The neural network was trained by a set of feasible and infeasible solutions generated with the use of a rule based expert system. Typically the training set was composed of 138 feasible schedules and 822 infeasible ones.



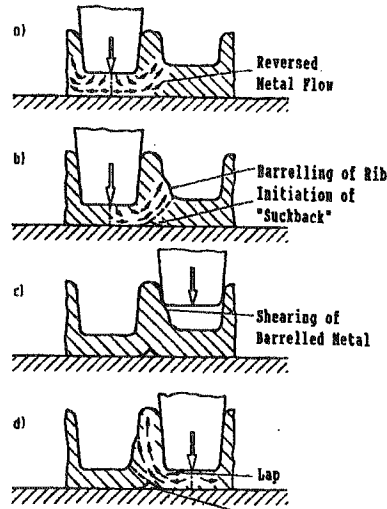
a) Bending Distortion

Welschhof and Kopp (1989)



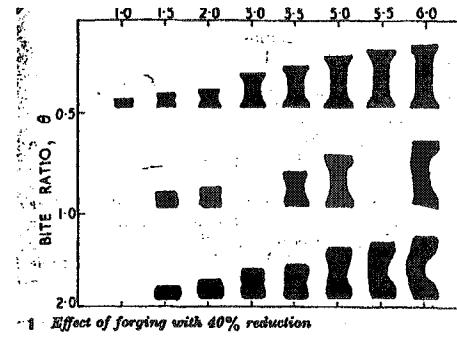
b) Foldover and Bulging

Etouney and Stelson (1990)



c) Suckback and Laps

Welschhof and Kopp (1989)



d) Buckling

Shutt (1963)

Figure 2.39: Forging Defects

Table 2.3: Technological Bounds due to Shutt (1963)

Constraint Name	Controlling Parameter	Parameter value	Minimum Allowable Bite Ratio (θ_{min})
Hourglass Shape limit (changing from single to double bulge)	Shape Factor (ϕ)	1.0-1.5	0.5
		1.5-2.5	1.0
		2.0-3.0	2.0
Lapping limit	Shape Factor (ϕ)	1	0.35
		1.5	0.52
		2	0.73
		ϕ	$\theta_{min} = \frac{1}{2.63} \times (\phi - 0.11)$

The network was able to identify if a given schedule is feasible or not with a success rate of 94%. The authors suggested that this procedure can be used as a first cut procedure to determine if a suggested schedule is feasible or not.

2.7 Feedback Systems in Metal Forming

The use of process shape feedback is the key to a successful adaptive scheduling algorithm. It overcomes the complex task of accurately predicting the flow of the forged material. Process control and programming complexity in metal forming operations is simplified while part shape accuracy is improved.

Traditional implementation of feedback control in metal forming was either concerned with avoiding overstressing of the forging equipment or improving the positioning precision of the forging equipment. Appleton et al. (1979); Lilly and Melligeri (1996); Aksakal et al. (1997); Ferreira and Osman (2000) suggested using feedback for compliance control of the robot positioning to compensate for accumulated positioning errors and unpredictability of workpiece material spread. Thomas and Tomlinson (1966) suggested the use of feedback to coordinate the operation of various equipment of the forging cell.

Hardt (1993) was the first to suggest controlling the generation of the forming schedules through a control process that utilizes shape feedback. In his paper he described how process feedback in a sheet bending operation could compensate for variations due to material thickness and yield strength. Shape feedback has also been used to simplify forming 3-D sheet metal panels using a reconfigurable die with a programmable surface (Hardt 1993; Walczyk et al. 1998; Walczyk and Hardt 1998; Walczyk et al. 2003). The die is first

set to the desired part shape and the panel is formed. It often occurs that the panel's shape mismatches the required shape due to material springback. Shape error is measured and used to readjust the die shape and the panel is pressed again. The process has been found to rapidly converge to the desired shape without prior planning for springback compensation while at the same time compensating for random fluctuations in process conditions.

2.8 Summary

- Of the two major approaches to develop flexible forging systems, automating the open die forging process promises to be more flexible and is therefore the one chosen.
- Automating open die forging cells relies on developing new schedule generation procedures.
- Cited forging schedule generation procedures are limited to cogging uniform cross-section beams with flat or radiused dies and relies on predicting the deformed shape of the workpiece using spread prediction models.
- Current spread prediction models are applicable to limited configurations and produce low quality estimates.
- Feedback systems has been reported to successfully generate sheet metal forming schedules without the need for accurate prediction of the deformed sheet shape between successive forming operations. This will be the main approach implemented in this study.
- Few studies were conducted to define the safe operating limits of the forging parameters (Technological bounds).
- The majority of research on open die forging pertains to cogging operations.
- The majority of the literature on open die forging targets enhancing the internal structure of the forged parts while few studies have been cited on the resultant dimensional and geometrical accuracies.
- Few studies were conducted on internal profile generation on open die forging cells.

Chapter 3

General Structure of the Incremental Forging Cell

The hardware configuration of the flexible forging cell is composed of a numerically controlled press, a robot for workpiece manipulation, a main supervisory computer and a vision feedback system (Section 3.1).

The general operation plan of the forging cell is composed of a process planning module, tool selection module, detailed scheduling module (forging schedule module) and shape feedback module (Section 3.3). The process planning module (Section 3.3.1) is assigned the task of generating an aggregate plan to forge the part in which the workpiece shape is broken down to a set of consecutive features. Portions (volumetric regions) on the unforged workpiece are then allocated to forge each of those features. A detailed forging schedule (Section 3.3.5) is then generated to forge each individual feature for which appropriate tools are selected to execute the schedule (Section 3.3.2).

The detailed forging schedule generation (the control procedure of which is presented in Section 3.3.3) can either depend on predicting the instantaneous shape of the workpiece using spread prediction models (Section 3.3.5) or on capturing the instantaneous shape of the workpiece by a shape feedback system (Section 3.2). In either case the forging schedule uses the shape error (Section 3.3.4) to plan the forging step. After the forging step is executed on the cell the schedule generation module either re-estimates or re-captures the new instantaneous workpiece shape to plan the following forging step. This control process iterates until the workpiece is forged to within the required tolerance. Technological bounds and other supporting knowledge bases necessary for the operation of the detailed forging schedule module are presented in Section 3.3.5.

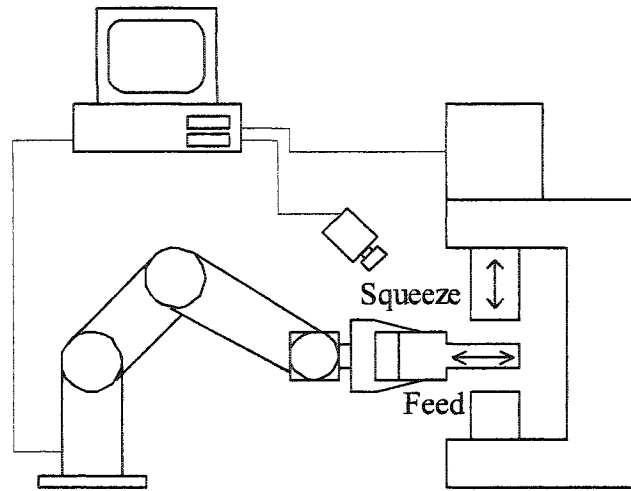


Figure 3.1: Flexible Manufacturing Cell Layout for Forged Metal Parts

3.1 Incremental Forging Cell Hardware Configuration

The configuration of the implemented flexible forging cell is based on an open-die forging architecture. This configuration has been implemented / recommended by numerous researchers aiming to develop a flexible forging system¹ (Schey and Abramowitz 1973; Appleton et al. 1979; Lilly and Jablolkow 1995; Aksakal et al. 1997; Ferreira and Osman 1999; Nye et al. 2001).

The forging cell is composed of a numerically controlled instrumented 2 GN hydraulic press; a six-axes Kawasaki JS10 robot for workpiece manipulation; a control PC that coordinates press and robot motions and generates adaptive schedules to forge the part; and a workpiece shape vision feedback system to capture the instantaneous workpiece shape (Fig. 3.1). The incorporation of shape feedback has not been implemented before and is based on Appleton et al. (1979) and Nye et al. (2001) conclusions that shape feedback is essential to compensate for the unpredictability of material spread during forging.

¹For different configurations of flexible forging cells refer to Section 2.2.

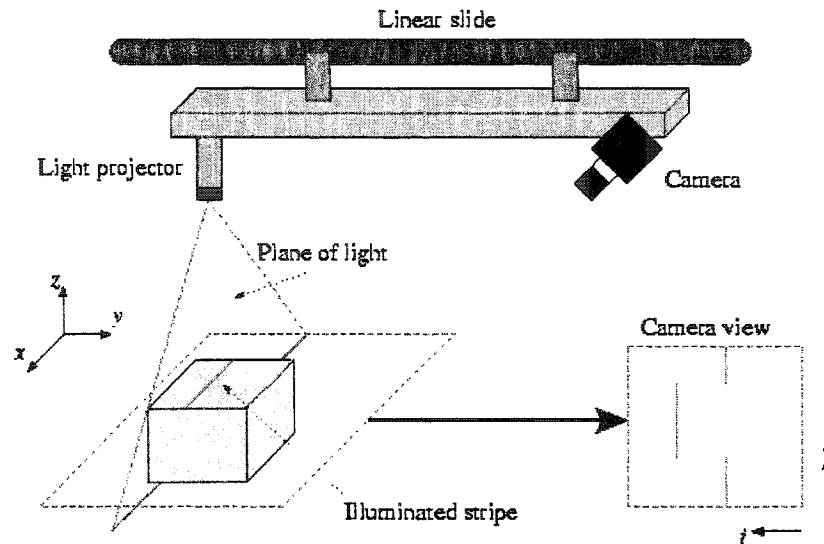


Figure 3.2: Structured Light Vision System Principle (Park et al. 2001)

3.2 Structured Light Vision Feedback System

The structure of the vision feedback system is shown in Fig. 3.2. It is constructed of a red laser projector that is calibrated to project a beam of $100 \mu\text{m}$ width at a distance of 15 cm from the object, and a digital camera with an infrared filter attached to the lens. The workpiece is held before the camera by the robot. The captured image is then processed by the main computer where successive sections of the workpiece are measured and used to construct a solid model of the workpiece.

Calibration of the Vision System

The calibration process is performed using the method described by Chen and Kak (1987) with the modified formulation described in Park et al. (2001). In this method a simple pinhole model is used for the camera and the lenses. A calibration matrix is used to map the (row, r ; column, c) positions of the captured image to their real world positions (x, y, z) through intermediate transformation to a homogeneous coordinate system $(\bar{x}, \bar{y}, \bar{z}, \rho)$. The calibration matrix and the transformation equations from the captured (r, c) image position to the world coordinate (x, y, z) are:

$$\begin{bmatrix} t_{11} & t_{12} & t_{13} \\ t_{21} & t_{22} & t_{23} \\ t_{31} & t_{32} & t_{33} \\ t_{41} & t_{42} & 1 \end{bmatrix} \begin{bmatrix} r_i \\ c_i \\ 1 \end{bmatrix} = \begin{bmatrix} \bar{x}_i \\ \bar{y}_i \\ \bar{z}_i \\ \rho \end{bmatrix} \quad (3.1)$$

$$\begin{bmatrix} x_i \\ y_i \\ z_i \end{bmatrix} = \begin{bmatrix} \frac{\bar{x}_i}{\rho} \\ \frac{\bar{y}_i}{\rho} \\ \frac{\bar{z}_i}{\rho} \end{bmatrix} \quad (3.2)$$

where,

t_{ij} are the coefficients of the calibration matrix.

r_i, c_i are the row and column positions of the i^{th} calibration point.

$\bar{x}_i, \bar{y}_i, \bar{z}_i, \rho$ are the homogeneous coordinates of the i^{th} calibration point.

x_i, y_i, z_i are the world coordinates of i^{th} calibration point.

Using Park et al. (2001) rearrangement the calibration matrix coefficients can be assessed using n calibration points as follows:

$$\begin{bmatrix} RC & 0 & 0 & RCX \\ 0 & RC & 0 & RCY \\ 0 & 0 & RC & RCZ \end{bmatrix} \begin{bmatrix} t_{11} \\ t_{12} \\ t_{13} \\ t_{21} \\ t_{22} \\ t_{23} \\ t_{31} \\ t_{32} \\ t_{33} \\ t_{41} \\ t_{42} \end{bmatrix} = \begin{bmatrix} x_1 \\ x_2 \\ \cdot \\ \cdot \\ x_n \\ y_1 \\ y_2 \\ \cdot \\ \cdot \\ y_n \\ z_1 \\ z_2 \\ \cdot \\ \cdot \\ z_n \end{bmatrix} \quad (3.3)$$

where,

$$RC = \begin{bmatrix} r_1 & c_1 & 1 \\ r_2 & c_2 & 1 \\ \cdot & \cdot & \cdot \\ \cdot & \cdot & \cdot \\ r_n & c_n & 1 \end{bmatrix} \quad (3.4)$$

$$RCX = \begin{bmatrix} -r_1x_1 & -c_1x_1 \\ -r_2x_2 & -c_2x_2 \\ \cdot & \cdot \\ \cdot & \cdot \\ -r_nx_n & -c_nx_n \end{bmatrix} \quad (3.5)$$

$$RCY = \begin{bmatrix} -r_1y_1 & -c_1y_1 \\ -r_2y_2 & -c_2y_2 \\ \cdot & \cdot \\ \cdot & \cdot \\ -r_ny_n & -c_ny_n \end{bmatrix} \quad (3.6)$$

$$RCZ = \begin{bmatrix} -r_1z_1 & -c_1z_1 \\ -r_2z_2 & -c_2z_2 \\ \cdot & \cdot \\ \cdot & \cdot \\ -r_nz_n & -c_nz_n \end{bmatrix} \quad (3.7)$$

A minimum of four calibration points are required to construct the calibration matrix. Five pins were attached to a board and placed in the view of the vision system. The world coordinates of the pins were used to calibrate the vision system where the mid point of each pin image was used. Figure 3.3 shows the location of the five pins on the image matrix as captured by the camera.

A block gauge was then used to determine the scatter and speckle error of the vision system (Fig. 3.4). The scatter error was estimated to be 1.1 mm for the rough data and 0.1 mm for the smoothed data². Based on experimental trials, the assembled vision system coupled with the iterative smoothing procedure can be confidently used to measure dimensions to within 0.5 mm. Calibration³ using gauge blocks resulted in an error of 0.23 mm.

The workpiece outer surface is then constructed from the vision system measured data. The assembly is performed by matching reference points on each measured surface. The assembled solid model is then used by the error algorithm to compute the shape difference between the instantaneous workpiece shape and the required one.

²Smoothing is performed by an iterative moving average procedure where the average of the nearest n points are used for m number of iterations.

³Two gauge blocks with a difference in height of 1 mm were used in the calibration.

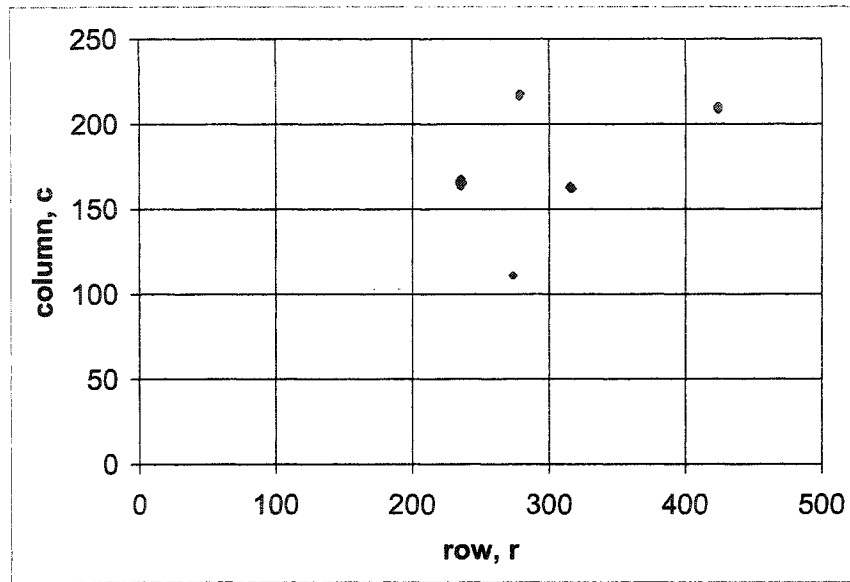


Figure 3.3: Vision System Calibration Image

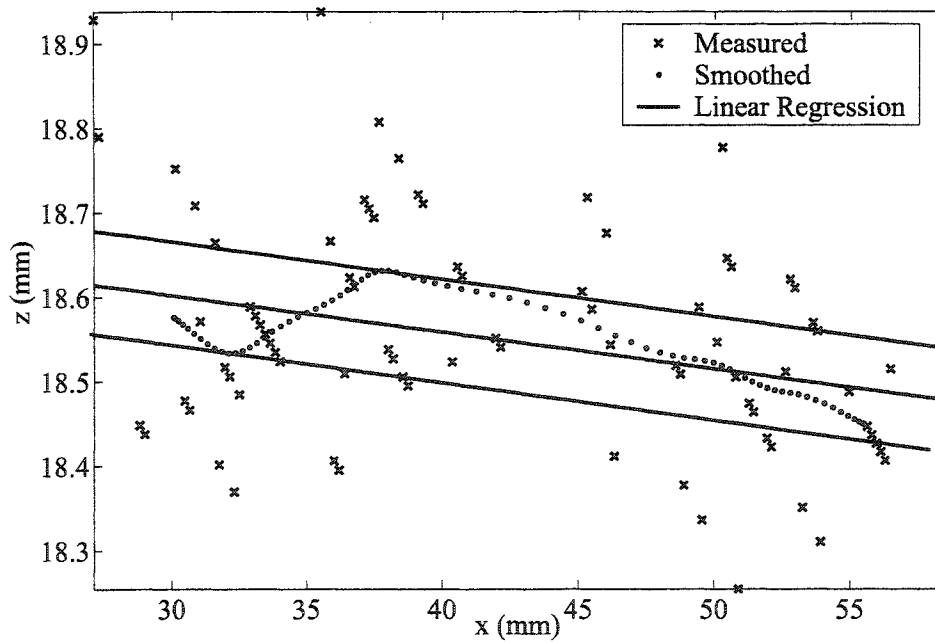


Figure 3.4: Scatter Error Assessment Using Blockgauges

3.3 Incremental Forging Operation Plan

Figure 3.5 presents the general operation plan for the flexible forging cell. The operation plan is composed of a process planning module (A1), tool selection module (A3), forging schedule module (A4) and a feedback module (A6).

The inputs to the process plan module (A1) are the initial and required workpiece shapes and the required tolerance grade. The process planning module then generates an aggregate forging schedule (henceforth referred to as the process plan) in which the workpiece is divided into a set of features, each to be generated by a forging operation. The process plan also specifies the operations execution sequence.

Appropriate forging tools are then selected and a detailed schedule (henceforth referred to as the forging schedule, or, in short the schedule) is generated by the forging schedule module (A4) to execute each individual operation. Candidate schedules are tested for feasibility on a virtual forging cell⁴ and one is selected for execution. A feedback system (A6) captures the instantaneous shape of the workpiece as it is being forged and the schedule is adaptively changed to compensate for any unpredictable shape changes. The shape control process is executed iteratively until the geometric and dimensional tolerances are met.

3.3.1 Process Plan (A1) and Operation Selection (A2)

In this study the process plan is defined as the sequence of operations used to generate multiple features on the workpiece. The objective of the process plan is to decompose the overall forging process into a number of basic operations. Each operation is performed by applying a series of tool paths composed of a series of squeezing actions along the forging feed direction. The process plan specifies the operations execution sequence based on the operation precedence technological constraints.

At this aggregate-level (process planning level) the raw material volume is divided into zones, each zone is assigned to produce a specific feature on the workpiece. Features are classified into either internal or external profile and appropriate tools are then selected based on the feature class, dimensional and geometrical attributes. It is the responsibility of the process planner to divide the required shape into a set of consecutive features specified in the required shape solid model. The raw material volume is then automatically divided into zones, each zone is assigned to produce a specific feature.

Few studies have been conducted on internal profiling, most likely due to the unpredictable nature of material spread in such operations. Forging

⁴The virtual forging cell is presented in Section 3.4.

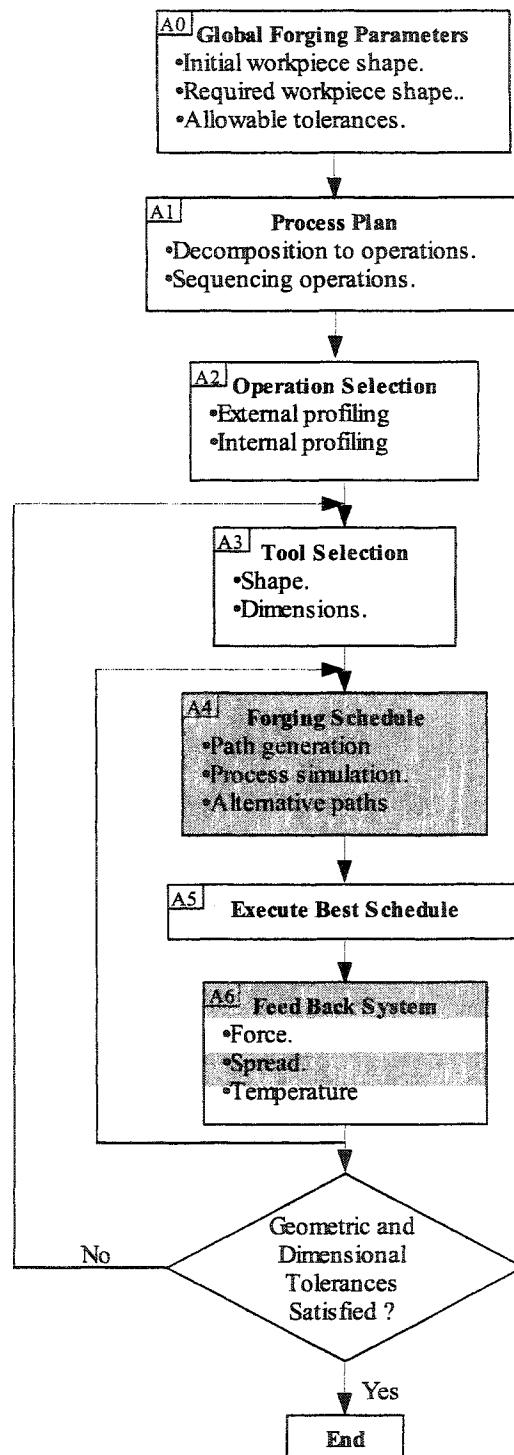


Figure 3.5: Incremental Forging Operation Plan (Shaded Areas are the Focus of This Research)

defects, especially lap formation, are also more pronounced in internal profiling adding a new degree of complexity in studying such operations. Lack of research on the internal profiling process and the complexity of material spreading are the main obstacles in studying internal profiling. No work was cited to predict spreading for an internal profiling operation.

For those reasons and from preliminary experimental studies on internal profiling⁵ it has been decided that generating schedules for internal profiles is out of the scope of this research.

Generating schedules for external profiles, however, has a lower degree of complexity as the majority of the literature on open die forging describes cogging operations (regarded in this research as the fundamental external profile generation operation). Yet generating forging schedules for external profiles is also hindered by the lack of models that predict spread in its general form⁶, (i.e. spread in all degrees of freedom not just side material spreading as been presented in the literature). This research will focus on generating schedules to forge external profiles on the incremental flexible forging cell.

3.3.2 Tool Selection (A3)

How the design of the forging die affects metal flow is still an open area for research. Some attempts to explore alternative forging die designs to the classical flat die were made, but they are not nearly sufficient. Benson and Hunt (1961); Johnson and Tomlinson (1966); Reddyhoff (1982) presented a variety of tools used for heavy forging operations. The majority of the cited literature pertains to flat tool forging as they are used to forge a variety of products. In this study flat dies will be used for the flexible forging cell.

3.3.3 Forging Cell Shape Feedback Control (A6)

Implementing feedback control is a key element proposed by this research to overcome the problems involved in accurately predicting material spread under the die. The benefits are expected to be that control and programming complexity will be greatly simplified while part shape accuracy will be improved.

⁵Several experiments on internal profiling were conducted using lead as modelling material. Unfortunately the lapping defect could not be prevented using various shapes of forging dies. It was concluded that incremental internal forging will always lead to lapping. Lapping in most of the experiments was so severe that the material did not deform at all and was only sheared and pressed under the forging die. This is similar to a machining process where the chips are cut and then pressed on the finished workpiece surface.

⁶Refer to Section 2.5 for patterns of material spread and for available spread prediction models (all are developed for cogging operation, especially the flat-tool cogging one).

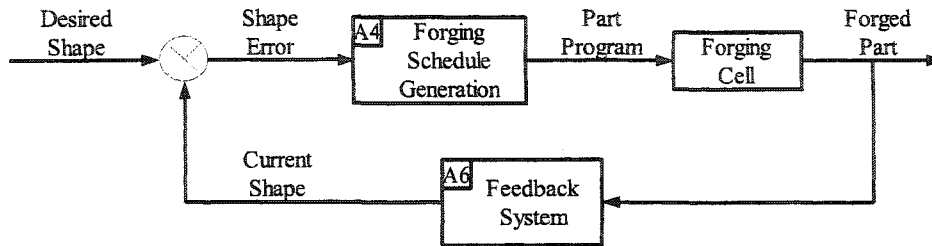


Figure 3.6: Control Schematic of the Forging Cell

Figure 3.6 presents a simplified control circuit for the cell operation. The instantaneous workpiece shape, as captured by the feedback system, and the desired shape are used to compute the shape error. A forging schedule, composed of several forging steps, is adaptively generated to reduce this error. After each forging step the shape error is reevaluated and the cycle iterates until the workpiece shape is within tolerance. An estimate of the spread, from the spread prediction knowledge base, can be used to improve the quality of the forging schedule, which should reduce the number of steps required to converge to the desired shape.

3.3.4 Error Computation Algorithm

Forging Cell Coordinates and Degrees of Freedom

The forging cell has four degrees of freedom (translation in x , y and z directions and rotation around the x axis) (Fig. 3.7). The press applies the squeezing action along the z axis while the robot is programmed to position the workpiece between the dies along the x and y axes and to rotate the workpiece in 90° increments around the x axis, if required. However, this study is concerned with generating external profiles using forging dies that extend beyond the workpiece in the lateral (y) direction and as such the operating degrees of freedom of the forging cell are reduced to three (translation in x and z directions and rotation around the x axis). Three main types of operation can be carried out on the flexible forging cell. The workpiece can be: a) incrementally squeezed along its height; b) incrementally squeezed along its width, and; c) occasionally if the length exceeds the tolerance limit an upsetting operation is applied (Fig. 3.8).

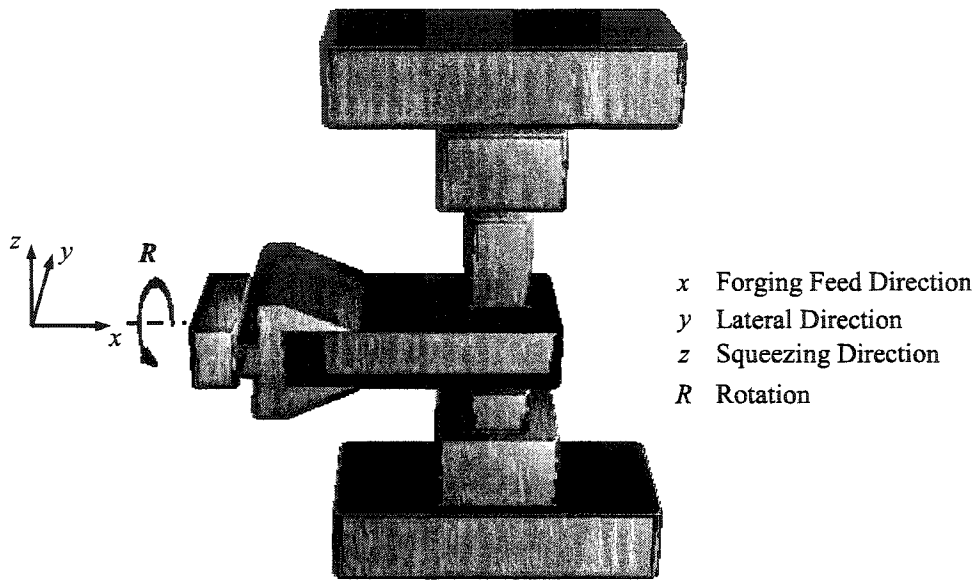


Figure 3.7: Forging Cell Coordinates

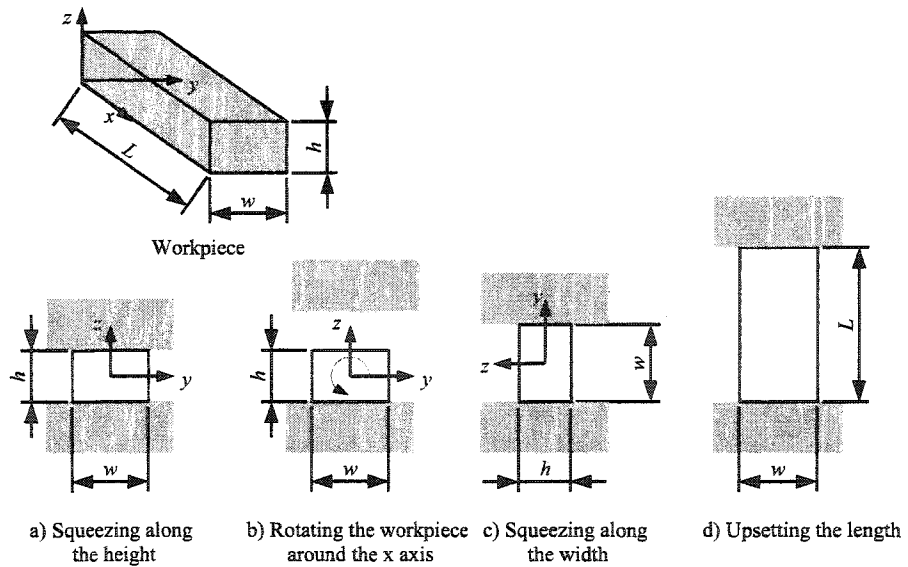


Figure 3.8: Types of Operations that Can Be Performed on the Cell

Shape Error Representation

The forging cell can forge the workpiece along its three local principal axes: height, width and length. To simplify the schedule generation process the vectorized shape difference⁷ (henceforth termed the shape error) will be computed along the three principal axes (length (x), width (y) and height (z)).

To illustrate how this type of error representation will simplify the schedule generation consider the case where the shape error in the width direction is +3 mm, then the corrective action would be to squeeze the width by 3 mm which can be accomplished by rotating the workpiece 90° then performing the squeezing operation (Fig. 3.8 a-c).

It is interesting to note that only positive (+ve) errors can be directly corrected by the forging operation while negative (-ve) errors are only indirectly corrected. Forging is carried out at the position of the (+ve) errors, the squeezing action redistributes the material and due to the constancy of volume it indirectly corrects (-ve) errors in other positions on the workpiece.

It must also be noted that the definition of the term error is stretched in this context as the workpiece only assumes its final shape at the final stage of the forging process. As forging progresses the workpiece is transformed to a number of intermediate shapes some of which might have little resemblance to the required shape.

To illustrate this statement, assume that a product of a rectangular cross-section and a monotonically decreasing height will be forged from an initial brick-shape billet (Fig. 3.9). The initial billet is chosen taller in height and shorter in length so that it can be systematically drawn out to the required shape. It is clear that the intermediate shapes of the forged billet are not even of the same class as the required final shape. It can also be seen that the profiles of the instantaneous and final shapes have different domains (the domain is the x , y , and z ranges on which the profile is defined). For this reason the vectorized shape error (the error components in the x , y and z directions) is computed at the intersection between the domains of the instantaneous and final shapes. This approach allows both the instantaneous and final shapes to be defined when computing the error.

General Requirements Of The Error Computing Algorithm

Development of the error algorithm must consider the following issues:

1. External profiles are considered in this study where the forging dies extends beyond the workpiece in the lateral (y) direction and as such the

⁷The shape difference is the difference between the instantaneous workpiece shape and the required shape.

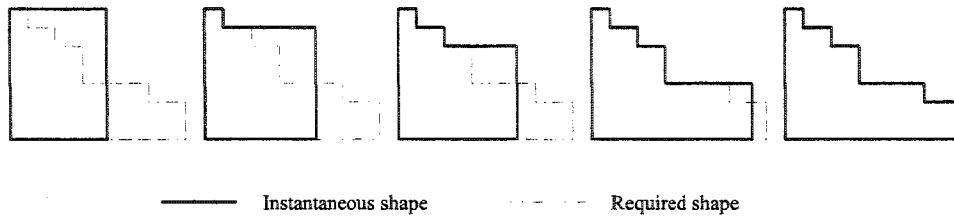


Figure 3.9: Instantaneous vs Required Forged Shapes of a Sample Workpiece

degrees of freedom of the cell is reduced to three: squeezing, feeding and rotation.

2. Only the outer surface is required to model the workpiece shape.
3. The forging cell can squeeze the workpiece height or width or upset its length (Fig. 3.8).
4. The vectorized shape difference (shape error) in the x , y and z directions will be computed for the intersection between the instantaneous and required shapes.
5. The forging operation can only directly correct positive errors, where the instantaneous shape dimension is greater than the required one, by squeezing the workpiece. On the other hand, negative errors are indirectly compensated for as a result of the constancy of volume.
6. To compute the shape error the current and required shapes of the workpiece must be referenced to the same global coordinate system. The alignment is carried out by matching selected reference points on both the current and required shapes. The reference points selected are those used to locate the workpiece on the robot gripper. They are specifically selected to be stationary non-deforming points on the holding surface of the workpiece.

Workpiece Modelling

The workpiece is modelled using a local coordinate system that complies with the right hand coordinate arrangement. The origin is set at the edge of the workpiece in such a way that most of the points will be in the positive octant of the coordinate system (Fig. 3.10). The outer surface of the workpiece is modelled by defining three pairs of surfaces along the three principal axes:

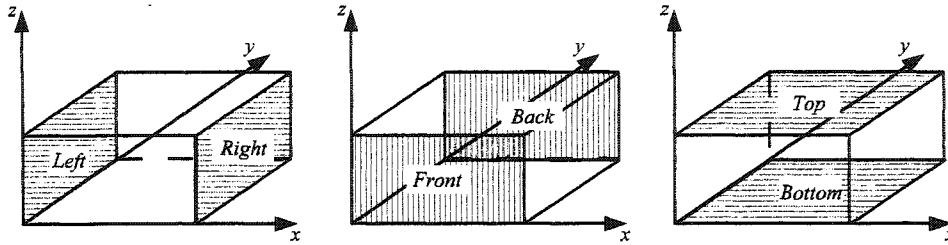


Figure 3.10: Workpiece Modelling

Table 3.1: Coordinate Assignment for the Workpiece Outer Surfaces

Surface	Independent Coordinate	Dependent Coordinates
<i>Right</i>	x	y, z
<i>Left</i>	x	y, z
<i>Back</i>	y	x, z
<i>Front</i>	y	x, z
<i>Top</i>	z	x, y
<i>Bottom</i>	z	x, y

height, width and length. Those surfaces that envelope the workpiece are named: left, right, top, bottom, front and back as illustrated in Fig. 3.10.

Each of the outer surfaces of the workpiece is defined by a dependent coordinate and two independent coordinates. The independent coordinates define the domain on which the surface is defined and the dependent one is assigned to the coordinate along which the error is to be computed. Table 3.1 defines the dependent and independent coordinates of the six outer surfaces of the workpiece.

The restrictions imposed by the forging operation are that the instantaneous workpiece cross-section between the dies must have a convex-shape and that the dependent coordinates of the outer surfaces must be uniquely defined for each point over their corresponding domains. These restrictions are necessary to allow the forging tools to have access to the forged surfaces.

A simple surface representation is applied in this study. It utilizes many of the MATLAB (MATLAB Version 6.1 2001) package built in functions. Each surface is stored in an $n \times 3$ matrix, where, n is the number of points used to define the surface and the three columns are used to store the x, y

Table 3.2: Workpiece Model Attributes

Surface Name	Attribute
<i>Top</i> surface	<i>.top</i>
<i>Bottom</i> surface	<i>.bottom</i>
<i>Right</i> surface	<i>.right</i>
<i>Left</i> surface	<i>.left</i>
<i>Front</i> surface	<i>.front</i>
<i>Back</i> surface	<i>.back</i>
Surface Projection on <i>xy</i> plane	<i>.proj.xy</i>
Surface Projection on <i>xz</i> plane	<i>.proj.xz</i>
Surface Projection on <i>yz</i> plane	<i>.proj.yz</i>

and z coordinates respectively. Linear and nonlinear interpolation⁸ are used to compute the surface coordinates corresponding to any point not defined by the surface matrix.

The instantaneous and the required workpiece shapes are stored in the structured variables *current* and *required* respectively. The structured variables attributes are defined in Table 3.2. Thus the top surface of the current shape of the workpiece is stored in the matrix *current.top*, the required top surface projection on the *xy* plane is stored in the matrix *required.proj.xy* and so on.

Error Calculation

For illustration the procedure used to compute the error in the z direction is presented here; the errors in the x and y directions are computed in a similar manner.

- The top and bottom surfaces are used to compute the height of the current and required shapes.
- The error is computed over the intersection area between the projection of the top and bottom surfaces on the *xy* plane for both the current and required shapes (Figs. 3.11 and 3.12).
- A grid is generated over the intersection of the projection of the top and bottom surfaces of the required and current shapes on the *xy* plane and

⁸Appropriate interpolation function is used for each surface class. The available interpolations are: nearest neighbourhood interpolation, bilinear interpolation, cubic spline interpolation and bi-cubic interpolation.

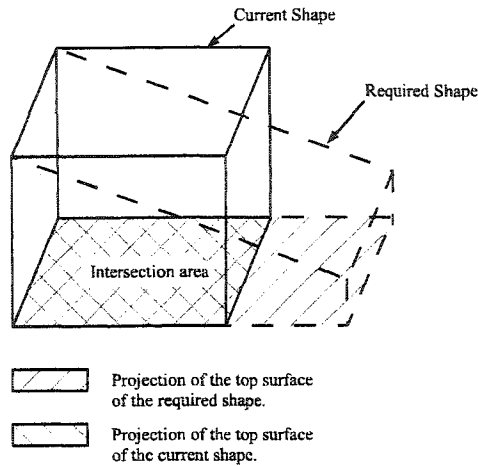


Figure 3.11: Projection Area for Sample Case

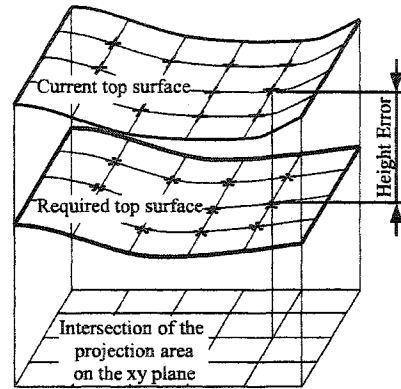


Figure 3.12: Error in Height Computation Method

the error is computed from the required and actual heights over the grid points (linear and nonlinear interpolation can be used to generate points not defined by the top or bottom matrices) (Fig. 3.12).

The error algorithm (Algorithm 3.1) is used to compute the error in height at each point on the generated data grid and returns the information in an $m \times 5$ matrix, where m is the number of points on the grid (number of rows). The first column is the error value, the second column the required height, the third column the current height, and the fourth and fifth columns are the x and y coordinates at which the z error is computed calculated.

3.3.5 Forging Schedule (A4)

The forging schedule module (A4) is used to generate a forging schedule to execute each individual operation based on the shape error and the technological and capacity constraints. The forging schedule specifies the tool paths and their execution sequence for generating each individual feature. A path specifies the bite and reduction values, number of strokes required and their sequence. Candidate schedules are simulated on the virtual forging cell (A42) and one is selected for execution. A real time feedback system captures the shape of the workpiece as it is being forged and the feedback information is used to adaptively change the forging schedule. The process iterates until the workpiece is within the prespecified dimensional and geometrical tolerances.

The forging schedule module (A4) is composed of three executive modules and six knowledge bases (Fig. 3.13). The path generation module (A41)

Algorithm 3.1 Error Algorithm (z Direction)

Inputs: Workpiece required and current top and bottom surfaces

Output: Error distribution (z direction)

- 1: Compute the intersection area between the projection of the top surfaces of the current and required shapes (in external forging this is also the intersection area between the bottom surfaces of the current and required shapes) on the xy plane (Fig. 3.12).

$$Area = current.top.proj.xy \cap required.top.proj.xy$$

- 2: Generate a mesh $[X \ Y]$ on the intersection area (Area), where X and Y are the matrices holding the x and y coordinates of the grid data points.

$$[XY] = mesh(Area)$$

- 3: Interpolate the z coordinate for each point on the grid data for the top and bottom surfaces of the current and required shapes.

$$\begin{aligned} Z_{req.top} &= interpolate([XY], current.top) \\ Z_{req.bottom} &= interpolate([XY], current.bottom) \\ Z_{current.top} &= interpolate([XY], required.top) \\ Z_{current.bottom} &= interpolate([XY], required.bottom) \end{aligned}$$

- 4: Compute the error in the height over the generated grid.

$$\begin{aligned} H_{req} &= Z_{req.top} - Z_{req.bottom} \\ H_{current} &= Z_{current.top} - Z_{current.bottom} \\ error.z &= H_{req} - H_{current} \end{aligned}$$

is the main module of the forging schedule generation. It generates a detailed forging schedule for each forging operation comprising the bite, squeeze and tool motion by consulting the spread prediction, technological bounds and other knowledge bases. The detailed schedule is then executed on a virtual forging cell and if the results are satisfactory (in terms of final shape and forging defects) it is executed. If the simulation results predict a problem an alternative tool path (A43) is generated and the modified schedule is reevaluated. The implemented forging schedule generation procedure divides the workpiece shape into a set of consecutive monotonic surfaces. The path generation algorithm⁹ is then used to generate the forging path.

Path Generation (A41)

A path¹⁰ consists of several strokes of the tool. Each stroke has an associated bite and reduction values. The path generation module utilizes the shape feedback from the feedback system, estimated material spreading from the spread prediction and the constraints imposed by the technological bounds to generate the forging path. The stroke sequence and the selection of the bite and reduction values are chosen to reduce forging shape defects.

A path generation algorithm (Algorithm 3.2) to forge surfaces defined by monotonic decreasing functions is presented in this section. The procedure can be used to forge surfaces defined by monotonic increasing functions simply by properly realigning the x coordinate to the feeding direction. The general formula for the monotonic decreasing function is given by:

$$z(x_2) < z(x_1) \quad \text{where} \quad x_2 > x_1 \quad (3.8)$$

The special characteristics of the monotonic decreasing function simplify the forging schedule. The material is drawn out with a constant squeeze value starting from the fixed end (start of the monotonic function) of the workpiece and moving to the free end of the workpiece. The monotonic decreasing function of the surface ensures that the error will increase gradually from a minimum value near the fixed end to a maximum at the free surface. The use of a constant squeeze value minimizes the incidence of overlaps¹¹ by reducing the possibility of reforging a previously forged region and assuring that the maximum squeeze value does not exceed the lapping limit. Another advantage of the procedure is that it does not require accurate prediction of the elongation as compared to other possible procedures.

⁹This algorithm is developed to generate surfaces defined by monotonic functions.

¹⁰Available path generation modules in the literature were developed for cogging operations. These are the same cogging schedule generation modules presented in Section 2.4

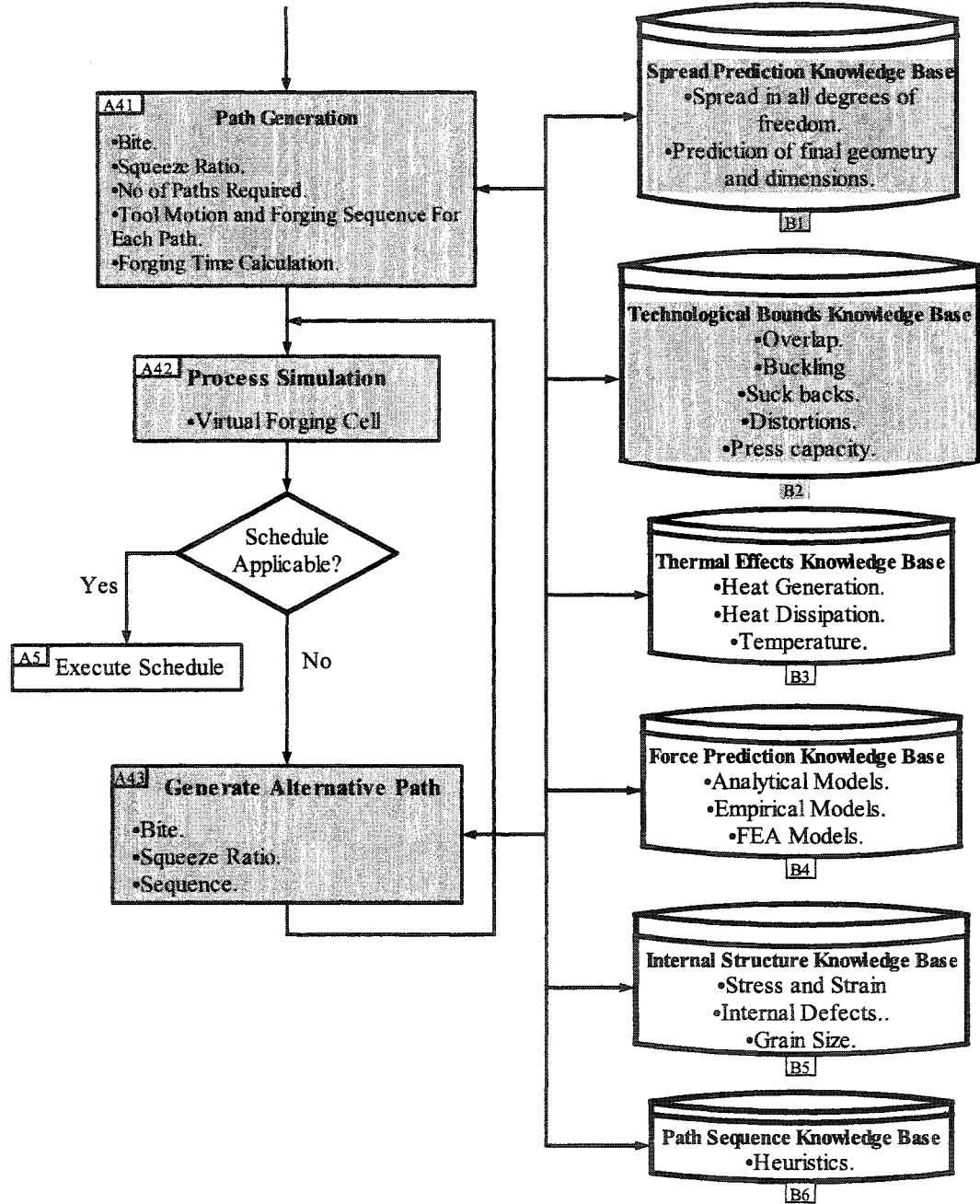


Figure 3.13: Forging Schedule Module (A4) (Shaded Areas are the Focus of This Research)

Algorithm 3.2 Path Generation Algorithm for Generating External Profiles Defined by Monotonically Decreasing Functions.

Inputs: Distribution of the Workpiece Shape Error. The preset tolerance limit

Output: Start of the forging path to be used for forging feed information. The direction of the squeezing action.

- 1: Starting from the fixed end of the workpiece scan the error function till the first location that exceeded the preset tolerance limit is found. This marks the starting point for the forging pass.
 - 2: Forge the workpiece from the starting point till to the end with a squeeze value equal to the tolerance limit.
-

Spread Prediction (B1)

Though the schedule can be generated without the need to estimate the spread¹² knowing the proportion of the material that spreads in each direction would enhance the quality of schedules generated by the adaptive scheduling procedure (as illustrated in Chapter 7). Several models have been presented in the literature for spread prediction¹³, mainly for cogging operations, they can only be used as rough estimators of the side material spread. Chapter 5 will introduce newly derived spread prediction models of better estimation precision.

Technological Bounds (B2)

A set of technological bounds are defined in the literature¹⁴. Technological bounds set an upper or lower limit on the quantitative values of the scheduling parameters. The most common technological bound is the press capacity. Other technological bounds are simple constraints to prevent defect formation, such as: central bursts; suck-backs; overlaps, buckling and other geometric distortions (Fig. 2.39). Those defects are by far more pronounced in internal profiling than in external profiling.

The most influential forging parameters are the bite ratio, θ , and the die width ratio, DWR . The bite ratio has a direct effect on the spreading of the material¹⁵ and on lap formation (Shutt 1963). Generally, the smaller the

since cogging schedules are composed of a single forging path.

¹¹This rule was derived from experimental experience.

¹²The control process of the forging operation does not require spread prediction (Section 3.3.3).

¹³Such models were presented in Section 2.5.

¹⁴ Refer to Section 2.6.

¹⁵Refer to Section 2.5.

Table 3.3: Implemented Technological Bounds due to Shutt (1963)

Constraint Name	Controlling Parameter	Parameter value	Minimum Allowable Bite Ratio (θ_{min})
Hourglass Shape limit (changing from single to double bulge)	Shape Factor (ϕ)	1.0-1.5	0.5
		1.5-2.5	1.0
		2.0-3.0	2.0
Lapping limit	Shape Factor (ϕ)	1	0.35
		1.5	0.52
		2	0.73
		ϕ	$\theta_{min} = \frac{1}{2.63} \times (\phi - 0.11)$

bite the lower the spread but the more likely a lap will be formed, and vice versa. The *DWR*, however, affects the penetration of the plastic strain to the center of the material (Wang and Cao 1994b, 1995). A large *DWR* results in better penetration of the plastic strain and the elimination of internal defects with a single bulge formation. On the other hand, a small *DWR* results in a lower depth of penetration of the plastic strain which leads to the formation of a double bulge on the free surface of the workpiece.

Table 3.3 summarizes the implemented technological bounds for safe working zones according to Shutt (1963), who studied different stability operating regions for the forging operation. His study included making physical models of plasticine and steel.

Wang and Cao (1994b), contrary to Shutt (1963), attributed the hourglass effect to the *DWR*. They experimentally found that a *DWR* of 0.5 marks the transition from tensile to compressive stress at the center of the workpiece. They recommended a *DWR* of 0.6 to avoid the hourglass effect and maintain better penetration of the plastic strain. Their conclusion was confirmed by reexamining Li and Zhou (1989) results, who, like Shutt (1963), attributed the transition to the effect of the shape factor, contradicting some of their own observations.

To illustrate the effect of improper choice of *DWR* the forging operation of a steel pyramid was simulated. The pyramid length, width, height and included angle are: 20 mm, 20 mm, 20 mm, and 28°, respectively. A 2 mm bite is chosen so that the *DWR* at the start of deformation is 0.1, lower than the recommended minimum of 0.6. The final shape after 8 deformation steps (Fig. 3.14) revealed that the material at the center of the workpiece did not deform at all. The deformation caused the nonhomogeneous bulging of the

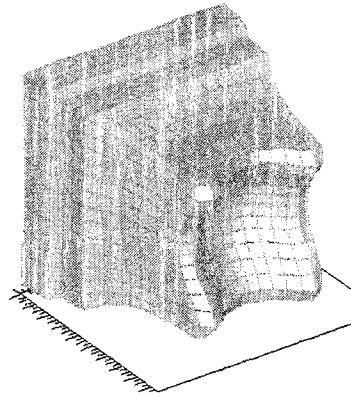


Figure 3.14: Improper Die Width Ratio

surface layers and the formation of a double bulge at the free surface. This effect is most pronounced when the forged region is near a free surface. Other experiments show that forging away from the free surface double bulges do not occur, rendering the bound on the *DWR* unnecessary.

A new technological bound (Section 4.1.2) was derived. The new bound is used to prevent the generation of the overlapping defect in forging an external profile defined by a linear relation between the height and the length of the workpiece where the workpiece has at least one free surface (Fig. 4.2).

In this research the technological bounds due to Shutt (1963); Wang and Cao (1994b) and the newly derived bound (Section 4.1.2) are implemented.

Force prediction (B4)

The most limiting constraint in commercial open die forging is press capacity. Many techniques are used for force prediction. For example, Kopp (1986) lists many empirical and analytical formulae for force prediction. The forging cell presented in this study will be used to forge small and medium size workpieces and thus press capacity is not an issue. Force prediction is not implemented in this study.

Internal Structure (B5)

Some studies have investigated the internal integrity of the material in the forging process, such as the homogeneity of the forming process (Siemer et al. 1986), elimination of voids (Dudra and Im 1990a,b), and avoiding internal cracks initiations (Gordon and Van-Tyne 1983). Workpieces for the forging cell presented in this study are assumed to be forged from homogeneous billets and

thus the starting internal structure is assumed to be free of defects, therefore an internal structure knowledge base is not implemented in this study.

Process simulation (A42)

FEM is the most widely used technique to simulate the forging process. FEM developed for forging operations can be found in the work of Voyiadjis and Foroozesh (1991); Qinchun et al. (1997); Kolmogorov et al. (1999); Ramakrishnan et al. (1999); Zabarar and Srikanth (1999); Pietrzyk (2000); Feng and Luo (2000). Applications of the FEM to predict material spread or to predict the stress strain distribution in forged products can be found in Kiefer and Shah (1990); Mitani et al. (1991); Wu et al. (1994); Rodrigues et al. (1994).

3.4 Virtual Forging Cell (A42)

The forging operation is simulated on the virtual cell using the non-linear FEA explicit code H3DMAP (Sauve 2000) as part of the forging schedule module (A4) (Fig. 3.13) where adaptive forging schemes are first simulated then an appropriate schedule is executed on the physical cell.

The workpiece and die mesh can be either generated by a custom FE preprocessor or by the finite element package FEMAP (FEMAP Version 8.0 2000). Steps in the forming sequence (i.e., workpiece position, die shape and workpiece and die relative motions) are implemented via a custom FE preprocessor that generates the H3DMAP input file. After the simulated forming step is completed, a custom post-processor extracts the workpiece shape, simulating the shape feedback system. The computed shape error is then used to drive the schedule generator to plan the next forming step. The virtual forging cell procedure is shown in Fig. 3.15.

All the virtual cell routines are operated under the MATLAB (MATLAB Version 6.1 2001) shell. FEMAP, developed FORTRAN or developed MATLAB routines can be used to create the solid models of the dies and the initial and final workpiece shapes. A main scheduling program then automatically calls the respective routines to compute the shape error, generate the finite element mesh, generate the H3DMAP input files, execute the simulation, import the results and generate other forging steps if necessary. Typical workpiece mesh contained 2,836 nodes and 2,604 elements and took 15 min to simulate on a 1.3 GHz AMD processor.

The explicit finite element solver is developed to solve dynamic problems. Forging is a static problem and to use the solver the solution is left to run for a long time in order to reach the steady state. Speeding up the convergence of the numerical solution can be achieved by using an artificial value of the material density or an artificial value of the forging speed¹⁶. It must be noted that using either approach will not affect the quality of the numerical solution as both parameters have no effect on static problems. In the simulations studies both approaches were used and it was found that the latter approach has better numerical stability.

3.4.1 Die Modelling

Die Shapes

The forging dies can be modelled to have any arbitrary shape. For the case studies presented in this study (Chapter 4) forging dies have a rectangular

¹⁶The artificial forging speed used is much higher than the actual forging speed. A typical value used would be 0.1 of the velocity of sound inside the material.

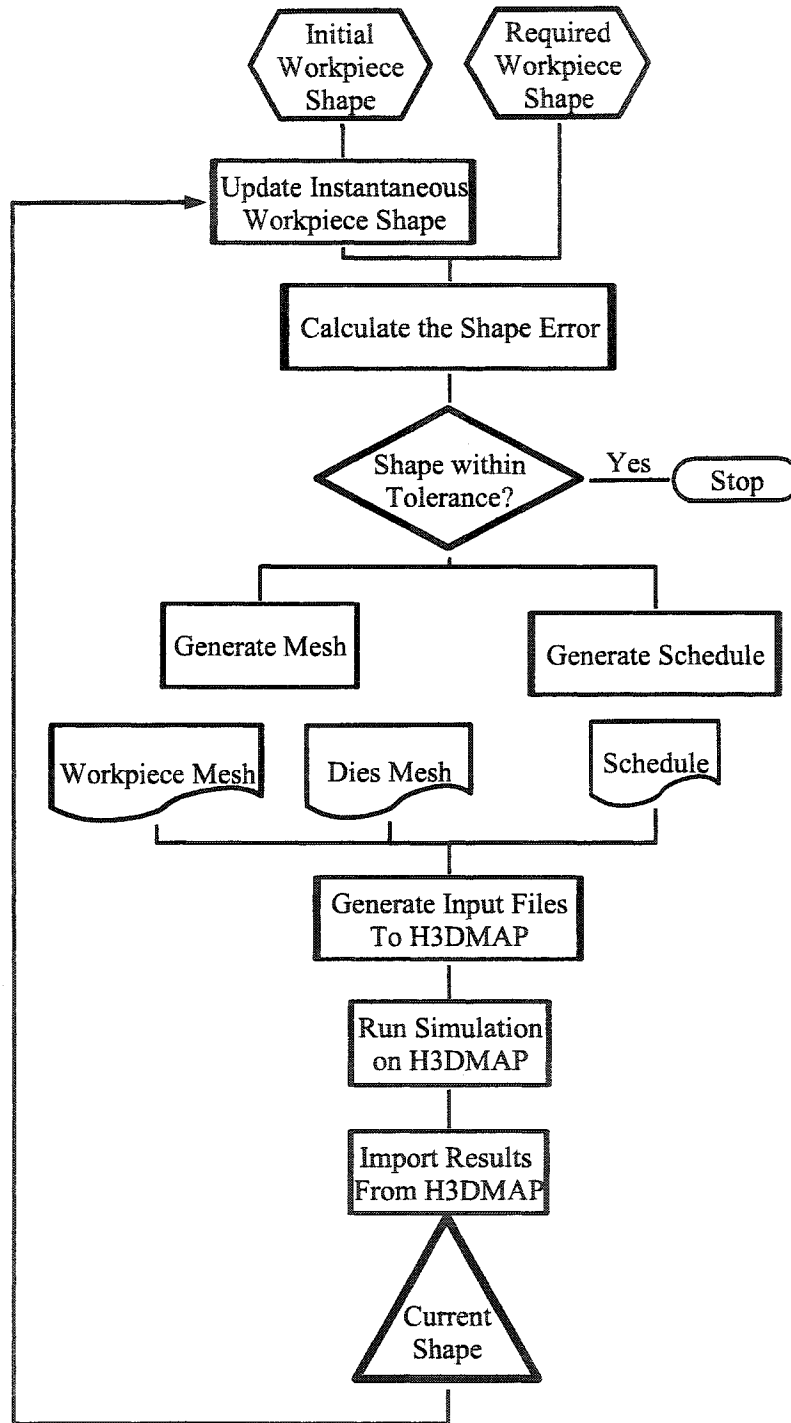


Figure 3.15: Virtual Forging Cell Procedure

Table 3.4: Simulated Die Material Properties, (Mild Steel Material) (Wong et al. 1996)

Property	Value
Young's Modulus of Elasticity	200 GPa
Poisson Ratio	0.3
Density	78 500 kg/m ³

brick-like shape to simulate flat-tool forging. For the implemented application of generating external profiles the die length is selected such that it extends beyond the workpiece width throughout the forging operation.

Material Model

The forging dies used are of steel and the simulated material model is a rigid isotropic elastic material model. The rigid elastic material model assumes the material will only deform elastically and not plastically¹⁷. The material properties used in the simulation are listed in Table 3.4. Note that the yield stress is not required as the material model assumes the material will not deform plastically, i.e., the material is treated as having an infinite yield stress.

3.4.2 Workpiece Modelling

Workpiece Shapes

Though normally the workpiece is assumed to be initially forged from a billet of a rectangular shape with dimensions which are approximately those of the final product, the workpiece material initial shape can be assumed to have any arbitrary shape.

Material Model

A custom built workpiece modelling and mesh generation module or FEMAP software can be used to generate the initial mesh of the workpiece. Lead, aluminum and mild steel were used as workpiece materials. The workpiece mate-

¹⁷This model is a standard material model in the H3DMAP package.

Table 3.5: Simulated Workpiece Material Properties, (Mild Steel Material) (Wong et al. 1996)

Property	Value
Yield Stress	200 MPa
Young's Modulus of Elasticity	200 GPa
Poisson Ratio	0.3
Density	78 500 kg/m ³
Hardening Modulus	80 MPa

rial model is selected to be an isotropic elastic plastic model. This model is a standard material model in the H3DMAP package that assumes the material will deform elastically until the yielding stress is reached and then plastically above that. The flow curve of this type of material model is given by

$$\sigma_y = \sigma_{y0} + E_T(\varepsilon_0 - \varepsilon)$$

where, σ_y is the instantaneous flow stress, σ_{y0} the yield stress, E_T the hardening modulus, ε_0 the total yield strain, ε the total strain (Sauve 2000). The material properties used in the simulation for mild steel, aluminum and lead are presented in Tables 3.5, 3.6¹⁸ and 3.7¹⁹ respectively.

Lead is considered as the most attractive simulating material for hot steel forming as it is hot worked at room temperature (Wong et al. 1996, 1995; Appleton et al. 1979; Schey and Abramowitz 1973). The basic characteristics of the stress strain curve of lead resembles those observed for hot steel especially that the work hardening of the material followed by softening as a result of dynamic recrystallisation (Wong et al. 1995). The major difference between lead and hot steel is that the coefficient of friction for steel forging is much higher than lead. Typical hot steel forging occurs under sticking friction

¹⁸The hardness modulus for aluminum is a computed artificial value to approximate the power relation to a straight line one. It was computed for a strain up to 0.69 and using a strain hardening exponent of 0.25.

¹⁹The hardness modulus for lead is an artificial value used to capture the strain hardening effect at the start of deformation and before recrystallisation.

Table 3.6: Simulated Workpiece Material Properties, (Pure Aluminum Material (Al1100)) (Wong et al. 1996)

Property	Value
Yield Stress	35 MPa
Young's Modulus of Elasticity	70 GPa
Poisson Ratio	0.33
Density	27 000 kg/m ³
Hardening Modulus	170 MPa

Table 3.7: Simulated Workpiece Material Properties, (Pure Lead Material) (Wong et al. 1996)

Property	Value
Yield Stress	14 MPa
Young's Modulus of Elasticity	14 GPa
Poisson Ratio	0.42
Density	114 000 kg/m ³
Hardening Modulus	16.7 MPa

condition (the friction factor m approaches unity) while typical coefficient of friction using lead $\mu = 0.1$ (corresponding to a friction factor m of 0.173) (Wong et al. 1996).

An alternative to lead (which is considered as a hazardous material) to simulate hot steel forging is aluminum (Nye et al. 2001; Aksakal et al. 1997; Ferreira and Osman 1997; Aksakal et al. 1993; Schey and Abramowitz 1973). Apart from its relative low cost it is also of the most reproducible quality. The major drawback of aluminum is its strain hardening and the development of secondary tensile stress at the free surface which requires periodic annealing.

3.4.3 The Scheduling Strategy

The implemented values of the forging parameters used by the forging schedule module (Algorithm 3.2 Section 3.3.5) in the numerical experiments are:

1. The dimensional tolerance limit is ± 1 mm.
2. The die length is chosen to ensure a bite that satisfies the technological constraints to have a lap free surface.
3. The starting bite was set to ensure a starting DWR of 0.6 thus providing adequate penetrations of plastic strain. This ratio decreases as the die approaches the free surface, violating occasionally the minimum allowable DWR . Experiments showed that this did not seriously promote the generation of double bulge at the free surface.

3.5 Summary

The general structure of the flexible forging cell was presented in this chapter. The cell hardware configuration is composed of a numerically controlled press, a robot for workpiece manipulation, a vision feedback system and a main control computer. The cell had three degrees of freedom where it can forge the workpiece along its height, width or length.

The general requirements of the forging operation plan were presented in Section 3.3. The main modules of the operation plan²⁰ are the forging schedule module (composed of the spread prediction module; the technological bounds knowledge base; and the virtual cell module) and the feedback module. Other modules has been identified in the general operation plan of the cell as modules that can be added later to enhance the capabilities of the developed forging cell.

²⁰Main operation plan modules are indicated by the shaded areas in Figs. 3.5 and 3.13.

A scheduling strategy has been presented for the adaptive forging procedure to forge external profiles defined by a monotonically decreasing or increasing functions. The strategy is simple and is presented here as a demonstration of the simplicity of developing schedules for the adaptive forging procedure. This scheduling algorithm (Algorithm 3.2) will be used later to generate 2-D and 3-D profiles as presented in Chapters 4 and 7.

Chapter 4

Case Studies

Illustrative case studies are presented in this chapter that are divided into two groups: case studies executed on the virtual forging cell and a validating case study that is executed on the physical cell (Section 4.2). The first case study (Section 4.1.1) demonstrates step by step the operation of the adaptive scheduling procedure for generating a $2\frac{1}{2}$ D surface. A comparison to possible schedule generation procedures, based on spread prediction models, for forging a wedge shaped workpiece is presented in Section 4.1.2. The convergence rate of the adaptive schedule generation procedure using different tolerance limits for forging the wedge shaped workpiece is presented in Section 4.1.2. A new technological bound on the maximum slope that can be forged has also been derived (Section 4.1.2). Finally a number of 3-D shapes of single or multiple features successfully generated by the adaptive schedule procedure are presented in Table 4.7.

4.1 Simulated Case Studies on the Virtual Forging Cell

4.1.1 Forging a 2^{nd} Degree Polynomial Surface

The virtual forging cell procedure (Fig. 3.15) was used to forge the workpiece shown in Fig. 4.1. The top and bottom surfaces are defined by 2^{nd} degree polynomial surfaces, with corresponding formulae given by:

$$z_{top} = \begin{cases} 12 & x = (0, 5) \\ -0.0156x^2 + 0.1563x + 11.609 & x = (5, 21) \end{cases} \quad (4.1)$$

$$z_{bottom} = \begin{cases} 0 & x = (0, 5) \\ 0.0156x^2 - 0.1563x + 0.3906 & x = (5, 21) \end{cases} \quad (4.2)$$

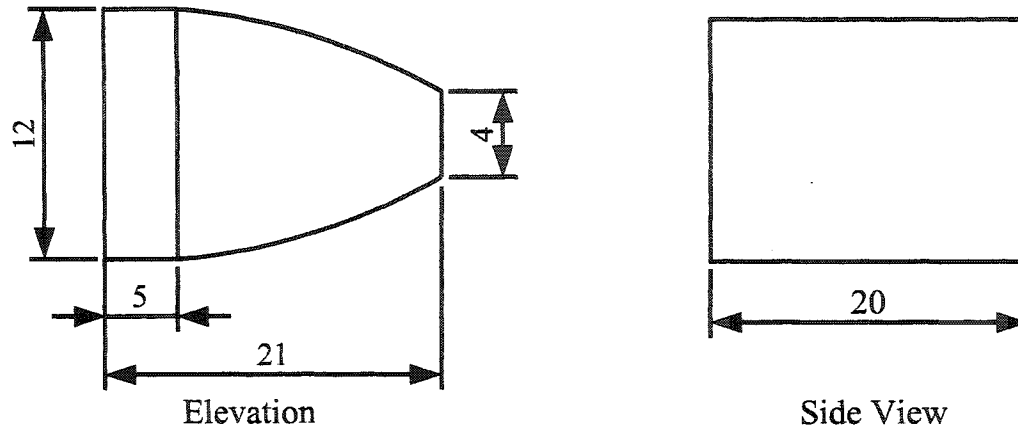


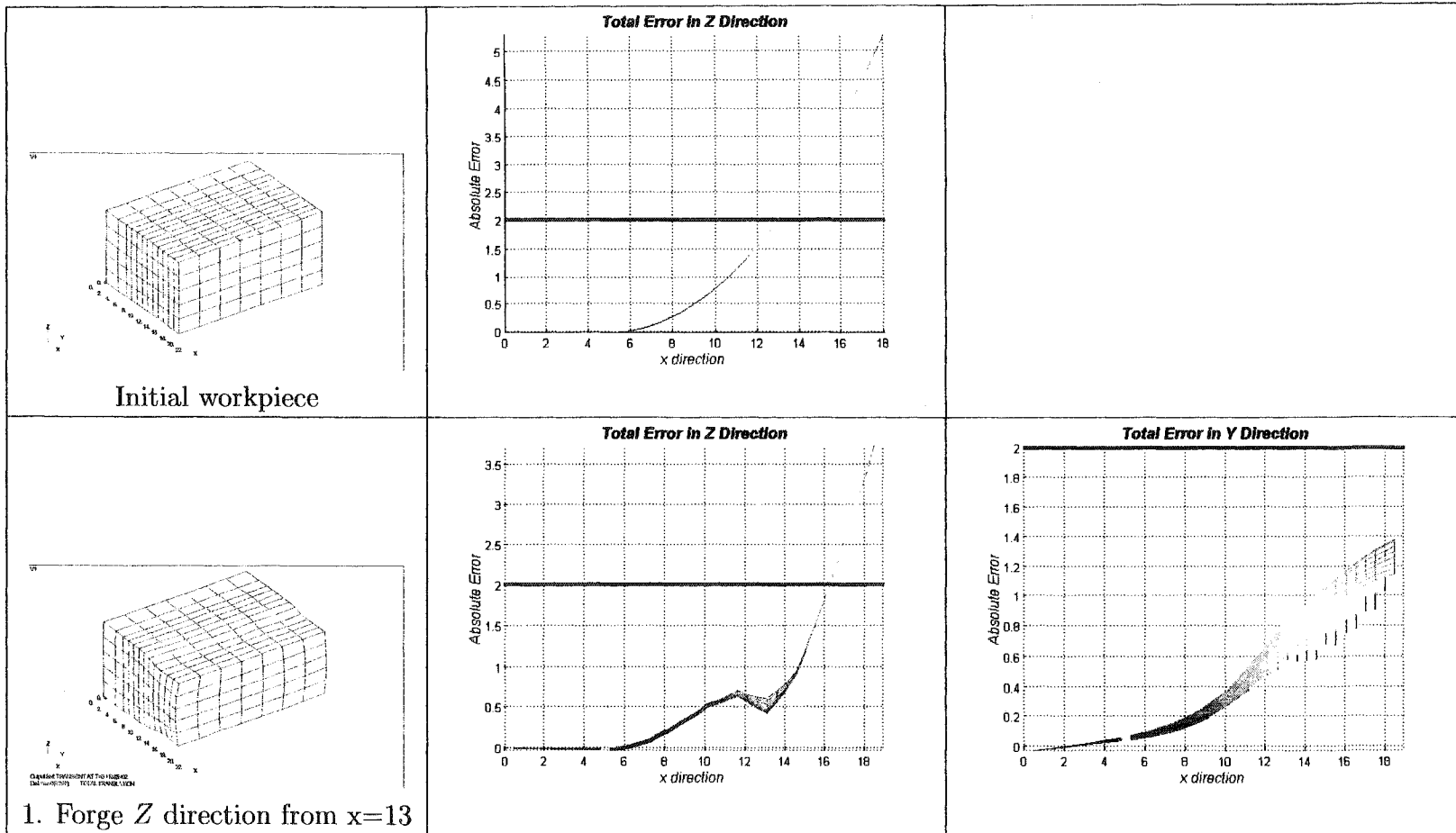
Figure 4.1: Workpiece With a 2nd Surface (all dimensions in mm)

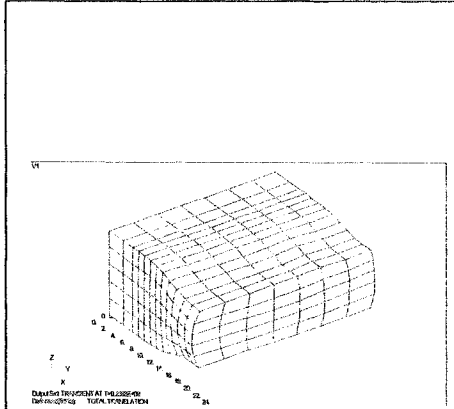
Table 4.1 shows the forging schedule for the product. The error axis for the Z and Y error columns is the total error on the dimension, so the ± 1 mm tolerance limit is represented by the 2 mm dark horizontal line on the error plot. At the start of the forging process the error in the Z direction first exceeds the preset limit at $x = 13$ mm, marking the start of the first forging pass. Thus for the first pass the squeeze value is 2 mm and the forging starts at $x = 13$ mm and ends at the end of the workpiece. The resulting workpiece shape after the first pass is shown by the two error figures corresponding to Step 1. Each line on the error figures represents measurements taken along element boundaries of the FE mesh surface. The forging step reduced the error along the Z direction. The error in the Y direction shows that as the material spreads the width of the workpiece starts to increase, with a maximum of 1.4 mm at the end of the workpiece.

The next forging step, Step 2, was determined by searching for the first occurrence on the x -axis where the error exceeded the preset limit of 2 mm, marked by the intersection of the error curve with the 2 mm line. This occurs on the error plot, for Z direction, at $x = 16$ mm. For the Y direction the workpiece is still within tolerance. Thus forging Step 3 is performed in the Z direction starting at $x = 16$ mm and ending at the end of the workpiece and with a squeeze value of 2 mm.

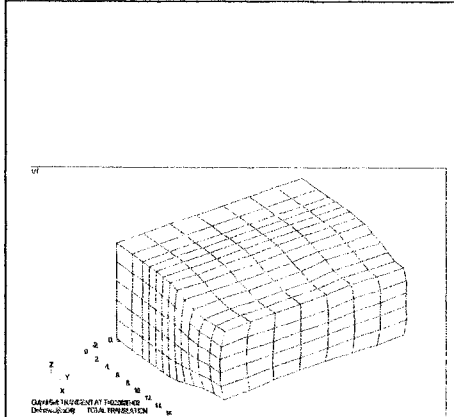
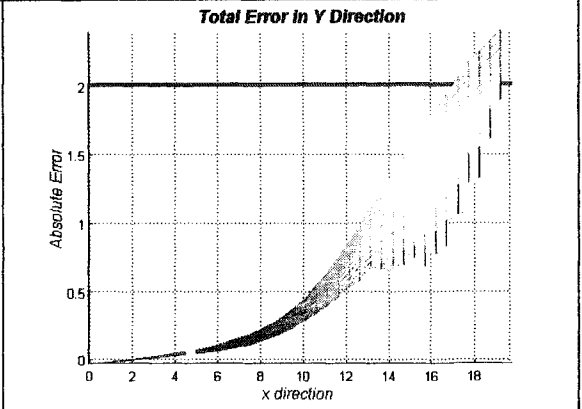
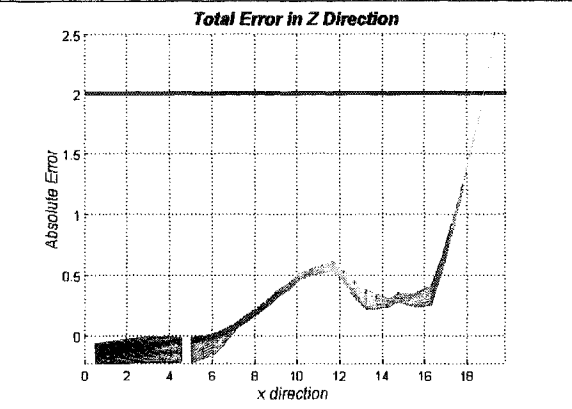
This procedure is repeated until the error in the Z and Y directions are within the preset tolerance limit of ± 1 mm. It should be noted that for Step 4 the procedure was prematurely terminated as the forging bite was 0.5 mm resulting in a very small die width ratio. Results showed that further forging resulted in the formation of double bulge on the free surface.

Table 4.1: Forging Schedule for 2nd Degree Surface

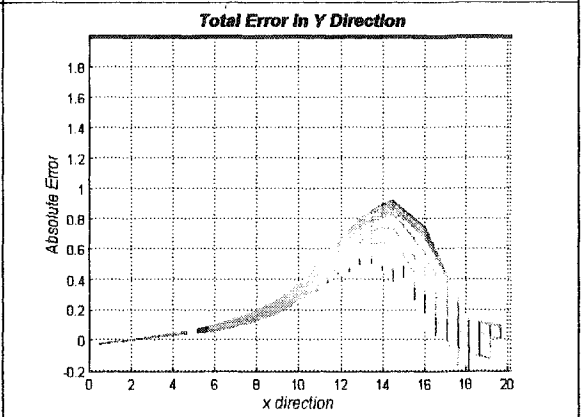
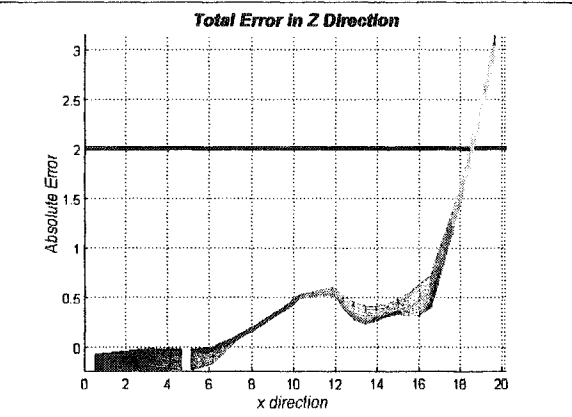


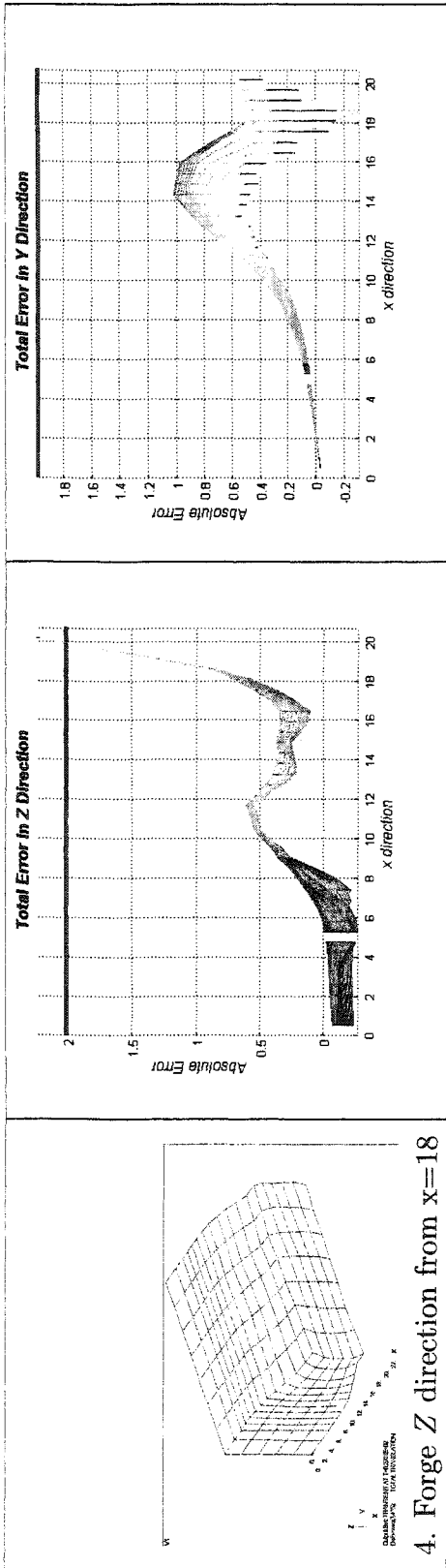


2. Forge Z direction from x=16



3. Forge Y direction from x=17





4. Forge Z direction from x=18

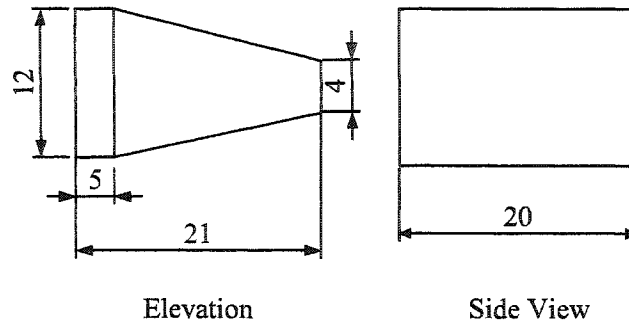


Figure 4.2: Wedge Workpiece (all dimensions in mm)

4.1.2 Forging a Wedge

The virtual forging cell procedure (Fig. 3.15) was used to forge a wedge (Fig. 4.2) from an initial block of material of 16.67 mm, 20 mm, 12 mm, length, width and height respectively. Table 4.2 shows the forging steps determined adaptively by the virtual forging cell procedure, where the final product dimensions are within ± 1 mm in seven steps.

Adaptive Schedule Convergence Rate

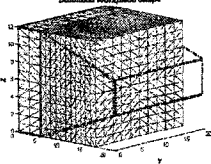
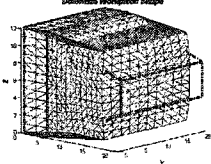
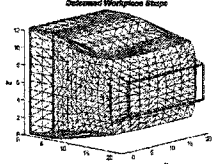
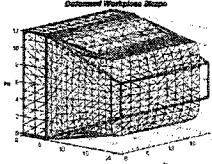
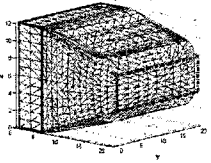
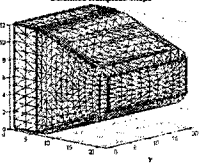
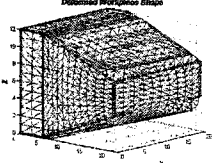
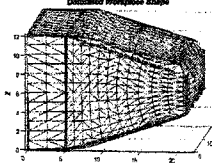
Several numerical experiments were conducted to assess the number of forging steps needed at different tolerance values. The results are shown in Fig. 4.3, which shows that the process will require a large number of steps for tight tolerances. Other experiments, not reported here, show that the convergence rate also deteriorates at much higher rate as the slope of the wedge increases. The 0.5 mm minimum allowable tolerance is much tighter than what to be expected in actual forging process. The edges of the workpiece will always deform nonhomogeneously and from experimental observations this can be controlled till up to 1.0 mm tolerance¹.

Forging a Wedge by Classical Technique

To demonstrate the benefit provided by the adaptive forging algorithm the same wedge (Fig. 4.2) previously forged by the adaptive forging algorithm will be forged using the Tomlinson and Stringer (1959) and the Tarnowski (1950) spread prediction formulae. The forging schedule is generated using the modified shape feedback control process (Fig.4.4) where vision shape feedback sys-

¹Figure 4.9 shows a typical non-recoverable hourglass defect of 5.7 mm at the end of the workpiece.

Table 4.2: Wedge Forging Steps

 <p>Initial workpiece</p>	 <p>Step 1 Forging in Z direction starting at $x=9$</p>	 <p>Step 2 Forging in Z direction starting at $x=12$</p>	 <p>Step 3 Forging in Y direction starting at $x=5$</p>
 <p>Step 4 Forging in Z direction starting at $x=15$</p>	 <p>Step 5 Forging in Z direction starting at $x=17$</p>	 <p>Step 6 Forging in Y direction starting at $x=12$</p>	 <p>Step 7 Forging in Z direction starting at $x=18$</p>

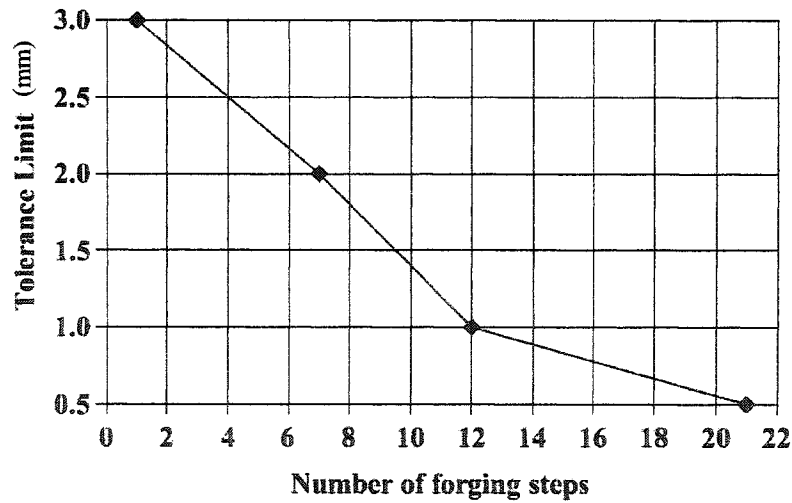


Figure 4.3: Adaptive Schedule Convergence Rate

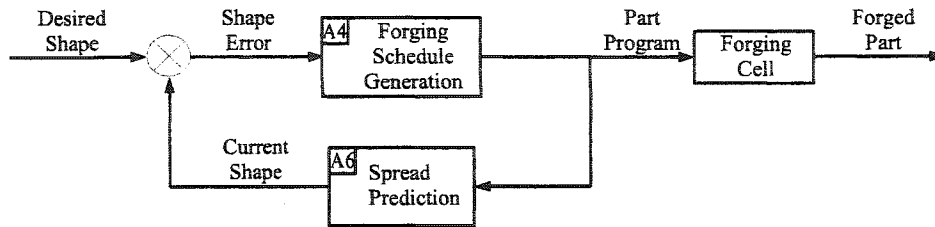


Figure 4.4: Control Schematic of the Forging Cell Based on Spread Prediction Models

tem is replaced by a spread prediction module to predict the instantaneous shape of the workpiece. The initial workpiece dimensions were computed from the constancy of volume requirement² and was found to be 16.6 mm, 20 mm, 12 mm, length, width and height respectively. The following assumptions are made for predicting the instantaneous workpiece shape by the spread prediction formulae:

- An accurate estimate of spread is available to predict changes in length and width after each forging step.
- Forged material directly squeezed by the dies experiences spreading while material not directly squeezed by the dies is rigid and does not experience plastic deformation. This simplification is necessary to comply with the assumptions made in the derivation of the spread coefficient (Tomlinson and Stringer 1959).
- A single step in taper forging represents a cogging operation.
- Spreading is evenly distributed in the positive and negative x directions.

The procedure to create the forging schedule is then:

- Starting from the holding surface of the wedge scan the shape error till the first position where the error is greater than the tolerance limit (i.e., 2 mm in this case) is found.
- Forge the workpiece starting from the point where the error was greater than the tolerance limit of 2 mm to the end of the workpiece.

²The exact volume should be 15.6 mm, 20 mm, 12 mm length width and height respectively. The extra volume is used to account for the machining allowance.

Table 4.3: The Forging Schedule Implementing the Tarnowski (1950) Formula for Spread Prediction

Forging Direction	Start	Bite	Start width	Start length	Spread	Start height	Final height	Final width	Final wedge length	Final total length
	mm	mm	mm	mm	mm	mm	mm	mm	mm	mm
Z	9	7.7	25	7.7	0.24	12	10	26.1	8.85	13.85
Z	13	0.85	26.1	8.85	0.03	10	8	26.28	10.99	15.99

- The starting bite was chosen greater than 7.5 mm to maintain a minimum starting die width ratio of 0.6.
- The thickness of the wedge, h , is defined by Eq. (4.3) and its width is 20 mm.
- The length width and height of workpiece refer to the workpiece's original orientation regardless of the current workpiece orientation during the forging step.

$$h = \begin{cases} 12 & x = (0, 5) \\ 12 - \frac{5}{20} \times 2 \times (x - 5) & x = (5, 21) \end{cases} \quad (4.3)$$

The Tarnowski (1950) formula, Eq. (4.4) is used to calculate the spread coefficient that is then used by the Schedule Generation Algorithm (Algorithm 4.1) to generate the forging schedule presented in Table 4.3 and the Tomlinson and Stringer (1959) formula, Eq. (4.5) is used to calculate the spread coefficient that is then used by the Schedule Generation Algorithm (Algorithm 4.1) to generate the forging schedule presented in Table 4.4. It should be noted that when forging in the y direction the height becomes the width.

$$s = \frac{B}{B + w_0} \quad (4.4)$$

$$s = 0.14 + 0.36 \times \frac{B}{w_0} - 0.054 \times \left(\frac{B}{w_0}\right)^2 \quad (4.5)$$

The error plots after simulating the forging process with these spread prediction formulae are presented in Table 4.5 and Table 4.6 respectively. The plots indicate that the final workpiece for both schedules is out of tolerance. The forging schedule based on either spread prediction formula failed to forge the workpiece within the required tolerance though the spread prediction error

Algorithm 4.1 Forging Schedule Generation Algorithm Using Spread Coefficient Predicting Formulae

Inputs: Initial and required workpiece shapes. Spread prediction formula to be used.

Output: Forging Schedule.

1: **repeat**

2: Use the initial and required workpiece shapes to compute the shape error distribution (use the Error Algorithm (Algorithm 3.1))

3: From the shape error distribution find the direction and location on the x axis, x_s where the shape error first exceeded the tolerance limit (2 mm in this case).

4: **if** The forging direction is the z direction **then**

5: The workpiece will be forged along its height with a squeeze equal to the tolerance limit starting from x_s to its free end.

6: To update the workpiece shape substitute for h_0 with the workpiece height at x_s , and for h_n with $h_0 - 2$. Then use the spread formula to estimate the spread coefficient \hat{s}_n and use it to estimate the updated workpiece width \hat{w}_n and length \hat{l}_n

$$\hat{w}_n = w_0 \times \left(\frac{h_0}{h_n} \right)^{\hat{s}_n}$$

$$\hat{l}_n = l_0 \times \left(\frac{h_0}{h_n} \right)^{1-\hat{s}_n}$$

7: **else if** The forging direction is the y direction **then**

8: The workpiece will be forged along its width with a squeeze equal to the tolerance limit starting from x_s to its free end.

9: To update the workpiece shape substitute for w_0 with the workpiece width at x_s , and for w_n with $w_0 - 2$. Then use the spread formula to estimate the spread coefficient \hat{s}_n and use it to estimate the updated workpiece height \hat{h}_n and length \hat{l}_n

$$\hat{h}_n = h_0 \times \left(\frac{w_0}{w_n} \right)^{\hat{s}_n}$$

$$\hat{l}_n = l_0 \times \left(\frac{w_0}{w_n} \right)^{1-\hat{s}_n}$$

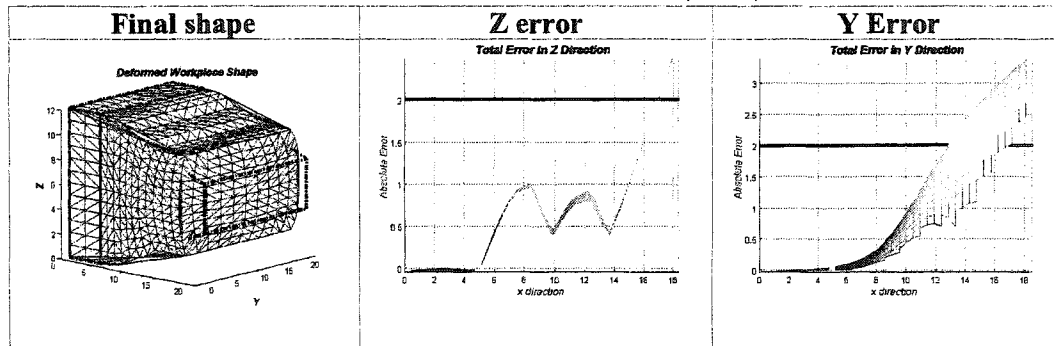
10: **end if**

11: **until** The workpiece dimensions are within the tolerance limit

Table 4.4: Scheduling Using the Tomlinson and Stringer (1959) Formula for Spread Prediction

Forging Direction	Start mm	Bite mm	Start width mm	Start length mm	Spread mm	Start height mm	Final height mm	Final width mm	Final wedge length mm	Final total length mm
Z	9	7.7	25	7.7	0.25	12	10	26.1	8.85	13.85
Z	13	0.85	26.1	8.85	0.15	10	8	27.04	10.68	15.68
Y	13	2.68	27.04	10.68	0.24	8	8.15	25	11.33	16.33

Table 4.5: Error Plots Based on the Tarnowski (1950) Formula Schedule



for a single step for both formulae was less than 0.4 mm. This poor performance can be attributed to the accumulation of error from the spread predicting formulae, and is remarkable in that this level of error has accumulated in so few forging steps. In contrast the adaptive scheduling approach succeeded in forging the workpiece within tolerance without the need to estimate the spread (Table 4.2).

Maximum Allowable Slope That Can Be Forged

The hourglass defect limits the maximum slope that can be forged by the process. A wedge of arbitrary width having a length L , base H , and an arbitrary slope (Fig. 4.5) is normally forged from a rectangular billet. The billet has the same width and height of the wedge but of different length W . The length of the required billet can be calculated from constancy of volume:

$$W \times H = \frac{1}{2}(H + H - 2 \times slope \times L) \times L \quad (4.6)$$

Rearranging:

Table 4.6: Error Plots Based on the Tomlinson and Stringer (1959) Formula Schedule

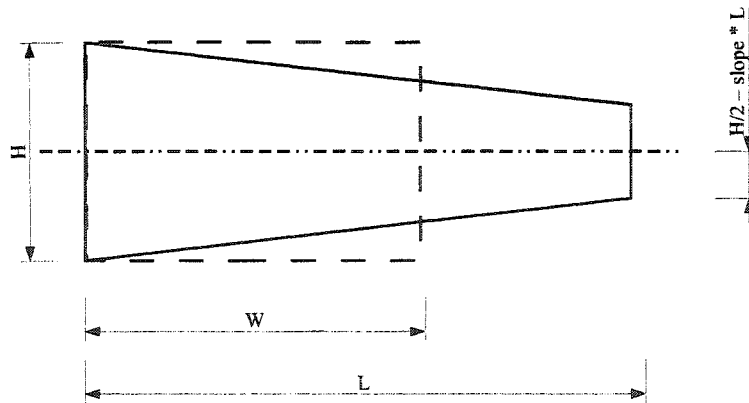
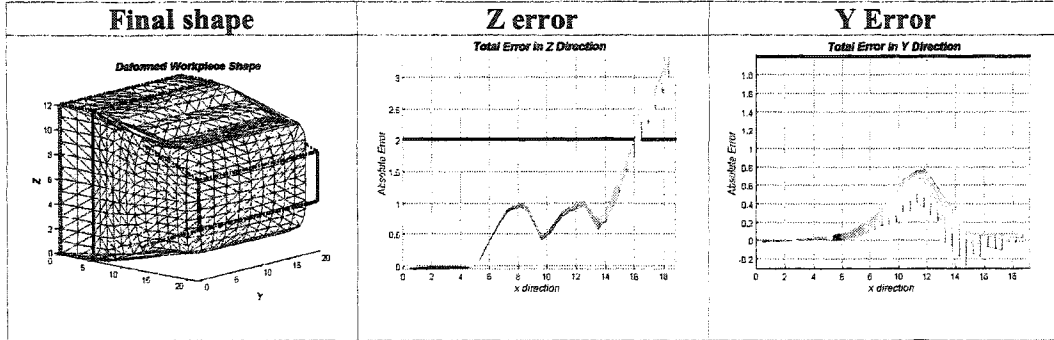


Figure 4.5: Maximum Allowable Slope

$$W = L\left(1 - \frac{L}{H} \times slope\right) \quad (4.7)$$

The hourglass defect (transition from single to double bulge) occurs when the DWR exceeds a critical value DWR_{min} (Wang and Cao 1994b). The maximum bite that can be used is limited by the initial workpiece length, W . Thus the constraint on the DWR is:

$$\left(DWR = \frac{W}{H}\right) \geq (DWR)_{min} \quad (4.8)$$

From Eq. (4.7) and Eq. (4.8)

$$\frac{L}{H} \left(1 - \frac{L}{H} \times slope\right) \geq (DWR)_{min} \quad (4.9)$$

Manipulating:

$$\left(\frac{L}{H}\right)^2 \times slope - \frac{L}{H} + (DWR)_{min} \leq 0 \quad (4.10)$$

For which the roots of the equation are:

$$\left(\frac{L}{H}\right) = \frac{1 \pm \sqrt{1 - 4 \times (DWR)_{min} \times slope}}{2 \times slope} \quad (4.11)$$

The solution can not have an imaginary part and since the slope and the bite ratio are positive real numbers, it follows that the limiting constraint is:

$$4 \times (DWR)_{min} \times slope \leq 1 \quad (4.12)$$

From which the allowable slope is:

$$slope \leq \frac{1}{4 \times (DWR)_{min}} \quad (4.13)$$

and the maximum slope for an allowable $(DWR)_{min}$ of 0.6 (Wang and Cao 1994b) is:

$$slope_{max} = \frac{1}{4 \times (DWR)_{min}} = 0.417 \quad (4.14)$$

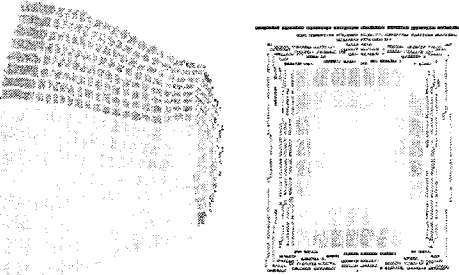
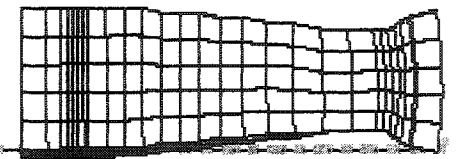
Equation (4.13) represents a new technological bound for incremental forming of tapered sections. This bound will be an element of the adaptive scheduling system.

4.1.3 3-D Geometries Forged on the Virtual Cell

The forging procedure presented in Sections 4.1.1 and 4.1.2 was used to forge the 3-D surfaces shown in Table 4.7. The last example of which represents forging a preform of a connecting rod. It also shows that forging a taper can be carried out with a bite that is less than the recommended one³ if the taper does not extend completely to the free end. The non-deforming material at the end enhances the material flow of the deforming section and restrains it from developing a hourglass shape. It also acts as a source of material that can absorb the non-uniform deformation, acting like a riser in a casting process.

³Recommended bite is the minimum bite that should be used to avoid the appearance of shape defects especially the hourglass shape defect.

Table 4.7: 3-D Shapes Forged in the Virtual Forging Cell

<i>Initial workpiece (mm)</i>	<i>Tolerance required (mm)</i>	<i>Number of forging steps</i>	<i>Bite</i>	<i>Required workpiece</i>
34*38*38	$\pm 1 \text{ mm}$	16 step	24mm	 <p>Pyramid of 38*38mm base, 38mm length and 19*19mm top surface, slope=0.25</p>
27*38*38	$\pm 0.5 \text{ mm}$	142 step	20mm	 <p>Pyramid of 38*38mm base, 40mm length and 14*14mm top surface, slope=0.4</p>
67*20*20	$\pm 1 \text{ mm}$	8steps	10mm	 <p>1. Rectangular block 10*20*20mm 2. Pyramid of 20*20mm base, 80mm length and 0.0625 slope 3. Rectangular block 5*20*20mm</p>

4.2 Wedge Forging on the Forging Cell (an Experimental Case Study)

The shape feedback control procedure (refer to Section 3.3.3) was used to forge a wedge (Fig. 4.6) from annealed aluminum using steel dies mounted on a programmable hydraulic press. The forging tolerance was set to ± 1.5 mm. Figure 4.7 shows the setup of the forging experiment.

4.2.1 Procedure

A workpiece template was made to aid in the feedback procedure. The template was sized to the upper limit of the dimensions of the workpiece. After each forging step the template was used to determine the position at which the workpiece dimension first exceeded the required dimension by the tolerance limit (Fig. 4.8). The workpiece was then marked at this location and a squeezing action of 3 mm was applied starting from the mark to the free end of the workpiece. After each squeezing operation the workpiece was inspected using the template and the width was measured using a vernier caliper to determine the next forging step. The forging schedule corresponding to this feedback control procedure is shown in Table 4.8.

4.2.2 Results

Figure 4.9 shows the dimensions of the forged workpiece. As shown on the figure the wedge is forged within the required tolerance. The free end of the wedge is to be cut where the nonhomogeneous deformation accounted for a 5.7 mm error at the end. Unfortunately this type of error can not be remedied by forging and the material has to be cut at this length. The width of the wedge was inspected by a vernier calliper and found to be 38.1 mm.

The initial block of material used had larger volume than that required to account for the machining allowance and free end error. The initial block was 67 mm length, 38.1 mm width and 38.1 mm height. The corresponding material utilization of the forging operation (taking into account the cut of the free end and the machining allowance) is 92%.

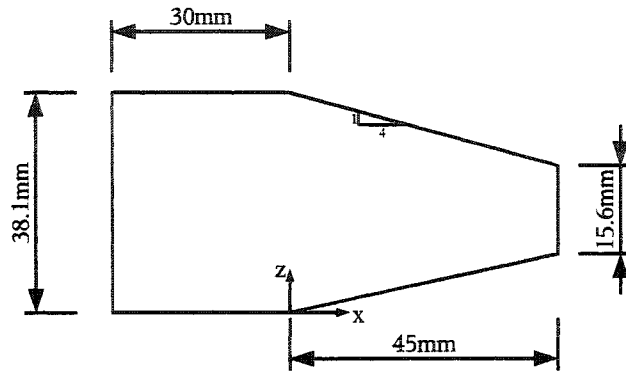


Figure 4.6: Wedge Workpiece (width=38.1 mm)

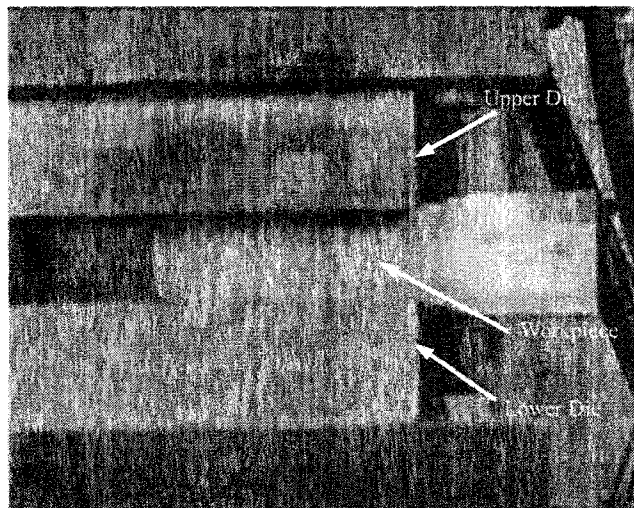


Figure 4.7: Experimental Setup for Forging a Wedge

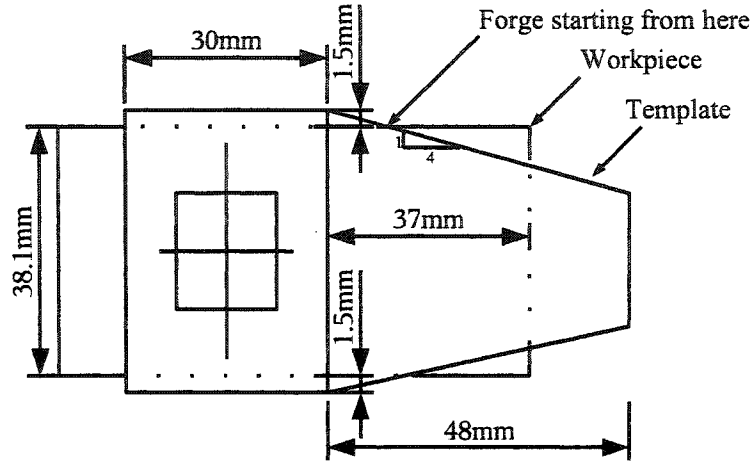


Figure 4.8: Inspection Procedure With Template

Table 4.8: Forging Schedule of Sample Workpiece

Forging Direction	Forging starts at x (mm)	Squeeze Value (mm)
z	6	3
z	12	3
z	18	3
z	24	3
z	30	3
y	0	3
z	10	3
z	23	3
z	30	3
z	36	3
z	42	3
y	0	3

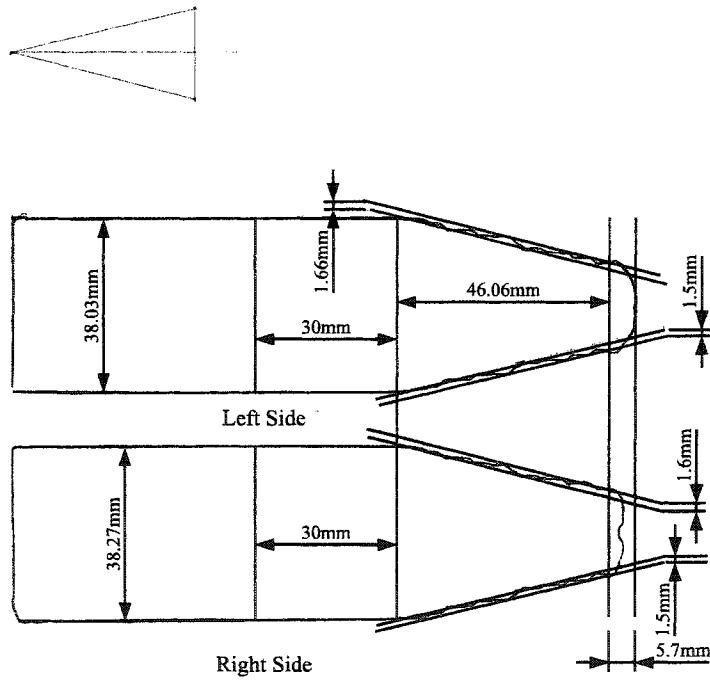


Figure 4.9: Measurements Results

4.3 Summary

The adaptive forging schedule procedure (developed in Section 3.3.5) was used to generate forging schedules that successfully forged a wedge within an arbitrarily targeted tolerance limit. Other forging schedule generation schemes based on spread prediction formulae failed to forge the same wedge within the same targeted tolerance limit.

A demonstration of the operation of the adaptive forging schedule procedure for forging a $2\frac{1}{2}$ -D profile was presented in Section 4.1.1 and a sample of generated 2-D and 3-D profiles were presented in Section 4.1.3.

The convergence rate of the procedure varied with the targeted tolerance on the forged profile, with tighter tolerances requiring disproportionately more forming steps. For this reason, there will be a trade-off between forging and machining time and costs.

A new technological limit on the slope of the profile that can be generated by the process, Eq. (4.13), has also been described (Section 4.1.2). By applying this technological limit as constraint in the adaptive control scheme, the generation of the lapping defects can be eliminated.

Chapter 5

Spread Prediction by the Upper Bound Method (B1)

5.1 Introduction

The developed adaptive control schedule can sometimes be trapped in redundant forging cycles of forging along the width, rotating then forging along the height. Such redundant forging cycles (henceforth termed overhead forging cycles) can be minimized by integrating an accurate spread prediction model with the adaptive schedule as will be demonstrated in Chapter 7. To achieve this result, however, new accurate spread prediction models are necessary. The development of such models is the focus of this chapter.

Current spread prediction models are of poor estimation quality¹ (Nye et al. 2001) and there is a need to develop more accurate models. Currently there are empirical, analytical, finite element and neural network spread prediction models (Section 2.5). Spread prediction models based on finite element analysis require long computation time rendering them unsuitable to be integrated to the online adaptive schedule model. Neural network models requires a comprehensive set of training data that has to be collected from experimental studies. Empirically derived models provide reasonable quality estimates but they are limited to a specific forging operation for specific die and workpiece material. In addition, they normally require lengthy experimental procedures to develop. On the other hand, upper bound spread prediction models are reported to provide comparably good estimates of the material spread in short computational time (Baraya and Johnson 1964; Sagar and Juneja 1979; Li and Zhou 1989; Aksakal et al. 1993, 1997; Nye 1999; Osman and Ferreira 1999). This property makes them a good candidate for online spread prediction for

¹Comparison of spread prediction models with measured spread is presented in Section 6.2.6.

the integration with the adaptive control scheduling model.

In this chapter new spread prediction models based on the upper bound method will be presented in which three approaches are incorporated to enhance the quality of the upper bound solution:

1. Relaxing the assumptions that the effect of the shear strain at the interface between the deforming and non deforming zones of the metal can be neglected (Section 5.3.1).
2. Assuming a material flow pattern that better represents the actual flow in a typical cogging operation² (Section 5.3.2)
3. Relaxing the inferred assumption that forging is a steady state process (Section 5.3.3). This assumption is implicit in all derived spread prediction models where the upper bound solution is only computed at the start of the deformation process and the velocity field is assumed to remain stationary until the end of deformation.

5.2 Formulation of the Upper Bound Method

An exact solution for the forming problem requires the construction of a boundary value problem consisting of integrating a set of continuum mechanics equations with respect to the variables describing the flow kinematics, stress state and body temperature, with specific boundary and initial conditions. The resultant stress field should be continuous and satisfy the equilibrium conditions at every point in the deformation zone (i.e., the net forces are equal to zero) and satisfy the boundary values. The velocity field should be continuous and satisfy the boundary values (at the die-workpiece interface).

The calculation of the exact loads or forces to cause a plastic flow is often difficult. Exact solutions require both the stress equilibrium and the kinematically admissible velocity fields of the metal flow to be satisfied simultaneously. In the absence of exact solutions to predict the required load to cause plastic flow in forming problems, even for simple cases, researchers used converging approximation procedures by relaxing in whole or part either the kinematic or statical boundary conditions and field equations (Hill 1963; Hosford and Caddell 1993; Kolmogorov et al. 1999).

In the Upper Bound solution the stress equilibrium constraint is relaxed, and knowing before hand the final shape of the workpiece, an artificial velocity field for material flow is constructed. This arbitrary velocity field is guaranteed to result in a total work that is equal to or greater than the

²Cogging is regarded as the fundamental incremental forging operation.

actual total work. The constructed velocity field must satisfy incompressibility and boundary conditions, and it may have a predefined discontinuity in it. The constructed kinematically admissible velocity field will have some free parameters that are determined by minimizing the total work.

The method requires a prior knowledge of the instantaneous shape of the considered body, together with the local yield functions at all points. For most forming operations the final shape of the material is dictated by the shape of the forming die, where the die bounds the flow pattern of the material and sets a boundary constraint on the velocity field. In contrast, for forming processes where the dies do not totally encapsulate the plastic region of the deformed material, as in the case of open die forging and rolling, one must assume the instantaneous shape of the metal as it is being deformed.

For forging, in particular, too many factors affect the instantaneous shape of the deformed metal making it hard to predict. Technological bounds are frequently used to set some boundaries for stability regions for different instantaneous shapes (Shutt 1963; Li and Zhou 1989; Wang and Cao 1994b), yet there are few published papers in this field. Hence, the upper bound method can only be used to predict the final shape of the workpiece in forging operations where the instantaneous shape is known before hand. It can thus be used to predict the forged dimensions of the workpiece assuming the deformed material will take a specific shape, known before hand either through experience or pilot experimental studies.

For simple cogging operations the deformed shape of the workpiece normally assumes a shape pattern that can be described conveniently with a polynomial function. Second and third degree polynomials³ have been reported to successfully approximate the actual forged shape (Shutt 1960; Baraya and Johnson 1964; Ferreira and Osman 1997; Aksakal et al. 1997; Nye 1999). However, assuming a uniform shape of deformation has been reported to successfully approximate the average increase in width (Tarnowski 1950; Tomlinson and Stringer 1959; Wisterich and Shutt 1959; Shutt 1960; Aksakal et al. 1997). For the adaptive forging schedule developed in this study only the average and maximum increase in width are required and knowing that the average increase in width can be used to compute the maximum increase in width, through a proper transformation function depending on the assumed degree of the deformation pattern, only uniform shape of deformation will be considered.

³Reader can refer to Section 2.5 on spread prediction methods in cogging operations.

5.2.1 Assumptions

The basis of the upper bound analysis is (as presented in Hosford and Caddell (1993)):

- An internal flow field is assumed and must account for the required shape change. As such, the field must be geometrically self-consistent.
- The energy consumed internally in this deformation field is calculated using the appropriate strength properties of the work material.
- The external forces (or stresses) are calculated by equating the external work with the internal energy consumption.
- Constant friction factor model for friction analysis is used.

In applying the upper bound method in forming the following simplifying assumptions are made (Hosford and Caddell 1993):

- The work material is isotropic and homogeneous.
- The material is assumed to be rigid perfectly plastic thus the yield stress is assumed to be constant and the effects of strain hardening and strain rate on flow stress are neglected.
- The elastic deformation and inertia forces are neglected
- The plastic deformation of the material follows the Levy-Mises flow rule and Von Mises yield criterion.

The total power is the summation of the deformation power, internal shearing power and power lost to overcome friction at the tool workpiece interface. Each is discussed in the following sections

5.2.2 The Deformation Power

The deformation power is the power required to forge the material plastically. The friction at the tool workpiece interface is ignored and the material is assumed to be free from internal discontinuities. The rate of work per unit volume for Von Mises material is:

$$\dot{w}_d = \sigma_{ij} \dot{\epsilon}_{ij} \quad (5.1)$$

and in terms of the stress deviators σ'_{ij} ($\sigma'_{ij} = \sigma_{ij} - \sigma_{mean}$):

$$\dot{w}_d = \sigma'_{ij} \dot{\epsilon}_{ij} \quad (5.2)$$

and for a perfectly plastic material following the Levy-Mises flow rule the infinitesimal work per unit volume is:

$$\dot{w}_d = \frac{2}{\sqrt{3}} \sigma_0 \sqrt{\frac{1}{2} \dot{\epsilon}_{ij} \dot{\epsilon}_{ij}} \quad (5.3)$$

where σ_0 is the flow stress. Integrating this infinitesimal work formula, Eq. (5.3), over the deforming volume the total deformation power is obtained as:

$$\dot{W}_d = \int_V \dot{w}_d dV \quad (5.4)$$

$$\dot{W}_d = \sqrt{\frac{2}{3}} \sigma_0 \int_V \sqrt{\dot{\epsilon}_{ij} \dot{\epsilon}_{ij}} dV \quad (5.5)$$

5.2.3 The Shear Power

The shear power is a direct result of discontinuities in the artificial velocity field. A discontinuity results in slipping and energy dissipation to overcome shear at the slip surface. The volume crossing a slip surface remains constant thus the velocity component normal to the surface remains constant and the discontinuity in the velocity field occurs in the velocity component tangent to the surface. Knowing the shear yield stress of the material, τ :

$$\tau = \frac{\sigma_0}{\sqrt{3}} \quad (5.6)$$

the shear power, \dot{W}_s , is calculated by integrating the energy dissipated along the shear surface, S , due to the velocity discontinuity, Δv :

$$\dot{W}_s = \frac{\sigma_0}{\sqrt{3}} \int_s |\Delta v| dS \quad (5.7)$$

5.2.4 The Friction Power

In plastic deformation processes friction occurs at the tool-workpiece interface. The friction resistance significantly affects the forming load and metal flow. The friction losses can be expressed as a function of the material shear stress in a similar manner as for the shear power.

The friction stress at the tool workpiece interface according to the constant shear friction model using the friction factor m , is given by Eq. (5.8):

$$\tau = m \frac{\sigma_0}{\sqrt{3}} \quad (5.8)$$

Hence the work dissipated to overcome friction knowing the velocity discontinuity, Δv , at the tool workpiece interface, A , is:

$$\dot{W}_f = \frac{m \sigma_0}{\sqrt{3}} \int_A |\Delta v| dA \quad (5.9)$$

5.2.5 Upper Bound Solution Procedure

The total dissipated power is the sum of the deformation, shear and friction powers.

$$\dot{W}_t = \dot{W}_d + \dot{W}_s + \dot{W}_f \quad (5.10)$$

Assuming a kinematically admissible velocity field described by a mathematical formulation $\dot{u}(x, y, z)$ that has some pseudo-free parameters, such as a scale or shape factor of the velocity distribution, the plastic strain rate can be calculated as follows:

$$\dot{\epsilon}_x = \frac{\partial \dot{u}_x}{\partial x} \quad (5.11)$$

$$\dot{\epsilon}_y = \frac{\partial \dot{u}_y}{\partial y} \quad (5.12)$$

$$\dot{\epsilon}_z = \frac{\partial \dot{u}_z}{\partial z} \quad (5.13)$$

The total power exerted by the tool given the die velocity, v_d , is:

$$\dot{W}_t = p_{av} A v_d \quad (5.14)$$

where p_{av} is the average pressure acting at the tool workpiece interface and A is the contact area. The average pressure, p_{av} , is calculated by equating the total power exerted by the tool to the total dissipated power as:

$$p_{av} = \frac{1}{A v_d} (\dot{W}_d + \dot{W}_s + \dot{W}_f) \quad (5.15)$$

The pseudo distribution parameters of the velocity field can be found by minimizing p_{av} , and thus the total power.

5.3 Metal Flow Analysis for Cogging Operation

In this section upper bound solutions to predict material spread for cogging between flat dies are presented. The fundamental assumptions of the upper

bound method, presented in Section 5.2.1, are applied here. Two artificial velocity fields are presented and the spread prediction of their associated solutions are compared to the actual and other spread prediction formulae.

There are two methods to study side spread for flat-tool cogging operations as presented in the literature.

- a) Indenting a flat die in the workpiece material and measuring the spread and elongation (Aksakal et al. 1997; Baraya and Johnson 1964; Sun et al. 1983; Kiefer and Shah 1990; Ferreira and Osman 1997; Mardanpour and Chitkara 1998; Nye 1999; Nye et al. 2001). This approach has the advantage of controlling the bite as forging progresses so the experimental setup is performed in a much more controlled environment with exact measurement of the extension, side spread and exact control on the bite, (in such case the bite is the die width) (Fig. 5.1). A difference between indentation and cogging is that the constraint imposed on the end surfaces of the deforming zone by the non-deforming part of the material is symmetric for indentation and nonsymmetric for cogging.
- b) Simulating the cogging operation and measuring the accumulated increase in length and the side spread of the material (Tarnowski 1950; Tomlinson and Stringer 1959; Appleton et al. 1979; Sun et al. 1983). In such a procedure there is much less control on the bite as the bite changes as the material deforms under the die. The die positioning error and inaccurate prediction of the expected extension after each squeezing action further increase the error in the applied bite rendering the experimental results and conclusions questionable. On the other hand, this procedure better represents the real forging process (as incremental forging is the net result of incremental cogging operations). In addition the constraint imposed by the non-deforming part of the material on the deforming zone is not the same on both end surfaces as presented in (Fig. 5.1).

The first presented upper bound solution (Section 5.3.1) is a generalization of the Aksakal et al. (1997) uniform pattern of deformation solution for flat-tool indentation problem. The main difference from the Aksakal et al. (1997) solution is that the shear work at the interface between the deforming and non-deforming zones of the workpiece was included. The equations have been re-derived such that the nomenclature is consistent. In addition, a proof of the Tarnowski (1950) spread formula is presented in Appendix D assuming a uniform pattern of deformation and analyzing only the friction work for a simple upsetting operation.

The second upper bound solution (Section 5.3.2) is derived for the cogging operation and taking into consideration the uneven restriction from the

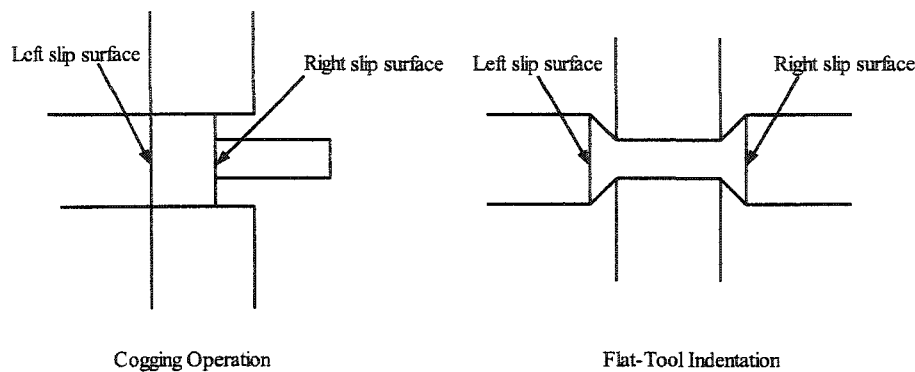


Figure 5.1: Flat Tool Indentation vs Cogging

non-deforming zone on the deforming one. A “fish bone” material spread pattern which closely resembles the spread pattern observed in pilot experimental and simulation studies is presented.

A new analysis approach based on the upper bound technique best suited for non-steady state forming operations (such as forging) is presented in Section 5.3.3 and its application in center indentation is demonstrated. The new method named “The Incrementally Updated Upper Bound Solution” gave the best results in terms of spread prediction for center indentation problems as will be shown in Section 6.2.6.

5.3.1 Homogeneous Pattern of Deformation - Center Indentation Case

Material spread in flat-tool cogging⁴ is often analyzed by studying spread in flat-tool indentation (Aksakal et al. 1993, 1997). The dies squeeze the metal along its height. As a result of the squeezing action the material spreads in the lateral and longitudinal directions. The aim of this model is to determine the proportion of the squeezed volume spreading in the longitudinal, forging feed direction and in the lateral, width direction. It must be noted that in generating the forging schedule the average and maximum values of the spread are required. The maximum is used for error computation and for die positioning at the start of the forging operation, and the average is used in calculating the value of the volume to be squeezed.

Actual metal flow normally assumes a higher-order shape of deformation, but as the average and maximum values of the forged width is of interest,

⁴Refer to Section 2.3.1 and Figs. 2.10 and 5.1.

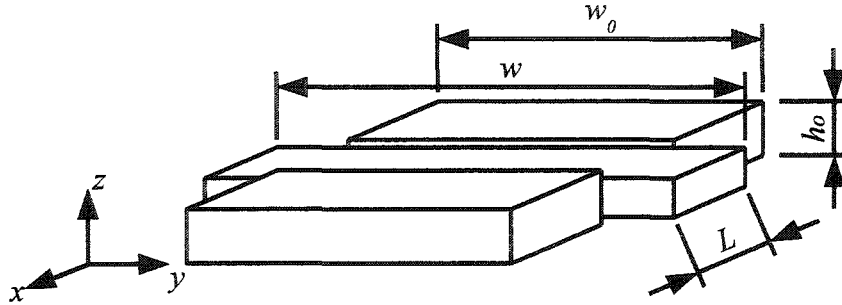


Figure 5.2: Homogeneous Deformation Pattern

a homogeneous parallel flow of the material is assumed.

Velocity Field

The assumed parallel velocity field results in a constant normal strain distribution with no shear components. Hence, the three spread directions are the principal directions and the squeezed volume will retain its geometric shape. Figure 5.2 shows the idealized flow pattern to be expected from such homogeneous pattern of deformation when cogging a rectangular bar between flat dies. The global coordinates are chosen such that the x -axis is the forging feed direction; the y -axis is the width / side spread direction and the z -axis is the squeezing direction.

At the start of the forging operation the deformed zone length, width and height are L_0^5 , w_0 , and h_0 , respectively. As the die indents the workpiece the deformed zone new length, width and height are L , w , and h , respectively.

The assumed velocity field is symmetric along the three major axes and thus only an octant of the deformed zone will be studied. The centroid of the deformed zone (henceforth referred to as the origin) is stagnant and at this point all three principal components of the velocity, v_x , v_y , v_z , are zero. The velocity components are assumed to vary linearly from zero at the origin to a maximum at the surface. At the start of the deformation process the surfaces of the studied octant are:

Left surface

$$x = 0 \quad (5.16)$$

Right surface

⁵ L_0 is also the bite and equals to the width of the forging die.

$$x = x_0 = \frac{L}{2} \quad (5.17)$$

Back surface

$$y = y_0 = \frac{w}{2} \quad (5.18)$$

Front surface

$$y = 0 \quad (5.19)$$

Top surface

$$z = z_0 = \frac{h}{2} \quad (5.20)$$

Bottom surface

$$z = 0 \quad (5.21)$$

Based on the assumption that the velocities vary linearly, the strain rates are constants. Using the spread coefficient, s , which has been previously defined⁶ as the ratio between the width strain and the height strain the relations for the strain rates are:

$$\dot{\epsilon}_y = -s \dot{\epsilon}_z \quad (5.22)$$

using the incompressibility condition:

$$\dot{\epsilon}_x + \dot{\epsilon}_y + \dot{\epsilon}_z = 0 \quad (5.23)$$

the longitudinal strain rate is:

$$\dot{\epsilon}_x = -\dot{\epsilon}_y - \dot{\epsilon}_z = -(1-s) \dot{\epsilon}_z \quad (5.24)$$

and the velocity components are obtained by integrating the corresponding strain rate:

$$v_x = \int_0^x \dot{\epsilon}_x dx = x \dot{\epsilon}_x \quad (5.25)$$

$$v_y = \int_0^y \dot{\epsilon}_y dy = y \dot{\epsilon}_y \quad (5.26)$$

$$v_z = \int_0^z \dot{\epsilon}_z dz = z \dot{\epsilon}_z \quad (5.27)$$

⁶Refer to Section 2.5.1.

The strain rate in the vertical direction, $\dot{\epsilon}_z$, is calculated by substituting the values of the velocity and the height (i.e., $v_z = -v_d$ and $z = z_0$) at the top surface in Eq. (5.27), where v_d is the die velocity at the top surface. Then:

$$\dot{\epsilon}_z = -\frac{v_d}{z_0} \quad (5.28)$$

and from Eq. (5.22) the width strain rate, $\dot{\epsilon}_y$, is:

$$\dot{\epsilon}_y = s \frac{v_d}{z_0} \quad (5.29)$$

and from Eq. (5.24) the longitudinal strain rate, $\dot{\epsilon}_x$, is:

$$\dot{\epsilon}_x = (1 - s) \frac{v_d}{z_0} \quad (5.30)$$

Thus the velocity field equations are obtained by substituting the values of the strain rates, Eqs. (5.28, 5.29, 5.30), into the velocity formulae, Eqs. (5.25, 5.26, 5.27):

$$v_x = (1 - s) \frac{v_d}{z_0} x \quad (5.31)$$

$$v_y = s \frac{v_d}{z_0} y \quad (5.32)$$

$$v_z = -\frac{v_d}{z_0} z \quad (5.33)$$

Work to Overcome Friction

The work to overcome friction is computed according to Eq. (5.9) and assuming a constant shear friction model with a friction constant of m :

$$\dot{W}_f = \frac{m \sigma_0}{\sqrt{3}} \int_A \sqrt{v_x^2 + v_y^2} dx dy \quad (5.34)$$

and from Eqs. (5.31 and 5.32):

$$dv_x = (1 - s) \frac{v_d}{z_0} dx \quad (5.35)$$

$$dv_y = s \frac{v_d}{z_0} dy \quad (5.36)$$

$$dx dy = \frac{z_0^2}{v_d^2} \frac{1}{s(1-s)} dv_x dv_y = C_2(s) dv_x dv_y \quad (5.37)$$

and assuming that the spread coefficient, s , is independent of the x, y position, the homogeneous pattern of deformation friction work is

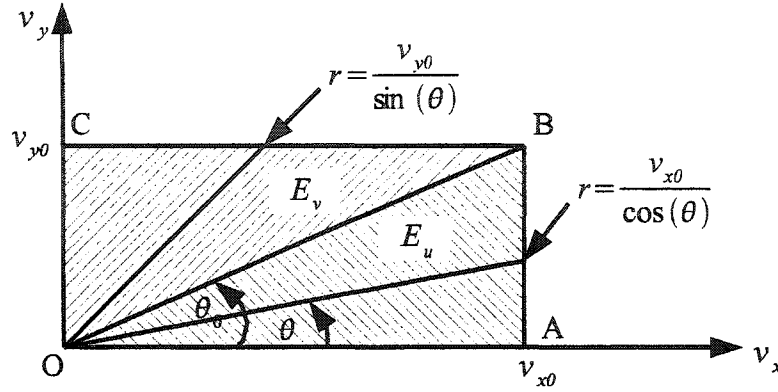


Figure 5.3: Integration Bounds of the Friction Work on the Interface Surface for (Cartesian And Polar Representations)

$$\begin{aligned}
 \dot{W}_f &= \frac{m \sigma_0}{\sqrt{3}} C_2(s) \int_0^{v_{x0}} \int_0^{v_{y0}} \sqrt{v_x^2 + v_y^2} dv_y dv_x \\
 &= C_3(s) \int_0^{v_{x0}} \int_0^{v_{y0}} \sqrt{v_x^2 + v_y^2} dv_y dv_x
 \end{aligned} \quad (5.38)$$

where,

v_{x0} is the x velocity component at the right surface ($x = x_0$).

v_{y0} is the y velocity component at the back surface ($y = y_0$).

The integral can be solved by transforming the cartesian co-ordinates to polar co-ordinates (Fig. 5.3). Thus:

$$v_x = r \cos \theta \quad (5.39)$$

$$v_y = r \sin \theta \quad (5.40)$$

$$\dot{W}_f = C_3(s) \int \int r \ r dr d\theta \quad (5.41)$$

where,

$$r = \begin{cases} \frac{v_{x0}}{\cos \theta} & \text{for } 0 \leq \theta \leq \theta_0 \\ \frac{v_{y0}}{\sin \theta} & \text{for } \theta_0 \leq \theta \leq \frac{\pi}{2} \end{cases} \quad (5.42)$$

substituting:

$$\begin{aligned}\dot{W}_f &= C_3(s) \left[\int_0^{\theta_0} \int_0^{\frac{v_{x0}}{\cos\theta}} r^2 dr d\theta + \int_{\theta_0}^{\frac{\pi}{2}} \int_0^{\frac{v_{y0}}{\sin\theta}} r^2 dr d\theta \right] \\ &= \frac{C_3(s)}{3} \left[v_{x0}^3 \int_0^{\theta_0} \frac{d\theta}{\cos^3\theta} + v_{y0}^3 \int_{\theta_0}^{\frac{\pi}{2}} \frac{d\theta}{\sin^3\theta} \right] \quad (5.43)\end{aligned}$$

The work against friction can be divided into two parts, work against friction in $\triangle OAB$, $C_3(s) E_u$, and work against friction in $\triangle OBC$, $C_3(s) E_v$ (Fig. 5.3). Thus the work against friction is:

$$\dot{W}_f = C_3(s) (E_u + E_v) \quad (5.44)$$

reformulating using ϕ and r_0 , where $\phi = \tan\theta_0 = \frac{v_{y0}}{v_{x0}}$ and, $r_0 = \sqrt{v_{x0}^2 + v_{y0}^2}$ E_u and E_v can be expressed as:

$$E_u = \frac{1}{6} v_{x0} v_{y0} r_0 + \frac{v_{x0}^3}{6} \ln (\sqrt{1 + \phi^2} + \phi) \quad (5.45)$$

$$E_v = \frac{1}{6} v_{x0} v_{y0} r_0 - \frac{v_{y0}^3}{6} \ln (\frac{\sqrt{1 + \phi^2} - 1}{\phi}) \quad (5.46)$$

The Shear Power

The shear work is a result of the velocity discontinuity between the sliding, deforming zone, and the stationary non-deforming zone (Figs. 5.1 and 5.2). The relative sliding occurs on the right side of the deformation zone, line AB (Fig. 5.3). Figure 5.4 shows the right surface of the deformed billet, $x = x_0$, on which the contact area where sliding occurs between the deformed and undeformed zone is identified.

The shear work formula is given by Eq. (5.7). In this case the shear work, \dot{W}_s , is:

$$|\dot{W}_s| = \frac{z_0^2}{s v_d^2} \frac{\sigma_0}{\sqrt{3}} \int_0^{v_{yi}} \int_0^{v_{z0}} \sqrt{v_y^2 + v_z^2} dv_y dv_z \quad (5.47)$$

The solution of this formula is similar to the solution of the frictional work formula and in its final form the shear work is

$$\begin{aligned}\dot{W}_s &= \frac{\sigma_0 z_0^2}{6 \sqrt{3} s v_d^2} \left[2 v_{yi} v_{z0} r_0 + v_{yi}^3 \ln (\sqrt{1 + \psi^2} + \psi) \right. \\ &\quad \left. - v_{z0}^3 \ln (\frac{\sqrt{1 + \psi^2} - 1}{\psi}) \right] \quad (5.48)\end{aligned}$$

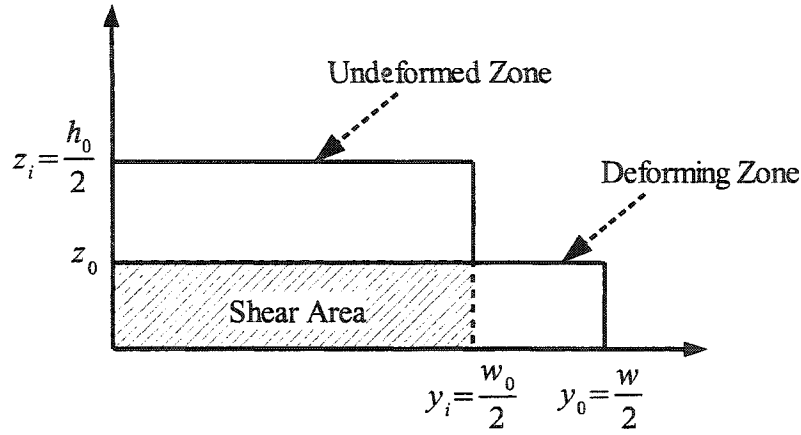


Figure 5.4: Sliding Area for Uniform Deformation Pattern

where,

$$r_0 = \sqrt{v_{yi}^2 + v_{z0}^2},$$

$$\psi = \tan^{-1} \frac{v_{z0}}{v_{yi}}$$

Deformation Work

The deformation work is calculated according to Eq. (5.5) restated here:

$$\dot{W}_d = \sqrt{\frac{2}{3}} \sigma_0 \int_V \sqrt{(\dot{\epsilon}_x^2 + \dot{\epsilon}_y^2 + \dot{\epsilon}_z^2)} dV \quad (5.49)$$

substituting the values of the strain rates, Eqs. (5.28, 5.29, 5.30), and manipulating, the deformation work becomes:

$$\dot{W}_d = \frac{2}{\sqrt{3}} \sigma_0 \frac{v_d}{z_0} \sqrt{1 - s + s^2} \frac{w h L}{2 2 2} \quad (5.50)$$

At any instantaneous height, h , the deformation work is:

$$\dot{W}_d = \frac{L w h}{2\sqrt{3}} \frac{v_d}{h_0} \sigma_0 \sqrt{1 - s + s^2} \quad (5.51)$$

and at the start of the deformation is:

$$\dot{W}_d = \frac{L_0 w_0}{2\sqrt{3}} v_d \sigma_0 \sqrt{1 - s + s^2} \quad (5.52)$$

The Total Power

The total power is the summation of all the powers:

$$\dot{W}_t = \dot{W}_d + \dot{W}_s + \dot{W}_f \quad (5.53)$$

Equating this power to the external power exerted by the tool, \dot{W}_t , Eq. (5.14) one obtains:

$$p_{av} A v_d = \dot{W}_d + \dot{W}_s + \dot{W}_f \quad (5.54)$$

$$p_{av} = \frac{4}{w L v_d} (\dot{W}_d + \dot{W}_s + \dot{W}_f) \quad (5.55)$$

The velocity fields and the spread coefficient, s , are found by minimizing the total work, or, the average pressure, p_{av} , by varying s , Eq. (5.56). This can be easily computed using any minimum search algorithm. In this research the Nelder-Mead simplex method (Olsson and Nelson 1975) was used to find the spread coefficient, s , corresponding to the minimum average pressure.

$$\min_s p_{av} \quad (5.56)$$

Algorithm 5.1 Homogeneous Pattern of Deformation Upper Bound Algorithm

Inputs: Initial workpiece height h_i , length l_i , and width w_i , final workpiece height h_f .

Output: The spread coefficient s .

The spread coefficient s is computed by numerically minimizing the average pressure p_{av} with respect to the spread coefficient using the Nelder-Mead simplex method

$$\min_s p_{av}$$

where the average pressure p_{av} is given by

$$p_{av} = \frac{4}{w L v_d} (\dot{W}_d + \dot{W}_s + \dot{W}_f)$$

and the deformation power \dot{W}_d is given by Eq. (5.52).

the shear power \dot{W}_s is given by Eq. (5.48).

and the friction power \dot{W}_f is given by Eq. (5.44).

5.3.2 Fish-Bone Pattern of Deformation - Continuous Cogging Case

An assumption in the homogeneous pattern of deformation is that the deforming zone is symmetrically restricted by the non-deforming zone (Fig. 5.1). However, in cogging operations (Fig. 5.5) the left and right surfaces of the deformation zones are subjected to uneven restriction by the non-deforming zones.

In order for the material to deform at the left surface, it must overcome the shear resistance against the undeformed region. In the simplest analysis it should overcome the shear resistive work in order to slip along the $ABCD$ area (Fig. 5.5). Similarly, the right surface of the deforming zone has to overcome the shear resistance against the previously deformed region, with a corresponding shear area $EFGH$. It can thus be seen that the material in the deforming zone is unevenly restricted by stagnant material from the left and right surfaces. This effect results in the fish-bone shape where the side spread of the material during deformation is higher at its right surface (lower resistance) than at its left surface (higher resistance) (an example is shown in Fig. 5.6). In this section an upper bound solution to predict side material spread for the fish-bone deformation pattern is developed.

Velocity Field

Figure 5.7 shows the fish-bone deformation pattern. The global coordinates coincide with the workpiece coordinates, where the x -axis is the forging feed direction, the y -axis is the width / side spread direction and the z -axis is the squeezing direction. A flat die indents the workpiece where the contact length with the die is the starting bite⁷ L_0 . The original width of the workpiece is w_0 , and the original height is h_0 . As the die indents in the workpiece the instantaneous deformation zone has a height h , width w , and length L . The origin at the start of deformation is set at the centroid of the deforming zone.

The assumed velocity field is symmetric along the x and z axes and thus only a quarter of the deformed zone will be studied. The centroid of the deformed zone (henceforth referred to as the origin) is a stagnant point and thus all three principal components of the velocity, v_x , v_y , v_z , are zero at this point. The velocity components also have their maximum value at the surface of the deformed zone. The velocity components of the velocity field are assumed to vary linearly from the origin to the surface.

Location Of The Centroid

The centroid is located on the z and x symmetric planes. The location

⁷The bite increases as the material flows under the die during the deformation operation.

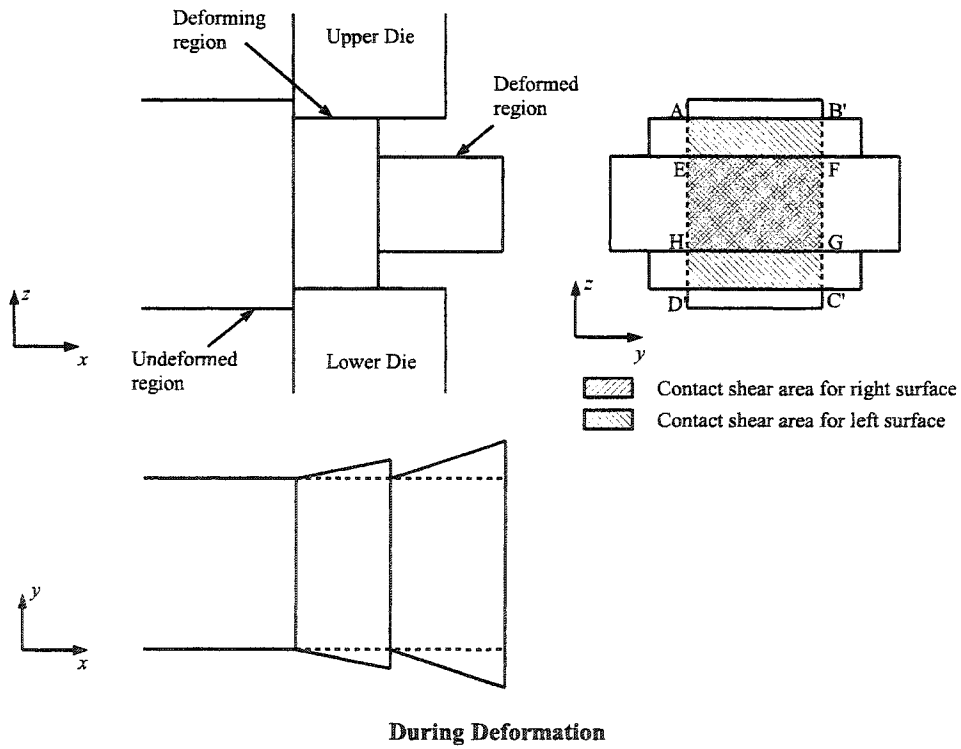
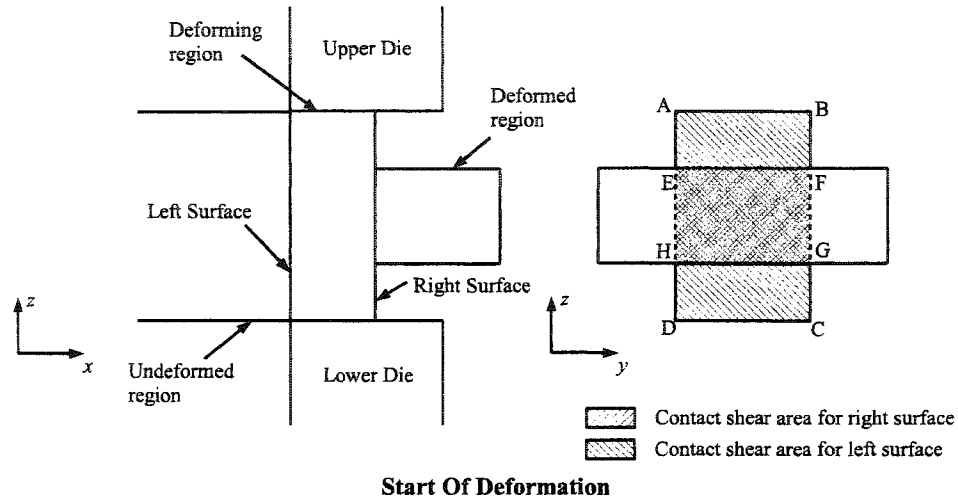


Figure 5.5: Development of Fish-Bone Deformation Pattern

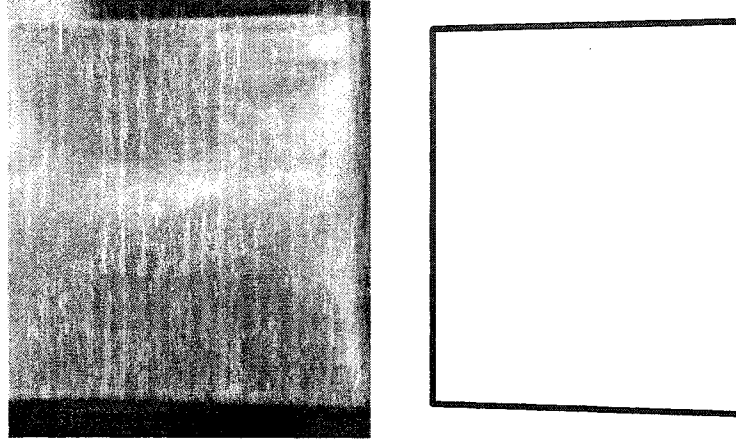


Figure 5.6: Typically Observed Fish-Bone Deformation Pattern in a Cogging Operation

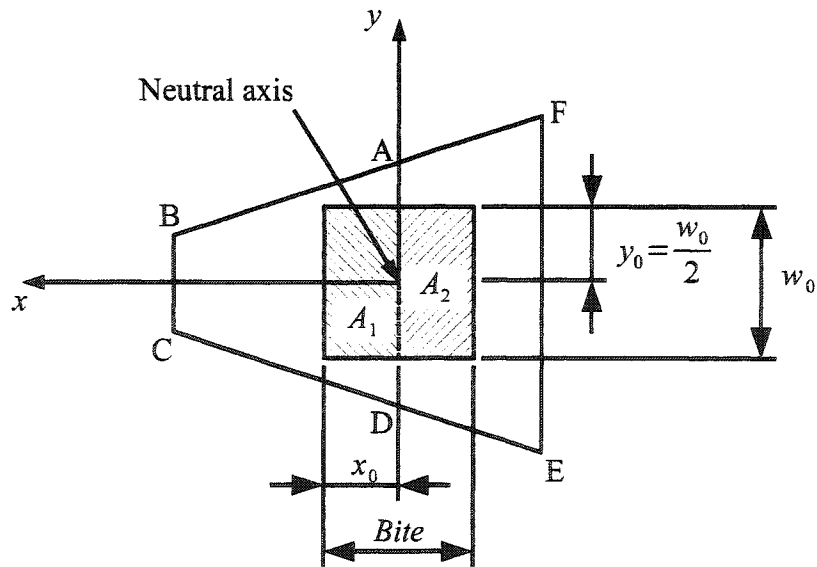


Figure 5.7: Fish-Bone Deformation Pattern

of the centroid along the x axis will move in the negative x direction as the deformation progresses. The instantaneous location of the centroid on the x -axis can be calculated using one of two simplifying assumptions.

- Vertical planes (planes parallel to the z -axis) will remain parallel to the z -axis, thus the location of the centroid at any arbitrary deformation height is calculated by equating the ratio of the undeformed area $\frac{A_1}{A_2}$ to the ratio of the deformed area $\frac{\text{area of } ABCD}{\text{area of } EFAD}$ (Fig. 5.7).
- At the start of the forging operation, as a result of symmetry and to satisfy the equilibrium conditions, the centroid should be located at the center of the deformation zone. $x_0 = \frac{\text{Bite}}{2}$.

For this analysis the upper bound solution is computed at the start of the deformation process and thus the second assumption is implemented. The longitudinal component of the velocity field, v_x , is symmetric around the yz -plane. The vertical component of the velocity field, v_z , is symmetric around the xy -plane. While the spread component of the velocity, v_y , has no axis of symmetry. In the analysis the studied deformation region will be divided into two zones: Zone-1 extends from $x = 0$ to $x = x_0$ and on which A_1 is located and Zone-2 extends from $x = 0$ to $x = -x_0$ and on which A_2 is located.

The surfaces of the studied deformation region at the start of deformation are:

Left surface

$$x = -\frac{\text{Bite}}{2} = -x_0 \quad (5.57)$$

Right surface

$$x = x_0 = \frac{\text{Bite}}{2} \quad (5.58)$$

Back surface

$$y = y_0 = \frac{w_0}{2} \quad (5.59)$$

Front surface

$$y = 0 \quad (5.60)$$

Top surface

$$z = z_0 = \frac{h_0}{2} \quad (5.61)$$

Bottom surface

$$z = 0 \quad (5.62)$$

The velocity component in the vertical direction, v_z , can be expressed in the same way as it was for the homogeneous pattern of deformation. It varies linearly from a value of zero at the xy -plane to the die velocity at the interface surface. Thus it can be expressed as:

$$v_z = -\frac{v_d}{z_0} z = -C_0 z \quad (5.63)$$

The velocity component in the spread direction, v_y , has the following characteristics:

$$v_y = \begin{cases} 0 & x = x_0 \\ 0 & y = 0 \\ v_{y\max} & (-x_0, y_0) \end{cases}$$

Assuming that the maximum value of the velocity component is given by:

$$v_y = 2 \alpha C_0 y_0 \quad \text{at} \quad (-x_0, y_0) \quad (5.64)$$

where α is a proportionality constant that reflects the balance of material spreading in the width and longitudinal directions. It will be optimized later to minimize the total work. This parameter is similar to the spread coefficient, s , of the homogeneous pattern of deformation.

A constructed function for v_y that satisfies the linearity and above mentioned conditions is:

$$v_y = \alpha C_0 y \left(1 - \frac{x}{x_0} \right) \quad (5.65)$$

The vertical and side strain rates, $\dot{\epsilon}_y$ and $\dot{\epsilon}_z$ are:

$$\dot{\epsilon}_y = \frac{\partial v_y}{\partial y} = \alpha C_0 \left(1 - \frac{x}{x_0} \right) \quad (5.66)$$

$$\dot{\epsilon}_z = \frac{\partial v_z}{\partial z} = -C_0 \quad (5.67)$$

from constancy of volume $\dot{\epsilon}_x$ is:

$$\dot{\epsilon}_x = -\dot{\epsilon}_y - \dot{\epsilon}_z = C_0 \left[\left(1 - \alpha \right) + \alpha \frac{x}{x_0} \right] \quad (5.68)$$

thus the velocity component in the longitudinal direction can be found by integrating Eq. (5.68):

$$v_x = \int_0^x \dot{\epsilon}_x dx = C_0 x \left[1 - \alpha \left(1 - \frac{x}{2x_0} \right) \right] \quad (5.69)$$

and the shear strain rate in the xy -plane is:

$$\dot{\epsilon}_{xy} = \frac{1}{2} \left(\frac{\partial v_y}{\partial x} + \frac{\partial v_x}{\partial y} \right) = -\frac{1}{2} \frac{\alpha C_0 y}{x_0} \quad (5.70)$$

The Total Power

The friction power can be calculated in accordance to Eq. (5.9):

$$\dot{W}_f = \frac{m \sigma_0}{\sqrt{3}} \int_{-x_0}^{x_0} \int_0^{y_0} \sqrt{v_x^2 + v_y^2} dx dy \quad (5.71)$$

The shear power can be calculated in accordance to Eq. (5.7):

$$\dot{W}_s = \frac{\sigma_0}{\sqrt{3}} \int_0^{y_0} \int_0^{z_0} \sqrt{v_y^2 + v_z^2} dy dz \quad (5.72)$$

The deformation power is calculated in accordance to Eq. (5.5):

$$\bar{\epsilon} = \sqrt{\frac{2}{3}} \sqrt{\dot{\epsilon}_x^2 + \dot{\epsilon}_y^2 + \dot{\epsilon}_z^2 + 2 \dot{\epsilon}_{xy}^2} \quad (5.73)$$

$$\dot{W}_d = \sqrt{\frac{2}{3}} \sigma_0 \int_{-x_0}^{x_0} \int_0^{y_0} \int_0^{z_0} \sqrt{\dot{\epsilon}_x^2 + \dot{\epsilon}_y^2 + \dot{\epsilon}_z^2 + 2 \dot{\epsilon}_{xy}^2} dx dy dz \quad (5.74)$$

The total power, W_t , can be calculated from Eq.(5.10), and the optimum value of α can be found by minimizing the average pressure, p_{av} , calculated from Eq. (5.75). As an analytical solution can not be found for W_t , both the integration and optimization are performed numerically. Algorithm 5.2 summarizes the fish bone upper bound model for spread prediction.

$$p_{av} = \frac{4}{w_0 B v_d} (\dot{W}_d + \dot{W}_s + \dot{W}_f) \quad (5.75)$$

Algorithm 5.2 Fish-Bone Pattern of Deformation Upper Bound Algorithm

Inputs: Initial workpiece height h_i , length l_i , and width w_i , final workpiece height h_f .

Output: The velocity field parameter α .

The velocity field parameter α is computed by numerically minimizing the average pressure p_{av} with respect to the spread coefficient using the Nelder-Mead simplex method

$$\min_s p_{av}$$

where the average pressure p_{av} is given by

$$p_{av} = \frac{4}{w_0 B v_d} (\dot{W}_d + \dot{W}_s + \dot{W}_f)$$

and the deformation power $\dot{W}_d =$ is computed by the numerical integration of Eq. (5.74).

the shear power \dot{W}_s is given computed by the numerical integration of Eq. (5.72).

and the friction power \dot{W}_f is given by the numerical integration of Eq. (5.71).

5.3.3 Incrementally Updated Upper Bound Method

The upper bound solution is used to compute the forged shape assuming a particular deformation pattern will occur (defined by the assumed velocity field). In the analysis of the solution the assumed velocity field is treated as if it is stationary throughout the forging operation and is only computed at the start of the forging action. However, the velocity field changes dynamically during a single forging step (Hill 1963).

An enhancement to the solution obtained by the upper bound method is to divide the total reduction in height into a number of smaller reduction intervals and to calculate the instantaneous upper bound solution at the start of each interval, update the shape assuming the velocity field will remain unchanged in this small interval then calculate the upper bound solution for the next interval using the updated shape. This procedure should be applied iteratively until the final deformed height is reached.

A demonstration of the operation of the process is given next for a center indentation problem assuming a homogeneous pattern of deformation. Such problem was treated earlier in Section 5.3.1 using a traditional upper bound solution. The velocity field components corresponding to the uniform pattern of deformation are given by Eqs. (5.31, 5.32, 5.33) and the upper bound solution of the spread coefficient, s , is given by Eq. (5.56). The deformed workpiece width and length can thus be predicted using Eqs. (2.3 and 2.2).

To apply the Incrementally Updated Upper Bound method the total reduction in height is divided into a number of equal increments, n . An upper bound solution for the spread coefficient is computed at the start of each increment, and is used to predict the updated geometry of the workpiece via Eqs. (2.3 and 2.2). The complete process is given in Algorithm 5.3. By using the updated method, changes to the spread coefficient caused by changes to the velocity field and workpiece geometry can be captured and used to improve the prediction accuracy.

Algorithm 5.3 Incrementally Updated Upper Bound Algorithm

Inputs: Initial workpiece height h_i , length l_i , and width w_i , final workpiece height h_f .

Output: Deformed workpiece length l_f , and width w_f .

- 1: Choose the number of increments, n .
- 2: Divide the total reduction in height ($h_i - h_f$) to smaller reduction in height increments of equal value; $\Delta = \frac{h_i - h_f}{n}$. Thus the instantaneous height, h_j , at the start of the interval j is

$$h_j = h_i - (j - 1)\Delta \quad 1 \leq j \leq n$$

- 3: For each reduction in height step use the upper bound method for homogeneous pattern of deformation to compute (via Eq. (5.56)) the spread coefficient s_j
- 4: The deformed width and length at the end of the interval can be computed (assuming that s_j will remain constant during the deformation interval)

$$w_{j+1} = w_j \left(\frac{h_j}{h_{j+1}} \right)^{s_j}$$

$$l_{j+1} = l_j \left(\frac{h_j}{h_{j+1}} \right)^{1-s_j}$$

- 5: Update the width, length and height of the workpiece at the end of the interval. Use the newly computed width, length and height as the starting width, length and height to be used with the upper bound solution to compute the new spread coefficient, s_{j+1} .
 - 6: Repeat steps 3 to 5 for all reduction intervals. The final dimension of the workpiece are those computed at the end of all iterations.
-

5.4 Summary

The upper bound method is the most widely used analytical solution for predicting the side material spread. It is best suited for online spread prediction and was reported to produce comparable results with other empirical and analytical spread prediction models. Existing solutions, however, have not been found accurate enough for this application. Three new spread prediction models that were aimed to reduce the spread prediction error were developed in this chapter. The predictions of the newly developed models will be compared to predictions of previous spread prediction models and experimental spread measurements in Chapter 6. In addition, the Incrementally Updated Upper Bound solution will be later used to accelerate the convergence rate of the adaptive scheduling procedure as presented in Chapter 7.

Chapter 6

Experimental Analysis of Side Material Spreading

6.1 Introduction

The experiments presented in this study were conducted to gain more knowledge into how the material flows as it is being forged by flat dies and to test the accuracy of different spread prediction models, including the ones derived in Chapter 5. Center indentation of the workpiece was selected as the test procedure as it guarantees precise control of the forging bite. This procedure has been adopted by several researchers to simulate actual material flow in cogging operations (Baraya and Johnson 1964; Aksakal et al. 1993; Ferreira and Osman 1997; Aksakal et al. 1997; Ferreira and Osman 1999; Osman and Ferreira 1999; Nye 1999; Nye et al. 2001).

6.2 Online Spread Assessment for Cogging Operation

As mentioned previously, a number of researchers have concluded that process variability in open die forging is great enough to require real-time process feedback. This section will describe an online spread prediction system developed in this work.

6.2.1 Instrumentation and Equipment

The experiments were conducted on an automated open die forging cell composed of an instrumented 2 GN hydraulic press and a PUMA 560 robot for workpiece manipulation (Fig. 6.1). Flat rectangular dies of 19.1 mm width

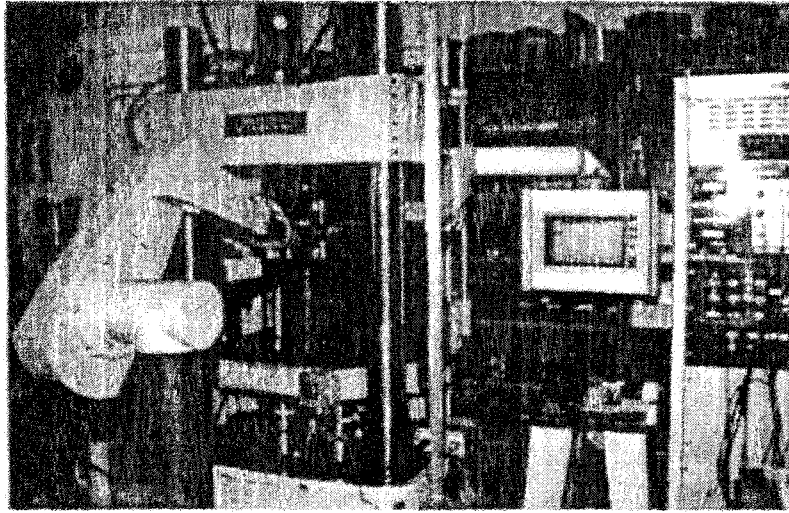


Figure 6.1: Experimental Setup Showing Press and Robot (Nye et al. 2001)

were manufactured from mild steel and fitted on the press to perform the cogging operation. A passive compliance end-effector with one degree of freedom was designed and built for online measurement of the elongation of the forged specimen. Specimens were clamped on the end-effector which was fitted on the robot gripper.

The press used is a single acting numerically controlled one in which the lower platen provides the squeezing action while the upper platen remains stationary. A displacement potentiometer is fitted on the press to measure and control the vertical travel to within 0.1 mm. The end-effector was calibrated using a vernier caliper and its calibrated measuring accuracy was found to be 0.3 mm. Signals from the end-effector and the vertical displacement potentiometer were captured in real time by a data acquisition system linked to a central computer on which the instantaneous specimen height and elongation were assessed. The overall measuring accuracy of the system was 0.1 mm in the squeezing direction and 0.3 mm in the elongation direction.

6.2.2 Experimental Setup and Procedure

Commercially pure aluminum (AL1100) in the annealed state at room temperature was used to simulate hot steel forging. Specimens were sanded lightly with emery paper before tests to remove surface oxides. Specimens and die surfaces were cleaned between tests with acetone. Tests were conducted without lubrication.

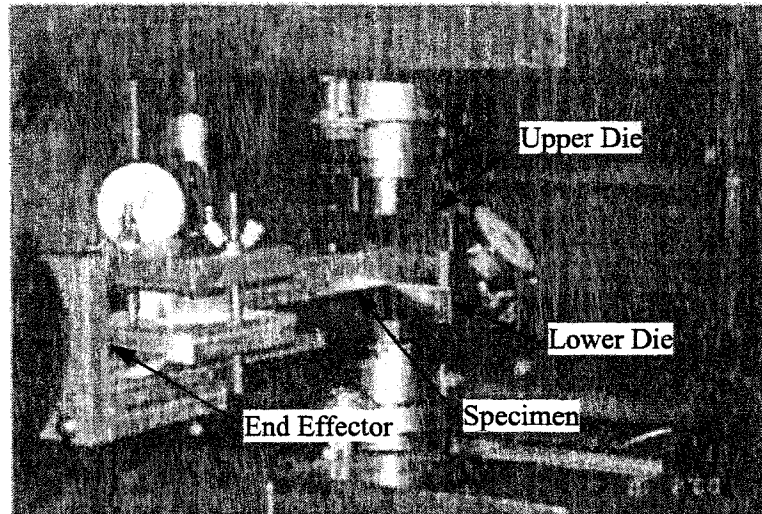


Figure 6.2: Experimental Setup Showing End-Effector, Tooling and Gauges (Nye et al. 2001)

A ring compression test was conducted using rings of standard dimensions¹ (Male and Cockcroft 1964) from the specimen material. The friction factor m according to Lee and Altan (1972) and Danckert (1988) calibration curves was found to be 0.2 and 0.16, respectively (Appendix B).

Each specimen was centrally indented, i.e., one forming step was performed with the ends of the specimen extending beyond the dies (Figs. 6.2 and 6.3). The manipulator, the robot, was programmed to accommodate for center-axis displacement of the specimens in the vertical, squeezing direction. For a single acting press as the one used the center-axis of the specimen travels half the reduction in height. The robot was programmed to compensate for such displacement by moving the end effector upwards.

6.2.3 Assessment of the Forged Width

The end-effector and the vertical potentiometer were used to assess the instantaneous length and height of the specimen. The instantaneous specimen width was calculated using the instantaneous height and length measurements. In forging the volume remains constant and the instantaneous width of the specimen was calculated by equating the volume before and after deformation.

¹Standard ring dimensions are: outer diameter= 19 mm ($\frac{3}{4}$ in), inner diameter= 9.5 mm ($\frac{3}{8}$ in), and height= 6.3 mm ($\frac{1}{4}$ in.)

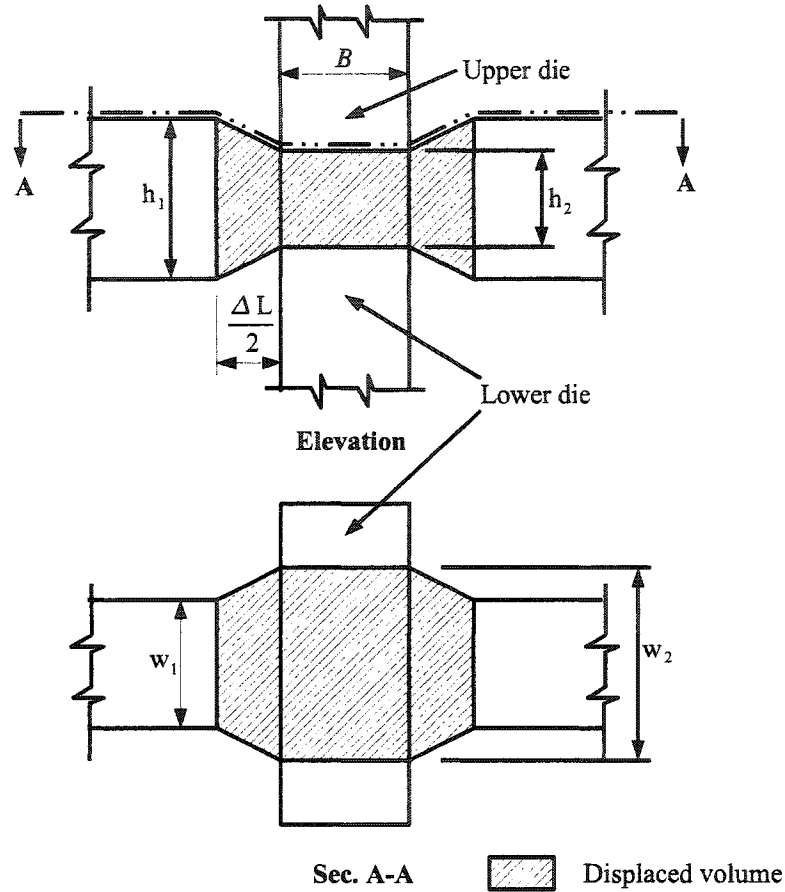


Figure 6.3: Displaced Volume for Center Indentation.

The displaced volume (the deforming volume of the specimen) corresponding to a uniform pattern of deformation² was used to calculate the average increase in width as shown in Fig. 6.3.

Equating the displaced volume before and after deformation:

$$w_1 h_1 B = w_2 h_2 B + 2 \left(\frac{\Delta L}{2} \frac{(h_1 + h_2)}{2} \frac{(w_1 + w_2)}{2} \right) \quad (6.1)$$

where,

B is the forging bite (in this case the die width).

ΔL is the measured elongation.

²The assumption of uniform pattern of deformation does not limit the procedure as one is interested in calculating the average value of the width.

h_2 the instantaneous height calculated as, $h_2 = h_1 - \Delta h$.

Δh is the squeeze value.

rearranging to calculate the instantaneous forged width:

$$w_2 = w_1 \frac{\left(h_1 B - \frac{(h_1 + h_2)}{2} \frac{\Delta L}{2} \right)}{\left(h_2 B + \frac{(h_1 + h_2)}{2} \frac{\Delta L}{2} \right)} \quad (6.2)$$

from which the increase in width Δw is:

$$\Delta w = w_2 - w_1 \quad (6.3)$$

and the corresponding instantaneous spread coefficient, s , can be calculated using the average forged width, w_2 .

$$s = - \frac{\epsilon_w}{\epsilon_h} = - \frac{\ln \frac{w_2}{w_1}}{\ln \frac{h_2}{h_1}} \quad (6.4)$$

6.2.4 Results

A pilot calibration of the overall setup was performed and then direct measurements of the spread for three different specimen dimensions were executed. The dimensions of the specimens used in each set were:

Experimental Set 1 width=19.1 mm, height=12.7 mm, bite=19.1 mm, resulting in a bite ratio, $\theta = 1$, shape factor, $\phi = \frac{2}{3}$, and, $DWR = \frac{3}{2}$.

Experimental Set 2 width=12.7 mm, height=19.1 mm, bite=19.1 mm, resulting in a bite ratio, $\theta = \frac{3}{2}$, shape factor, $\phi = \frac{3}{2}$, and, $DWR = 1$.

Experimental Set 3 width=19.1 mm, height=19.1 mm, bite=19.1 mm, resulting in a bite ratio, $\theta = 1$, shape factor, $\phi = 1$, and, $DWR = 1$.

Five specimens were used for each experimental set each to be forged in a forging trial. The difference between the trial results for any given experimental set indicates the inherent variability in the process.

Calibration of the System

To calibrate the online measurement setup, two dial gauges were attached to the press to measure the vertical displacement of the press and the elongation of the test specimen. The press was programmed to squeeze a square specimen of initial height and width of, 19.1 mm, to a final height of 7.8 mm in approximately 1 mm increments. At each increment the press came to a complete

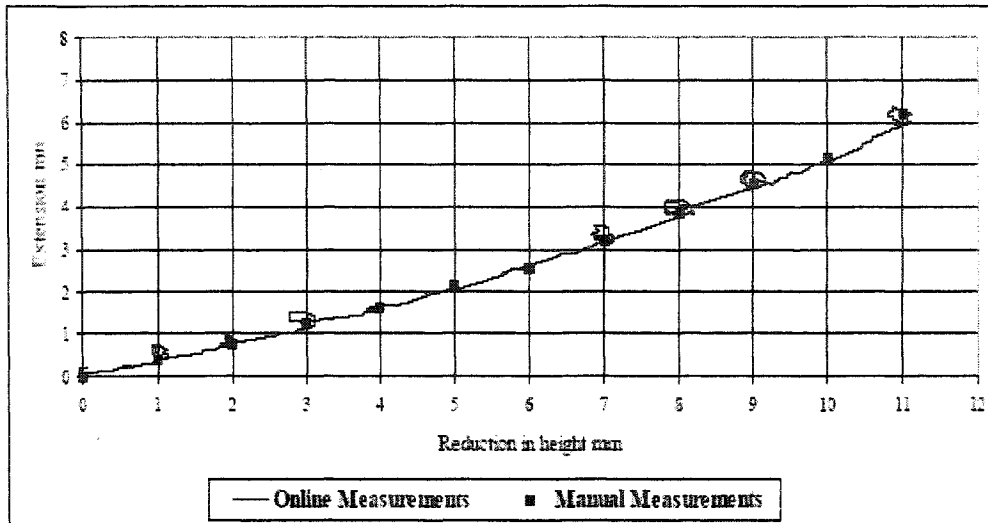


Figure 6.4: Manual vs Online Measurement Readings

halt so dial gauge readings could be recorded. The manual dial gauge readings and the measured data acquisition system readings are shown in Fig. 6.4.

The results of this test show that the compliance end-effector measurements provide a good estimate of the elongation. Figure 6.4 also shows a number of irregular loops in the acquired measurement data. Two factors affected the system as the press motion was paused after each reduction increment to take a manual measurement. First, the servo position control system of the press was found to 'hunt for position' as it reached the predefined stopping height, leading to the horizontal oscillating motions of the curve near the stop positions. Second, the PUMA robot possesses limited stiffness and accuracy, and the servo drives on the joint axes would often 'buzz' due to loads applied to the end-effector. This servo-induced vibration from the robot led to variations in the elongation measurement, witnessed by the vertical motions of the curve in Fig. 6.4.

Online Measurement of the Increase in Length and Width

The main forming trials were run without pauses, and this vibratory behaviour was not observed in the measurement data. Three sets of experiments each composed of five trials were conducted and the measurements of the elongation vs the reduction in height are plotted in Figs. 6.5, 6.7 and 6.9. It may be noted that the curves are relatively smooth, which, given the lack of stiffness in the experimental apparatus, suggests that elongation measurement

through manipulator displacement due to compliance will be robust in practice. Trial data number five for Experimental Set 3 is an outlier caused by the passive compliance end-effector jamming during the experiment and giving biased measurements. As such this trial data was omitted in further analysis of the experimental results.

The average increase in the forged width of the specimens was computed according to Eq. (6.3) and the corresponding spread coefficient according to Eq. (6.4). The increase in width vs the reduction in height for the three sets of experiments are presented in Figs. 6.6, 6.8 and 6.10, and the spread coefficient vs the reduction in height in Figs. 6.11 - 6.13

6.2.5 Analysis of the Results

The results presented in Section 6.2.4 showed that online indirect width measurements were consistent with little variation. The difference between different trial measurements, for any given experimental set, of the forged width did not exceed 0.5 mm, rendering the procedure robust and reliable. Figs 6.5 -6.10 show that material spread in width direction is nearly equal to and sometimes greater than, the elongation of the specimens, where the proportion of material spreading in the width direction increases with the reduction in height. This observation shows that assessing material spreading is essential for scheduling flat-tool cogging operations.

The spread coefficient was found to change significantly with the reduction in height. Three zones can be visually identified on the spread coefficient - height reduction graph³ (Fig. 6.14).

Zone I At the start of deformation the plastic deformation does not penetrate deep inside the forged material. As a result the deformation is a surface one rendering the effective forged height less than the workpiece height. This zone is characterized by rapid drop in the spread coefficient, which starts from a fairly large value, to a near constant value as the two bulges merge together to form a single bulge.

Zone II As the material deforms homogeneously and the plastic strain penetrates to the center of the workpiece the spread coefficient drops slowly as the bite ratio decreases due to the increase in the workpiece width. This should be the recommended operating zone for cogging operations as the deformation is homogeneous and distortions are minimized. In the

³For Experimental Set 1 as the original height is small the graph starts with zone II. The first point apparent error is attributed to the small change in height used in computing the spread at this point which was less than the measuring accuracy of the measuring instrument.

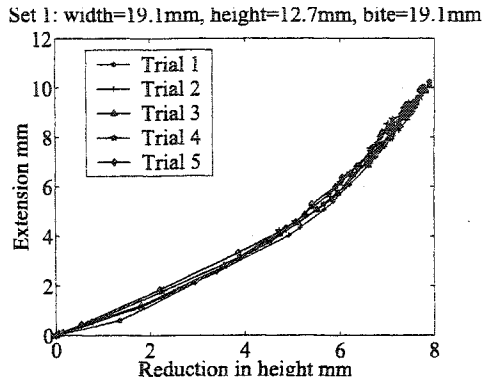


Figure 6.5: Elongation in Length vs Reduction in Height for Experimental Set 1

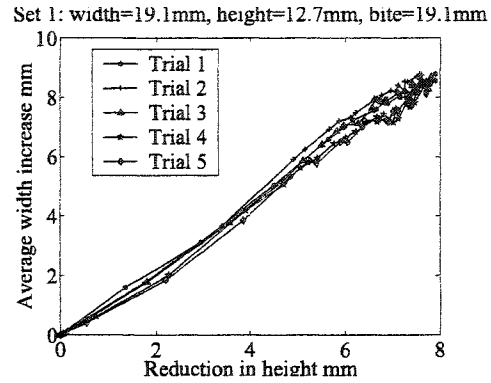


Figure 6.6: Increase in Width vs Reduction in Height for Experimental Set 1

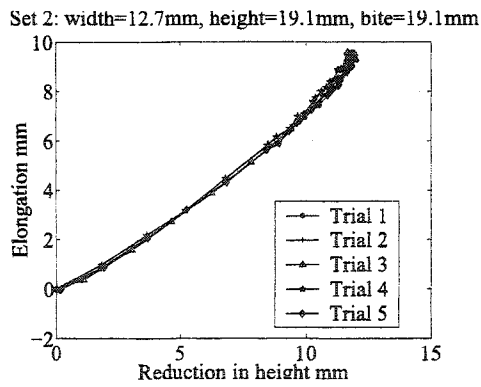


Figure 6.7: Elongation in Length vs Reduction in Height for Experimental Set 2

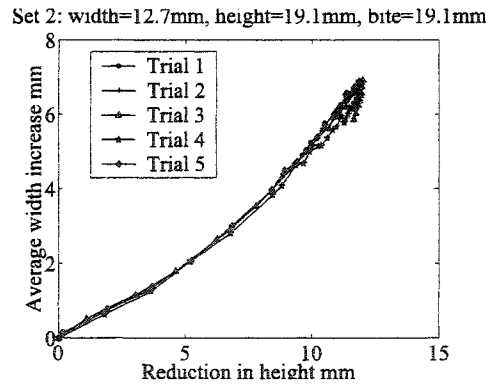


Figure 6.8: Increase in Width vs Reduction in Height for Experimental Set 2

Set 3: width=19.1mm, height=19.1mm, bite=19.1mm

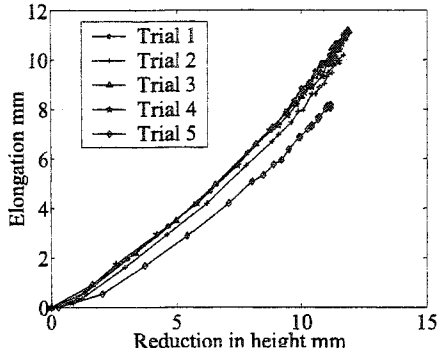


Figure 6.9: Elongation in Length vs Reduction in Height for Experimental Set 3

Set 3: width=19.1mm, height=19.1mm, bite=19.1mm

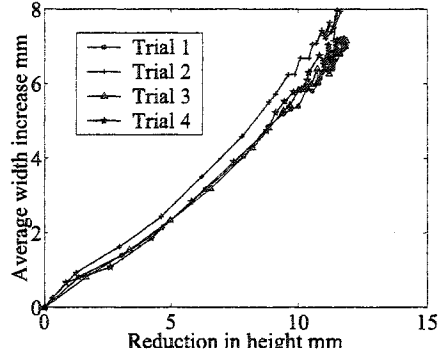


Figure 6.10: Increase in Width vs Reduction in Height for Experimental Set 3

Set 1: width=19.1mm, height=12.7mm, bite=19.1mm

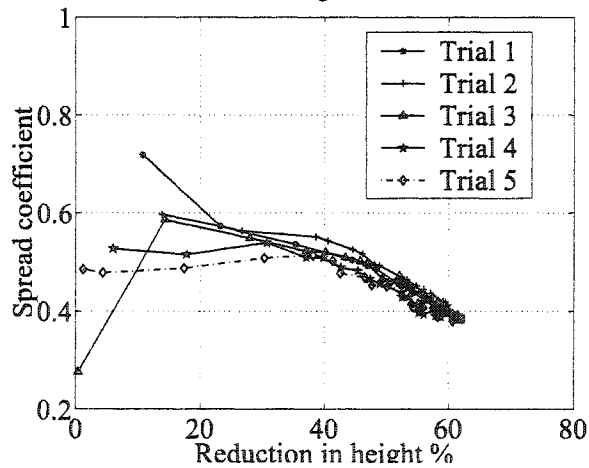


Figure 6.11: Forged Spread vs Reduction in Height for Experimental Set 1

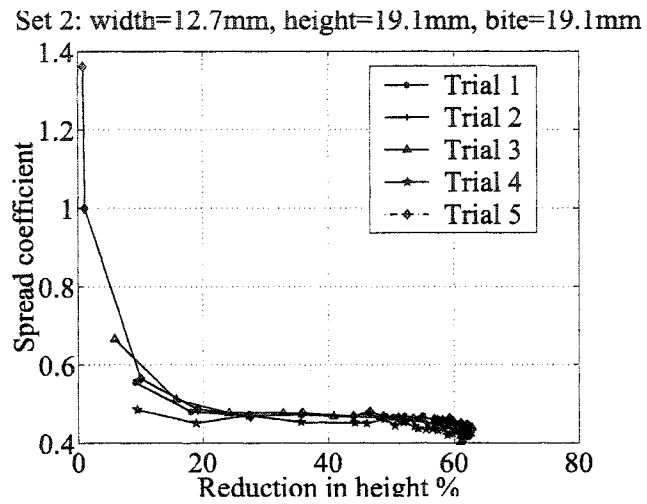


Figure 6.12: Forged Spread vs Reduction in Height for Experimental Set 2

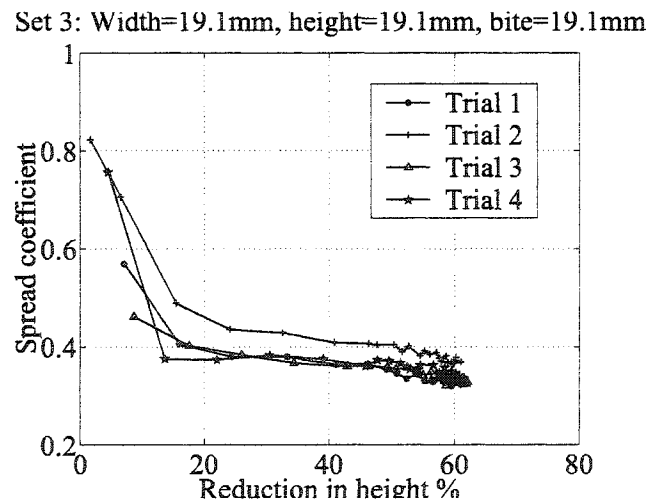


Figure 6.13: Forged Spread vs Reduction in Height for Experimental Set 3

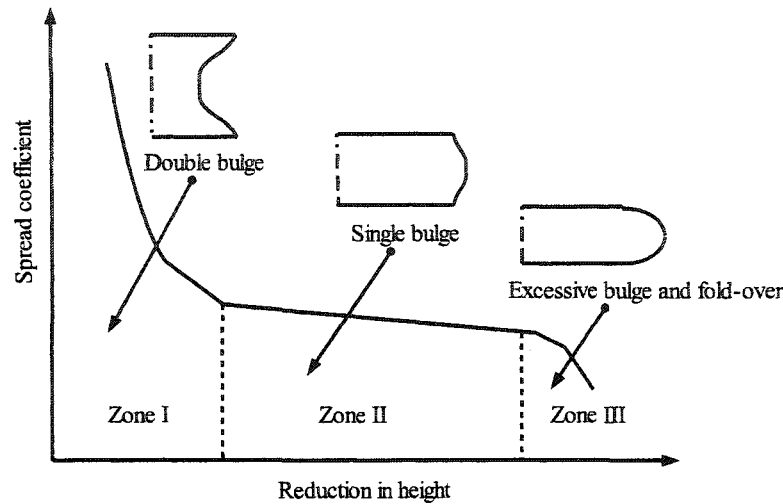


Figure 6.14: Variation of Spread Coefficient With the Reduction in Height

experiments, zone II was normally associated with a reduction in height ranging from 10% to 50%. This implies that the current implemented reduction in height in industry⁴ (10%-15%) can be safely increased, making it possible to reduce the time to produce any given product and enabling higher squeeze values that give better plastic penetration enhancing the internal structure of the forged material.

Zone III This zone is characterized by an increase in the drop of the spread coefficient as the material starts to deform nonhomogeneously and the length increases rapidly due to excessive bulging of the sides and fold-over. In each case this zone was reached only after dramatic reduction (e.g. > 50%) had occurred and was associated with severe nonhomogeneous deformation rendering it of little practical use.

6.2.6 Comparison to Theoretical Spread Predicting Models

Figures (6.15 - 6.18) compare the average deformed width with several spread predicting empirical and analytical models⁵. The deformed width, w_2 , was computed knowing the spread coefficient s , according to Eq. (6.5). The comparison reveals that for all models the error in estimating the deformed width

⁴Such practised reduction is limited by the capacity of the presses in use.

⁵Refer to Table 2.2 and Section 2.5.

increases as the reduction in height increases. Thus, all models give fairly good estimates for the current operating range of the reduction in height as practised in the industry (10% - 15%). The divergence starts to increase rapidly for reduction in height ratios above 15%.

$$w_2 = w_1 \times \left(\frac{h_2}{h_1} \right)^s \quad (6.5)$$

Observations

One can observe the following from Figs. 6.15 - 6.18

- The Wang and Cao (1995) model diverged rapidly⁶ from the true measured value of the width for reduction ratios greater than 25% (Fig. 6.15) and thus was not included in the collective comparison charts (Figs. 6.16 - 6.18).
- The Shutt (1960) model overestimated the average deformed width and had the maximum deviation from the true measured width compared to the other estimation models for all Experimental Sets and reductions in height. The model estimates the forged width to within 1 mm for reduction ratios below 25%.
- The Tomlinson and Stringer (1959) and the Tarnowski (1950) models gave good estimates of the forged width for reduction in height below 50% for Experimental Set 1 and below 40% for Experimental Sets 2 and 3.
- The Hill (1963) analytical model and the Baraya and Johnson (1964) empirical formula gave the best estimates (compared to other models) for experimental sets 2 and 3 for which the shape factor, ϕ , was 1. The estimation error was below 0.5 mm. For Experimental Set 1, (shape factor $\phi = \frac{2}{3}$) the Baraya and Johnson (1964) and the Hill (1963) models prediction performed poorly for reduction ratios between 35% and 50%. It must also be noted that the deviation between the two estimates did not exceed 1 mm for all Experimental Sets.
- The Homogeneous Pattern of Deformation Upper Bound solution derived in Section 5.3.1 gave better estimates for width prediction compared to the Tomlinson and Stringer (1959) and the Tarnowski (1950) models. It managed to accurately model the trend between the reduction in height and the forged width. It can be used to estimate the width to within 1

⁶Divergence and quality of estimate was determined based on an error threshold of 1 mm.

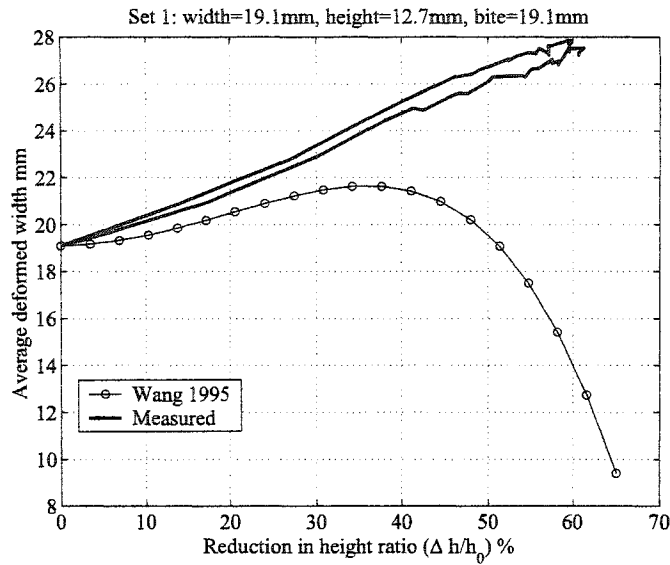


Figure 6.15: Estimated vs Measured Average Forged Width Using Wang and Cao (1995) Spread Predicting Formula Set 1

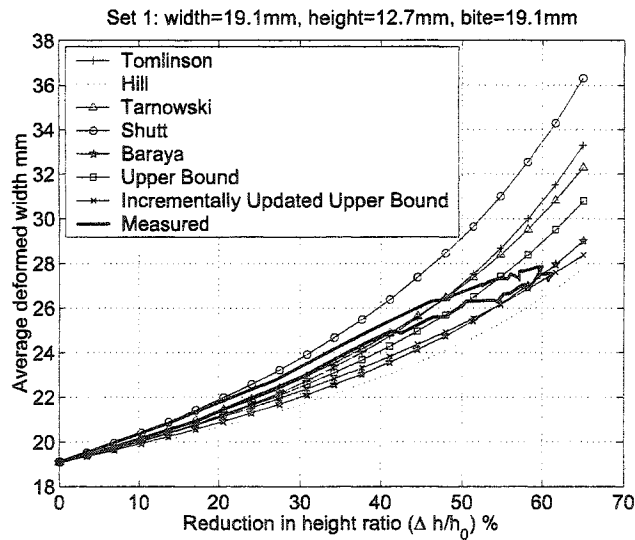


Figure 6.16: Estimated vs Measured Average Forged Width According to Various Spread Predicting Formulae Set 1

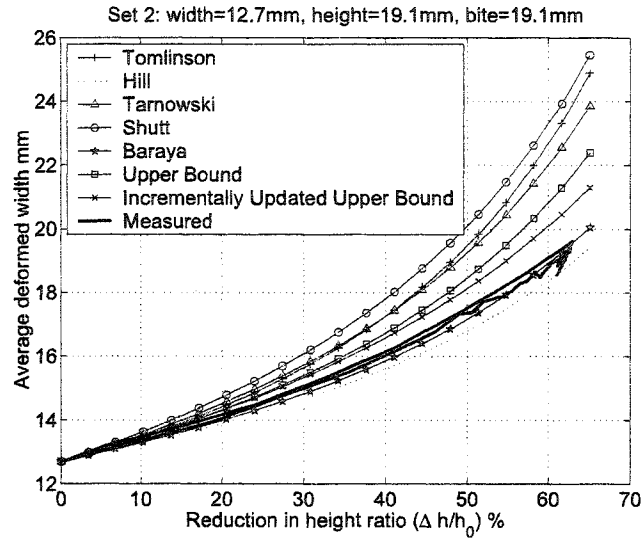


Figure 6.17: Estimated vs Measured Average Forged Width According to Various Spread Predicting Formulae Set 2

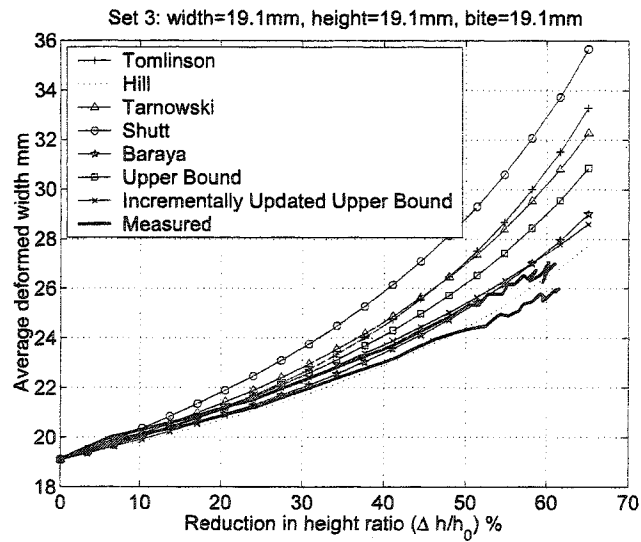


Figure 6.18: Estimated vs Measured Average Forged Width According to Various Spread Predicting Formulae Set 3

Table 6.1: Average Forged Width Estimation Error Using Different Formulae

Model	Set 1 Error (mm)	Set 2 Error (mm)	Set 3 Error (mm)	Maximum Error (mm)
Incrementally Updated Upper Bound	1.2	1.5	1.7	1.7
Hill (1963)	1.9	0.7	0.8	1.9
Baraya and Johnson (1964)	1.5	0.4	2	2
Upper Bound	2.6	2.6	3.9	3.9
Tarnowski (1950)	4.1	4	5.4	5.4
Tomlinson and Stringer (1959)	5.1	5.1	6.4	6.4
Shutt (1960)	8.1	5.6	8.7	8.7
Wang and Cao (1995)	18.8	10.7	13.2	18.8

mm for reduction in height below 45%. Above this threshold reduction in height, it tends to overestimate the forged width.

- The Incrementally Updated Upper Bound solution derived in Section 5.3.3 gave a much better estimate than other upper bound solutions. The estimation error was less than 1 mm for Experimental Sets 1 and 2, and for a reduction in height less than 58% for Experimental Set 3. The Incrementally Updated Upper Bound solution had the smallest observed estimation error, 1.6 mm, for all Experimental Sets and for all observed reductions in height (0-63 %).

For each data set a regression formula was developed for the relation between the reduction in height and the average deformed width⁷. It was found that a quadratic formula best fits the data where the error associated with the formula for all data sets is within ± 0.5 mm. Using the regression formula the maximum error in average forged width estimation was calculated for all predicting formulae for a reduction in height ranging from 0% to 65%, and is presented in Table 6.1.

⁷Regression models are presented in Appendix C.

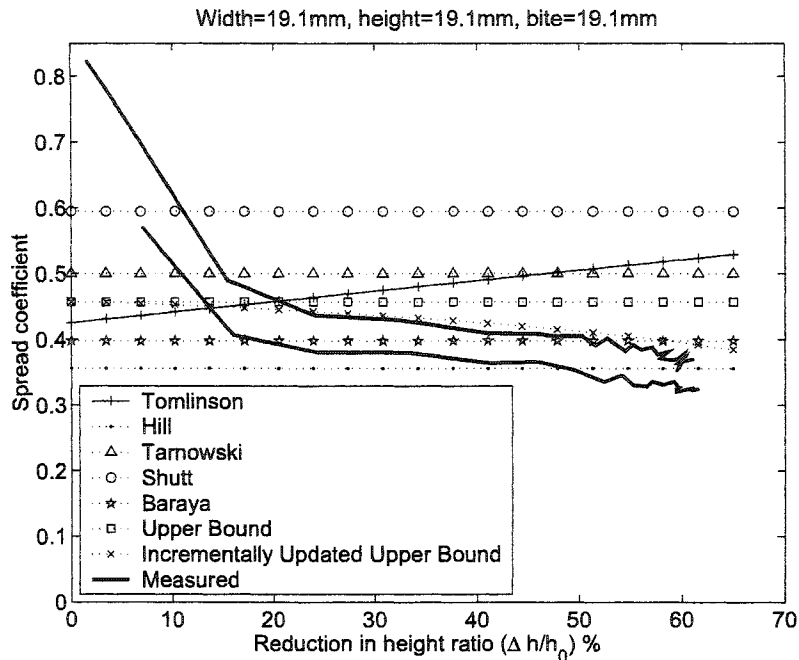


Figure 6.19: Theoretical Models Estimating the Spread Coefficient vs Actual Spread Coefficient for Experimental Set 3

The results indicate that the Incrementally Updated Upper Bound solution gave the best results for all data sets where the maximum observed error at 65% reduction ratio was 1.7 mm. The Hill (1963) and the Baraya and Johnson (1964) prediction models also gave good estimates of the forged width. Their estimation errors were 1.9 mm and 2 mm, respectively.

Figure (6.19) is a sample curve that shows the variation of the spread coefficient with the reduction in height. The Incrementally Updated Upper Bound model predicted the decrease in the spread coefficient with increasing the reduction in height. Except for the Tomlinson and Stringer (1959) model that predicted the reverse of the observed relation, all other spread predicting models assumed that the spread will remain constant with increasing the reduction in height.

The curves also show that a significant error in estimating the spread coefficient is encountered in all predicting formulae. This fact might be attributed to the inherent process variability. Even under highly controlled lab conditions the measured spread coefficient shows a large degree of uncertainty.

In conclusion, any of the Incrementally Updated Upper Bound, the Hill (1963), or the Baraya and Johnson (1964) models can be used to ade-

quately predict the forged width in single step flat-tool cogging operations. Unfortunately, for scheduling a flexible forging cell multiple consecutive cogging operations will be needed to forge any given part. This means that the error will increase with the number of forging steps. It is believed that the current estimation error, a minimum of which is 1.7 mm for the particular case studied, is inadequate for successive cogging steps and planning a forging sequence for a flexible forging cell even for as high tolerance limit as ± 3 mm. In addition, the above mentioned models are limited to flat-tool cogging with a linear forging feed motion assuming a single mode of spreading exists (i.e., single bulge of sides in this case). Complex die shapes and/or forging feed motions have not been studied and no models are currently available that study spread prediction for such cases. For generating successful forging schedules for a flexible forging cell it is necessary to measure online the deformed shape of the workpiece and to re-adjust the schedule frequently to accommodate for any unpredicted changes in the shape. This result emphasize the need for an adaptive control scheme based on online shape feedback.

6.3 Summary

Experimental results in this chapter showed that there are three distinctive phases of material deformation as it is being forged (Fig. 6.14). At the start of the squeezing action the deformation is nonhomogeneous and is concentrated on the surface layers. As the squeezing continues the deformation penetrates inside the material and the deformation process can be regarded as homogeneous. Further squeezing of the material leads to excessive deformation at the center while the surface is constrained by the friction between the workpiece and the die leading to the initiation of high tensile stresses on the outer surface. Such stresses might result in crack formation and to a nonuniform deformation pattern.

The experimental results also showed that reduction in height ratios of 10-50% corresponding to the homogeneous deformation phase, can be safely implemented in the adaptive forging schedule procedure. These values are much higher than the current practised reduction in height ratios of 10-15%; a limit that might be attributed to the press capacity constraint and not to the deformation severity. The increased allowable reduction ratio will help reduce the time to produce any given product and will enable higher squeeze values that give better plastic penetration thus enhancing the internal structure of the forged material.

The spread coefficient was found to decrease as the reduction in height increases as observed on the spread-vs-reduction in height curves (Figs 6.11, 6.12 and 6.13). This nonstationarity behaviour of the spread coefficient dur-

ing the deformation process was the main drive to develop the Incrementally Updated Upper Bound solution since traditional upper bound spread prediction models assumes that the spread coefficient remains constant during the deformation process.

A comparison between spread prediction models (including the newly developed models of Chapter 5) for flat tool center indentation were presented in Section 6.2.6. The results showed that the Incrementally Updated Upper Bound solution had the least estimation error. Other models varied significantly in their performance. Typical estimation errors for estimating the deformed width of a workpiece of an original width of 19.1 mm varied from 2 mm to 18.8 mm. Most models performed poorly in predicting the spread coefficient which might be attributed to the inherited process variation that is oversimplified by the spread prediction models.

Spread prediction models are applicable to limited configurations. Their estimation error is adequate for single-step cogging operations. However, the propagation of the estimation error in a forging schedule, consisting of multiple consecutive cogging operations, render the propagated spread prediction models estimation error unacceptable. For this reason online shape feedback is necessary for a successful forging schedule generation procedure.

Chapter 7

Intelligent Forging Schedule Procedure

Shape feedback control to assist in generating the forging schedule was proposed in Chapter 3 and it was demonstrated in Chapter 4 that shape feedback control can be solely used to successfully and easily generate forging schedules to forge 2-D and 3-D profiles. In contrast, using conventional spread prediction models to generate the forging schedule failed to forge a wedge workpiece within the preset tolerance limit (Section 4.1.2).

Even though the shape feedback control approach performed better, examining its behaviour shows that it does not benefit from anticipating the consequences of its decisions. While conventional spread prediction calculations perform poorly when used directly to generate schedules, they can be used as an approximate tool for predicting the consequences of a proposed forging step. In this chapter the predictive capabilities of the spread prediction models are integrated into the adaptive scheduling procedure to intelligently plan the forging schedule. Figure 7.1 shows the Intelligent Forging Schedule procedure.

The desired and instantaneous¹ workpiece shapes are used to compute the shape error that drives the forging schedule. A forging path (Fig. 7.1 b) comprising a number of consecutive height squeezing actions along the forging feed direction is then generated and an estimate for the width is calculated using the spread prediction models. If the estimated increase in width is within the allowable tolerance the forging path is executed on the physical cell.

However, if the estimated increase in width is greater than the allowable tolerance, extra (overhead) forging operations will be inevitable to bring the width to within the required tolerance. The aim of the Intelligent Forging Schedule Procedure is to use the predictive capabilities of the spread prediction

¹As captured by the feedback system.

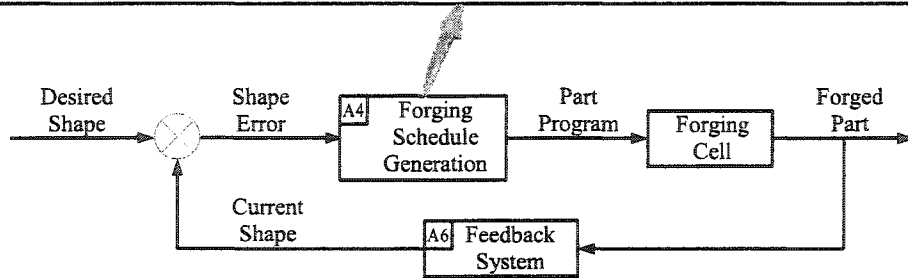
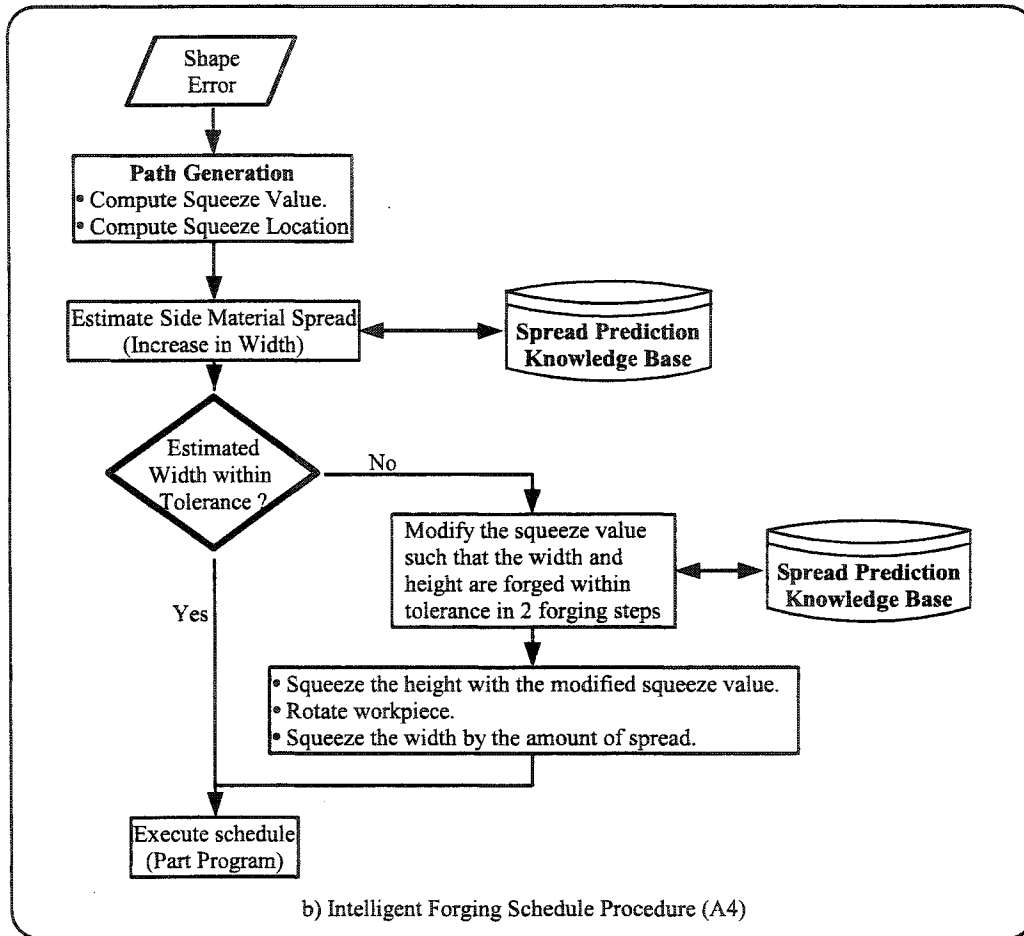


Figure 7.1: Intelligent Forging Cell Procedure

models to reduce the number of overhead cycles² that are necessary to maintain the workpiece dimensions within tolerance.

7.1 Optimum Schedule of Overhead Cycles

The overhead forging cycles, if not controlled, might result in a large number of iterations before the workpiece converges to the required shape. In this section the use of the spread estimate from spread prediction models to plan the forging cycle is proposed. In such a case the height of the workpiece will be over-squeezed to a shorter height (h) than the required one (h_f) so that after applying the second squeezing action along the width (w), material spread in the height direction will bring the height to the required value (h_f) (Fig. 7.2).

The procedure is based on first estimating the spread coefficients (\hat{s}_1 and \hat{s}_2) for forging the workpiece along its height and width respectively, then using the estimates to determine the required intermediate workpiece shape as follows:

- Estimate the spread coefficient (\hat{s}_1) for forging along the height direction using the spread prediction model. Use the bite, the original height (h_i) and original width (w_i) as inputs.
- Estimate the spread coefficient (\hat{s}_2) for forging along the width direction using the spread prediction model. Use the bite, the final height (h_f) and final width (w_f) for inputs.

Using the estimates of the spread coefficients the following relations can be derived:

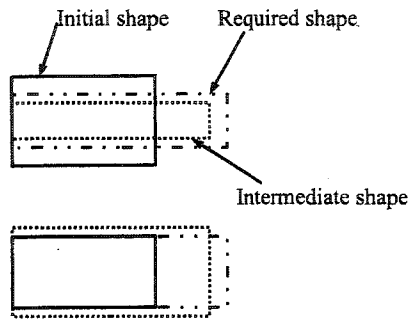
$$w = w_i \left(\frac{h_i}{h} \right)^{\hat{s}_1} \quad (7.1)$$

$$h_f = h \left(\frac{w}{w_f} \right)^{\hat{s}_2} \quad (7.2)$$

From which by substituting the value of the intermediate width (w) in the height (h) equation and manipulating:

$$h = \left(\frac{h_f}{h_i^{\hat{s}_1 \hat{s}_2}} \left(\frac{w_f}{w_i} \right)^{\hat{s}_2} \right)^{\frac{1}{1-\hat{s}_1 \hat{s}_2}} \quad (7.3)$$

²Overhead forging cycles are iterative forging operation caused by material spread and are typically formed of forging along a dimension, rotating and forging along another dimension.



		Forging Step 1 Squeeze the height by $2 \cdot R_h$	Forging Step 2 Squeeze the width by $2 \cdot R_w$
Elevation			
Plan			

Figure 7.2: Optimum Overhead Cycle Schedule

Algorithm 7.1 Optimum Overhead Scheduling Algorithm

Inputs: Initial workpiece height h_i and width w_i , final workpiece height h_f and width w_f

Output: Optimum oversqueezed height h .

- 1: Use h_i and w_i and the Incrementally Updated Upper Bound Algorithm (Algorithm 5.3) to estimate the spread coefficient for the first squeezing step \hat{s}_1 .
- 2: Use h_f and w_f and the Incrementally Updated Upper Bound Algorithm (Algorithm 5.3) to estimate the spread coefficient for the second squeezing step \hat{s}_2 .
- 3: The optimum oversqueezed height is:

$$h = \left(\frac{h_f}{h_i^{\hat{s}_1} \hat{s}_2} \left(\frac{w_f}{w_i} \right)^{\hat{s}_2} \right)^{\frac{1}{1-\hat{s}_1 \hat{s}_2}}$$

Thus in order to reduce the number of overhead forging steps to only two the workpiece should be first squeezed along its height to an intermediate height (h). Then the workpiece is rotated and forged along its width to the final required width (w_f). The spread in the height direction during the second forging operation will bring the height to the required value of h_f .

7.2 Illustrative Example

To illustrate how spread prediction can be used to minimize the number of overhead forging cycles consider cogging a rectangular billet of initial height and width of 200 mm and 100 mm, respectively, to a square one of 100 ± 1 mm height and width (Fig. 7.3). The forging schedule based only on feedback information³ is shown in Table 7.1

The forging schedule based on the Intelligent Forging Schedule is shown in Table 7.2. The estimation of the amount of over-squeeze was performed using Eq. (7.3) and the Incrementally Updated Upper Bound model for spread prediction (Section 5.3.3). The estimates of the spread coefficients for forging along the height and along the width were $\hat{s}_1 = 0.4274$ and $\hat{s}_2 = 0.4563$, respectively. The computed intermediate height according to Eq. (7.3) was $h = 84.5 \approx 85$ mm which is the value used in the Intelligent Forging Schedule Table 7.2.

³The simple schedule is based on computing the shape error, forging the workpiece where the error is maximum and repeating until the required tolerance is met.

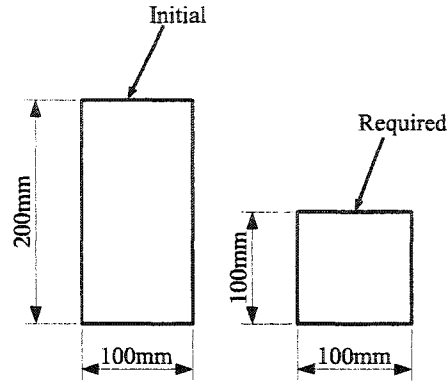


Figure 7.3: Intelligent Forging Schedule Illustrative Example

Table 7.1: Feedback Control Forging Schedule

Step	Forging Direction	Reduction (mm)	Instantaneous Width (mm)	Instantaneous Height (mm)
1	Height	100	134.5	100
2	Width	34.5	100	114
3	Height	14	106	100
4	Width	6	100	102.5
5	Height	2.5	101.1	100
6	Width	1.1	100	100.5

Table 7.2: Intelligent Forging Schedule

Step	Forging Direction	Reduction (mm)	Instantaneous Width (mm)	Instantaneous Height (mm)
1	Height	115	142.8	85
2	Width	42.8	100	100.6

As presented the number of overhead forging steps required to forge the part was reduced from six to only two using the Intelligent Forging Schedule procedure. The height was over-squeezed by 15 mm in the first squeezing operation. When the width was squeezed in the following forging step material spread in the height direction brought the height to the required 100 mm value. Thus, while a minor addition to the complexity of the control scheme, a predictive capability can have a dramatic impact on the effectiveness of the adaptive forging schedule generation system.

Chapter 8

Conclusions and Recommendations

8.1 Summary of Achievements and Conclusions

8.1.1 Adaptive Scheduling for the Incremental Forging Cell

Researchers have recommended online measurement of material flow to overcome the low estimation quality of the spread prediction models (Appleton et al. 1979; Lilly and Melligeri 1996; Aksakal et al. 1997; Ferreira and Osman 2000; Nye et al. 2001) but until now such system has never been implemented. In a forging schedule consisting of several forging steps the accumulation of the spread prediction error results in an unacceptable estimation error of the instantaneous workpiece shape. This was the main reason it was decided that the actual, real time, measurements of the workpiece shape should be incorporated to adaptively generate the forging schedule.

Adaptive forging schedules to forge external profiles using flat dies were introduced in this work. Two schedule generation levels are presented. The first is an aggregate schedule generation model (Process Plan, Section 3.3.1) in which the required shape is divided into a set of features¹, each to be generated by a forging operation. The raw material volume is then divided into zones; each zone is assigned to produce a specific feature.

The second schedule generation level (Forging Schedule (A4), Section 3.3.5) generates the detailed schedule to execute each individual operation. This

¹It is the responsibility of the process planner to divide the required shape into a set of consecutive features specified in the required shape solid model.

schedule is adaptively generated based on the instantaneous shape error computed from the instantaneous and the required workpiece shapes. The control process of the adaptive schedule generation is based on the following iterative procedure:

- Capture the instantaneous shape of the workpiece using the shape feedback system.
- Compute the shape error between the instantaneous and required workpiece shapes.
- Generate a forging schedule composed of several forging steps to reduce the shape error.
- Iterate until the workpiece shape is within the preset tolerance.

The beauty of this procedure is that not only it is simpler to implement than an *a-priori* approach, but illustrative case studies forged on the virtual forging cell showed that it successfully forged external profiles (given an arbitrarily set tolerance limit) when *a-priori* approaches failed. In addition, the illustrative case studies showed that the new scheme could forge 2-D and 3-D profiles as easily (in terms of programming effort) as forging a uniform billet. Longitudinal profiles² of moderate shape complexity have also been forged on the cell.

The convergence rate of the procedure varied with the allowable tolerance on the forged profile, with tighter tolerances requiring disproportionately more forming steps. For this reason, there will be a trade-off between forging and finish machining time and costs.

A new technological limit on the slope of the profile that can be generated by the process, Eq. (4.13), has also been described (Section 4.1.2). By applying the technological limits as constraints in the adaptive control scheme, forging shape defects, namely the hourglass defect and lapping, can be reduced or eliminated.

A paper describing the adaptive control procedure used for generating 2½-D profiles was submitted for publication in *the International Journal of Machine Tools and Manufacture* (Elbadan and Nye 2003), and a paper describing the adaptive schedule used to generate 3-D profiles is currently under preparation (Elbadan and Nye 2004a).

²Longitudinal profiles are profiles that are defined along the forging feed direction.

8.1.2 Spread Prediction Models

Three new spread prediction models were developed in this research to improve the prediction quality of the instantaneous workpiece shape to provide predictive capability for the adaptive forging schedule model.

The developed spread prediction models use upper bound solutions in which a uniform deformation pattern was assumed. This pattern provides a good estimate of the average change of the forged workpiece dimensions, which is an information required by the forging schedule generation module.

The first model relaxed the assumption made by Aksakal et al. (1997) that the shear work at the interface between the deforming and non-deforming zones of the workpiece can be neglected. In this model the shear constraint is assumed to be symmetric for both sides of the deforming metal. The second model was derived for cogging operation in which the asymmetric nature of the shear work constraint between deforming and non-deforming metal is incorporated.

Upper bound solutions for forging problems were often derived at the start of the forging operation. Such solutions thus ignore the non-stationarity of the process. A modified Incrementally Updated Upper Bound solution was derived in the third presented model where the upper bound solution is updated at discrete points in time during the forging operation.

Experimental results showed that the Incrementally Updated Upper Bound model provided the best estimate of the instantaneous workpiece shape compared to other spread prediction models (The worst estimation error, compared to measured spread from conducted experiments, was less than 1.7 mm for reductions in height ratios up to 65 %).

The comparison of the measured spread and the estimates of the spread prediction models was published in the *Journal of Engineering Materials and Technology* (Nye et al. 2001). A paper describing the Incrementally Updated Upper Bound spread prediction model is currently under preparation (Elbadan and Nye 2004b).

8.1.3 Intelligent Forging Schedule Procedure

The adaptive forging schedule procedure developed in this research was sometimes found to require redundant forging cycles (termed in this research overhead forging cycles). The Intelligent Forging Schedule Procedure presented in Chapter 7 was developed to minimize the number of overhead forging cycles. The procedure utilizes the shape prediction capability of the Incrementally Updated Upper Bound model to calculate the required amount of over-squeezing that is necessary to forge the height and width in fewer forging steps. A case study showed that adding a predictive element to the adaptive forging sched-

ule procedure significantly improved performance; in the particular example forging steps dropped from six to two.

8.1.4 Incremental Forging Limitations

The proposed incremental forging operations are intended as a “near-net shape” processes in which the dimensional and geometrical quality of the generated surfaces are limited by the uncontrollable behaviour of material spread. As the dies partly constrain the material flow, only partial control on the material spread can be achieved. Shape distortions are inevitable and finishing operations are required. It is recommended that the incremental forging cell proposed in this study be used to forge products to within ± 1 mm tolerance. This is perceived to be a much tighter limit than what is practised especially if forging is performed hot, where oxides and scales are to be removed.

Other limitations on the incremental forging operations are attributed to either the implemented scheduling or error algorithms. Those limitations could be relaxed through the development of more sophisticated algorithms to handle scheduling and error assessment.

Limitations Imposed by the Scheduling Algorithm

The developed adaptive algorithm is currently limited to forging external profiles where the dies extend beyond the workpiece width. Convexly shaped dies including flat, radiused, bevelled and chamfered dies, can be used. Forged workpieces must have convexly shaped symmetric cross-sections to ensure full access to the forged surface by the double acting dies.

Limitations Imposed by the Error Algorithm

The forging cell is limited to forge the workpiece in three principal directions (height, width and length) and the error computation algorithm was developed to calculate the error along those three directions. For this reason the current implementation of the adaptive scheduling procedure is limited to forging workpieces of rectangular cross-sections. The procedure can be extended to forge arbitrary convexly shaped cross-sections with minor modifications. The workpiece model is composed of a set of consecutive features. Each feature must have a convex shape to be processed by the error algorithm.

8.1.5 Programming Environment of the Virtual Forging Cell

MATLAB (MATLAB Version 6.1 2001) was used as the main operating shell from which the preprocessing, finite element and postprocessing operations were performed. FEMAP (FEMAP Version 8.0 2000) package or developed MATLAB routines can be used to generate the workpiece and dies solid models. Forging operating parameters can be included through the developed user interface under MATLAB. A main scheduling routine then uses this information to simulate the forging operation and generate the forging schedule.

8.2 Recommendations for Future Work

- Research on the tool shape's effect on material flow is still required. New die designs may help improve the operation of the incremental forging process.
- The literature review has shown that there are few papers that addressed incrementally forging internal profiles. Given the potential of such process further research is needed in this area. (This process was investigated earlier in this research with little success in avoiding the lapping defect).
- Further research on technological bounds for incremental forging is required. The automated form of this process is still novel and currently a narrow range of forging parameters can be used based on known bounds. It is felt existing bounds may be too conservative. Better bounds would increase process flexibility.
- The main operating modules to generate a forging schedule that forges workpieces within a prespecified tolerance limit have been developed (Fig. 3.13). The development and integration of a thermal effect knowledge base, force prediction knowledge base, internal structure knowledge base and path sequence knowledge base will enhance the operation of the developed forging schedule module. This integration will also extend the applicability of the developed forging schedule procedure to generate forging schedules to forge large scale workpieces that are not necessary forged from fault free billets.
- Perhaps the most profitable area of research that would accelerate the development of the incremental forging operation is to construct a knowledge base that captures the experience of practising forgemasters. A

great amount of forging knowledge exists in practice, and capturing it in Expert Systems will definitely widen the applicability of the automated process.

- Extending the adaptive scheduling procedure to include 3-D bending operations is believed to be possible with minor modifications. The major research effort is expected to be invested in developing a technological bound knowledge base for such operations.

Bibliography

- Aksakal, B., F. Osman, and A. Bramley. *Analysis for the Automation of Small Batch Manufacturing Using Open Die Forging*. Annals of CIRP, 42:273–278, 1993.
- Aksakal, B., F. Osman, and A. Bramley. *Upper-Bound Analysis for the Automation of Open Die Forging*. Journal of Materials Processing Technology, 71:215–223, 1997.
- Appleton, E., W. Heginbotham, and M. Kohno. *Experimental Study into the Use of an Industrial Robot as a Manipulator for Open Die Forging of Light Workpieces*. Technical Paper MS79-296, Society of Manufacturing Engineers SME, 1 SME Drive PO Box 930 Dearborn, Michigan, 48128, 1979.
- AVANTOP KC1.1 Milling Cutter. AVANTEC, Gerokstraße 22, D-75428 Illingen, Germany, 2004.
URL http://www.avantec.de/e_2_5_1b.html
- Baraya, G. and W. Johnson. *Flat Bar Forging*. Proc. 5Th Int. Conf. MTDR, pages 449–469, 1964.
- Barnett, K. *Research Initiatives for the Forging Industry*. Journal of Materials Processing Technology, 98:162–164, 2000.
- Belova, L., L. Dmitriev, I. Dzyuina, and I. Shalagaeva. *Theoretical - Experimental Research and Development of Open-Die Forging Process Conditions for Large Ingots*. English Translation of Soviet Forging and Sheet Metal Stamping Technology, (3):102–105, 1987.
- Benson, R. and R. Hunt. *Tools for Heavy Forging Work*. Journal of the Iron and Steel Institute, pages 390–401, August 1961.
- Berger, B., E. Neuschütz, and P. Angott. *Analysis of Technical Forging Parameters for Open-Die Forging and Calculating of Forging Schedules*. Metallurgical Plant and Technology, pages 110–114, May 1982.

- Bramley, A. *UBET and TEUBA: Fast Methods for Forging Simulation and Preform Design*. Journal of Materials Processing Technology, 116:62–66, 2001.
- Braun-Angott, P. and B. Berger. *An Upper Bound Approximation for Spread and Pressure in Flat Tool Forging*. Proc. Int. Conf. Num. Methods in Ind. Forming, pages 165–174, 1982.
- Cai, A. and M. Li. *Multi-Point Forming of Three-Dimensional Sheet Metal and the Control of the Forming Process*. International Journal of Pressure Vessels and Piping, 79:289–296, 2002.
- Chen, C. and A. Kak. *Modeling and Calibration of a Structured Light Scanner for 3-D Robot Vision*. Proceedings of the IEEE International Conference on Robotics and Automation, Raleigh NC, pages 807–815, March 1987.
- Danckert, Joachim. *Analysis of the Ring Test Method for the Evaluation of Frictional Stresses in Bulk Metal Forming Processes*. Annals of the CIRP, 37(1):217–220, 1988.
- Dudra, S. and Y. Im. *Analysis of Void Closure in Open-Die Forging*. International Journal of Machine Tools Manufacture, 30:65–75, 1990a.
- Dudra, S. and Y. Im. *Investigation of Metal Flow in Open-Die Forging with Different Die and Billet Geometries*. Journal of Materials Processing Technology, 21:143–154, 1990b.
- Elbadan, Amr and Tim Nye. *An Adaptive Scheduling Algorithm for Generating $2\frac{1}{2}$ D Profiles for an Intelligent Flexible Forging Cell*. Submitted to the International Journal of Machine Tools and Manufacture, 2003.
- Elbadan, Amr and Tim Nye. *Adaptive Scheduling for Generating 3-D Convex Profiles on an Intelligent Flexible Forging Cell*. To be Submitted, 2004a.
- Elbadan, Amr and Tim Nye. *The Incrementally Updated Upper Bound Spread Prediction Model*. To be Submitted, 2004b.
- Ettouney, O. and K. Stelson. *An Approximate Model to Calculate Foldover and Strains During Cold Upsetting of Cylinders, Part I: Formulation and Evaluation of the Foldover Model*. Transactions of the ASME, Journal of Engineering for Industry, 112:260–266, 1990.
- European Powder Metallurgy Association. *Raw Material Utilisation and Energy Requirements of Various Manufacturing Processes*. Retrieved May 12, 2004, from

http://www.epma.com/rv_pm/PM%20Process/7.%20ECONOMIC%20ADVANTAGES/1.%20Economic%20Advantages%20Menu.htm, 2004.

FEMAP Version 8.0. Finite Element Modelling and Postprocessing. Structured Dynamics Research Corp., P.O. Box 1172, Exton, PA 19341, 2000.

Feng, J. and Z. Luo. *A Method for the Optimal Control of Forging Process Variables Using the Finite Element Method and Control Theory*. Journal of Materials Processing Technology, 108:40–44, 2000.

Ferreira, J. and F. Osman. *Investigation Into Bar Forging Using Semi-Circular Tool*. Advances in Materials and Processing Technology, pages 885–860, 1997.

Ferreira, J. and F. Osman. *A New Environment for Profile Forming Using a Theory Driven Machine*. 2nd ESAFORM Conference on Material Forming, Guimaraes, Portugal, 1999.

Ferreira, J. and F. Osman. *Design and Analysis of a Computer Integrated Open Die Forging Cell*. 5Th Asia-Pacific Symposium On Advances in Engineering Plasticity and Its Applications (AEPA 2000), June 12-16, 2000.

Gordon, W. and C. Van-Tyne. *Analysis of Central Burst in Forging*. Manufacturing Engineering Transactions 11Th NAMRAC 1983 Madison, pages 238–242, 1983.

Hardt, D. *Modeling and Control of Manufacturing Processes: Getting More Involved*. Journal of Dynamic Systems, Measurement and Control, 115:291–300, 1993.

Hill, R. *A General Method of Analysis for Metal-Working Processes*. Journal of Mech. Phys. Solids, 11:305–326, 1963.

Hosford, William F. and Robert M. Caddell. *Metal Forming Mechanics and Metallurgy*, chapter 8. PTR Prentice-Hall a Pearson Education Company, Upper Saddle River, NJ 07458, 2nd edition, 1993.

Hung, C. and S. Kobayashi. *Three Dimensional Finite Element Analysis on Open Die Block Forging Design*. Journal of Engineering for Industry, 114:459–464, 1992.

Hydraulic Press Buyers' Guide. The Cordylen Group, Ltd., *Stamping Journal*, July / August 2003.

URL http://www2.thefabricator.com/Buyers_Guides/2003HydPressBrkBG.pdf

- Johnson, T. W. and A. Tomlinson. *A Survey of Developments in Open Die Forging*. Metal Forming, pages 427–475, November 1966.
- Kiefer, B. and K. Shah. *Three Dimensional Simulation of Open Die Press Forging*. Journal of Engineering Materials and Technology, 112:447–485, 1990.
- Kim, P., M. Chun, J. Yi, and Y. Moon. *Pass Schedule Algorithms for Hot Open Die Forging*. Journal of Material Processing Technology, 130:516–523, 2002.
- Kolmogorov, V. L., V. P. Fedotov, and A. V. Gorshkov. *Three-Dimensional Analysis of the Stress-Strain State in the Process of Plastic Deformation of Metals*. Journal of Materials Processing Technology, 95:55–64, 1999.
- Kopp, R. *The Theory of Open-Die Forging in the Course of Historical Change*. Steel Research, 57:125–129, 1986.
- Kopp, R. and T. Bechmann. *Open Die Forging With a Six-Axis Robot As Forging Manipulator*. Proc. of 5Th Int. Conf. On Tech. of Plasticity (ICTP) 7-10 Oct. 1996 Columbus OH., 1996.
- Kopp, R., L. Schaeffer, and G. Schuler. *Incremental Forging With Integrated Open Die Forging Press*. Metallurgical Plant and Technology, 5:76–81, 1982.
- Lahoti, G. and S. Kobayashi. *Flat Tool Forging*. Proc. of 2nd NAMRAC, pages 73–87, 1974.
- Lee, C. H. and T. Altan. *Influence of Flow Stress and Friction Upon Metal Flow in Upset Forging of Rings and Cylinders*. Journal of Engineering for Industry, pages 775–782, August 1972.
- Li, Y. and D. Zhou. *An Upper-Bound Strip Technique for Predicting Spread in Forging*. Journal of Mechanical Working Technology, 18:109–119, 1989.
- Lilly, K. and A. Jablokow. *Intelligent Open Die Forging*. International Journal of Industrial Engineering, 2:216–222, 1995.
- Lilly, K. and A. Melligeri. *Dynamic Simulation and Neural Network Compliance Control of an Intelligent Forging Center*. Journal of Intelligent and Robotic Systems, 17:81–99, 1996.
- Male, A. T. and M. G. Cockcroft. *A Method for the Determination of the Coefficient of Friction of Metals Under Conditions of Bulk Plastic Deformation*. Journal of the Institute of Metals, 93(65):38–46, 1964.

- Mardanpour, S. and N. Chitkara. *Plane Strain Indentation of Thick Blocks Between Opposed Flat Rigid Punches of Unequal Width, Two at the Top and One at the Bottom - II*. NAMRAC XXVI May 19-22, 1998 Atlanta, Georgia, pages MF 98–228, 1998.
- MATLAB Version 6.1. Development Environment. The Math Works, Inc., 3 Apple Hill Drive Natick, MA 01760-2098, May 2001.
- Melligeri, A. and K. Lilly. *Application of Neural Networks in Compliance Control of an Integrated Robot/Forge Processing Center*. Advances in Manufacturing Systems, pages 445–450, 1994.
- Mitani, Y., V. Mendoza, and K. Osakada. *Analysis of Rotor Shaft Forging by Rigid-Plastic Finite Element Method*. Journal of Materials Processing Technology, 27:137–149, 1991.
- Narayanasamy, R. and K. Pandey. *A Study on the Barrelling of Sintered Iron Preforms During Hot Upset Forging*. Journal of Material Processing Technology, 100:87–94, 2000.
- Nielsen, L., S. Lassen, C. Andersen, J. Gronbaek, and N. Bay. *Development of a Flexible Tool System for Small Quantity Production in Cold Forging*. Journal of Materials Processing Technology, 71:36–42, 1997.
- Nieschwitz, P., F. Ecken, and E. Siemer. *Pass Schedule Calculation Program "Comforge" for Open-Die Forging Plants*. Metallurgical Plant and Technology, 11(5):54–68, 1988.
- Nye, T. *A Control Strategy and Upper Bound Solution for Non-Flat Tool Open Die Forging Automation*. Proceedings ASME MED, 10:746–753, 1999.
- Nye, T., A. Elbadan, and G. Bone. *Real-Time Process Characterization of Open Die Forging for Adaptive Control*. Journal of Engineering Materials and Technology, 123:511–516, 2001.
- Nye, Timothy J. *Preliminary Status Report for Flexible Forging Technology*. Technical report, ERC for Net Shape Manufacturing, Ohio State University, March 1988.
- Oberg, Erik, Franlin D. Jones, Holbrook L. Horton, and Henry H. Ryffel. *Machinery's Handbook*. Industrial Press INC., 26Th edition, 2000.
- Olsson, Donald M. and Lloyd S. Nelson. *The Nelder-Mead Simplex Procedure for Function Minimization*. Technometrics, 17(1):45–51, 1975.

- Osman, F. and J. Ferreira. *Investigation Into the Automation of Incremental Forming Process*. Proceedings of the Institution of Mechanical Engineers Part B, Journal of Engineering Manufacture, 213(3):311–315, 1999.
- Pahnke, H. *Fundamentals of Programmed Forging*. Metallurgical Plant and Technology, pages 92–101, May 1983.
- Park, J., G. Desouza, and A. Kak. *Dual-Beam Structured Light Scanning for 3-D Object Modeling*. In Third International Conference On 3-D Digital Imaging and Modelling, Quebec, Canada, pages 65–72. 2001.
- Park, K., D. Yang, and Y. Kang. *Precision Forging Design and Analysis in Electronics Part Manufacturing*. Proceedings of the Institution of Mechanical Engineers, Part B, Journal of Engineering Manufacture, 213:11–20, 1999.
- Pietrzyk, M. *Finite-Element Simulation of Large Plastic Deformation*. Journal of Materials Processing Technology, 106:223–229, 2000.
- Qinchun, Yang, Qu Shengnian, Zhu Qi, and Min Naiyan. *FE Simulation Method for a Forging System*. Journal of Materials Processing Technology, 63:678–683, 1997.
- Ramakrishnan, N., Krishna M. Singh, R. K. V. Suresh, and N. Srinivasan. *An Algorithm Based on Total-Elastic-Incremental-Plastic Strain for Large Deformation Plasticity*. Journal of Materials Processing Technology, 86:190–199, 1999.
- Reddyhoff, Michael. *The Integrated Forge*. Proceedings Forging Industry Association June 22-24, 1982, Hyatt Regency O'Hare, Chicago, Illinois, pages 1–8, 1982.
- Rodrigues, J., P. Martins, and M. Marques. *The Plast 3 System and its Application to the Simulation of an Open Die Forging Operation*. Journal of Materials Processing Technology, 47:111–125, 1994.
- Sagar, R. and B. Juneja. *An Upper Bound Solution for Flat Tool Forging Taking into Account the Bulging of Sides*. International Journal of Machine Tool Design and Research, 19:263–258, 1979.
- Sagar, R. and B. Juneja. *Open Die Forging of a Four Sided Irregular Disc*. International Journal of Machine Tools and Manufacture, 31(3):315–328, 1991.

- Sauve, R. *H3DMAP Version 6.2 - A General Three Dimensional Finite Element Computer Code for Linear and Nonlinear Analysis of Structures*. Ontario Power Technologies Report No 181.1-H3DMAP-1998-Ra-0001-R01, pages 1–245, November 2000.
- Schey, J. and P. Abramowitz. *Incremental Forging of Parts With Cross-Ribs*. Technical Paper MF 73-164, Society of Manufacturing Engineers, 1973.
- Shutt, A. *A Note On Spread in Indenting*. Applied Scientific Research, pages 389–392, 1960.
- Shutt, A. *An Investigation of the Technological Bound of Flat-Tool Press Cogging*. Journal of the Iron and Steel Institute, 201:208–212, 1963.
- Siemer, E., P. Nieschwitz, and R. Kopp. *Quality Optimized Process Control of Open Die Forging*. Stahl Und Eisen, 106:383–387, 1986.
- Standring, P., J. Moon, and E. Appleton. *Plastic Deformation Produced During Indentation Phase of Rotary Forging*. Metals Technology, pages 159–166, April 1980.
- Sun, L., G. Li, and S. Kobayashi. *Analysis of Spread in Flat Tool Forging by the Finite Element Method*. Manufacturing Engineers Transactions 11Th NAMRAC, pages 224–231, 1983.
- Szyndler, R. and B. Klimkiewicz. *Design of the Open-Die Elongation Process Using Optimization Technique*. Journal of Materials Processing Technology, 34:157–162, 1992.
- Tamura, K. and J. Tajima. *Optimisation of Open Die Forging Condition and Tool Design for Ensuring Both Internal Quality and Dimensional Precision by Three-Dimensional Rigid-Plastic Finite Element Analysis*. Ironmaking and Steel Making, 30(5):405–411, 2003.
- Tarnowski, I. *New Researches in the Field of Technology*. Moscow, Gostekhizdat, as reported in Tomlinson and Stringer (1959), 1950.
- Teti, R., A. Langella, and D. D'Addona. *An Intelligent Computation Approach to Process Planning in Multiple Step Cold Forging*. Annals of CIRP, 48:175–178, 1999.
- Thomas, L. and A. Tomlinson. *Computer Control for Automation of Heavy Forging Production*. Journal of the Iron and Steel Institute, pages 423–433, May 1966.

- Tomlinson, A. and J. Stringer. *Spread and Elongation in Flat Tool Forging*. Journal of Iron and Steel Institute, pages 157–162, October 1959.
- Tsujimura, Y. and M. Gen. *Parts Loading Scheduling in a Flexible Forging Machine Using an Advanced Genetic Algorithm*. Journal of Intelligent Manufacturing, 10:149–159, 1999.
- Voelcker, Herbert B. and Aristides A. G. Requicha. *Geometric Modeling of Mechanical Parts and Processes*. Computer, 10(12):48–57, December 1977.
- Voyiadjis, George Z. and Mehrdad Foroozesh. *A Finite Strain, Total Lagrangian Finite Element Solution for Metal Extrusion Problems*. Computer Methods in Applied Mechanics and Engineering, 86:337–370, 1991.
- Walczyk, D. and D. Hardt. *Design and Analysis of Reconfigurable Discrete Dies for Sheet Metal Forming*. Journal of Manufacturing Systems, 17:436–440, 1998.
- Walczyk, D. and Y. Im. *A Hydraulically-Actuated Reconfigurable Tool for Flexible Fabrication: Implementation and Control*. Journal of Manufacturing Science and Technology, 122:562–568, 2000.
- Walczyk, D., J. Hosford, and J. Papazian. *Using Reconfigurable Tooling and Surface Heating for Incremental Forming of Composite Aircraft Parts*. Journal of Manufacturing Science and Engineering, 125:333–343, 2003.
- Walczyk, D., J. Lakshamikanthan, and D. Kirk. *Development of a Reconfigurable Tool for Forming Aircraft Body Panels*. Journal of Manufacturing Systems, 17:287–296, 1998.
- Wang, S. and Q. Cao. *The Investigation of FM Heavy Forging Process by the Moire Method, Part I: Single Reduction Results*. Journal of Materials Processing Technology, 43:195–209, 1994a.
- Wang, S. and Q. Cao. *The Investigation of the FM Heavy Forging Process by the Moire Method, Part II: Consecutive Reduction Results*. Journal of Materials Processing Technology, 43:211–220, 1994b.
- Wang, S. and Q. Cao. *Investigation of FM Heavy Forging Process by the Moire Method, Part III: a Direct Forging Process Standard*. Journal of Materials Processing Technology, 47:311–322, 1995.
- Welchhof, K. and R. Kopp. *Incremental Forging - Flexible Metal Forming Process Improves Utilisation of Material and Energy*. Steel Research, (2):74–80, 1989.

- Wisterich, J. and A. Shutt. *Theoretical Analysis of Bloom and Billet Forging*. Journal of the Iron and Steel Institute, pages 163–176, October 1959.
- Wong, S., P. Hodgson, C. Chong, and P. Thomson. *Physical Modeling with Application to Metal Working Especially to Hot Rolling*. Journal of Materials Processing Technology, 62:260–274, 1996.
- Wong, S., P. Hodgson, and P. Thomson. *Comparison of Torsion and Plane-Strain Compression for Predicting Mean Yield Strength in Single and Multiple-Pass Flat Rolling Using Lead to Model Hot Steel*. Journal of Materials Processing Technology, 53:601–616, 1995.
- Wright, P., D. Bourne, J. Coyler, G. Schatz, and J. Isai. *A Flexible Manufacturing Cell for Swaging*. Mechanical Engineering, pages 75–83, October 1982.
- Wu, W., G. Li, and J. Tang. *Finite Element Analysis of Three Dimensional Metal Flow in Cold and Hot Forming Processes*. Annals of CIRP, 43:235–239, 1994.
- Zabaras, Nicholas and Akkram Srikanth. *An Object-Oriented Programming Approach to the Lagrangian FEM Analysis of Large Inelastic Deformations and Metal-Forming Processes*. International Journal for Numerical Methods in Engineering, 45:399–445, 1999.

Appendix A

Comparison Between Machining, Open Die Forging and Adaptive Forging of a Typical Product

To illustrate the potential benefits¹ to be gained from developing a flexible forging cell a comparison between machining and flexible forging of a sample product (Fig. A.1) is presented here. The product is to be manufactured from mild steel ASTM A197 within ± 1 mm tolerance.

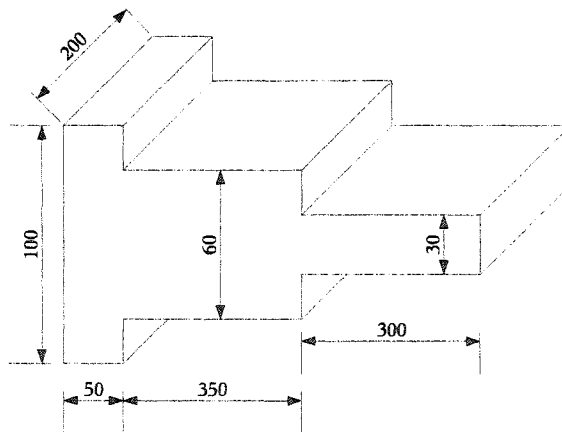


Figure A.1: Sample Workpiece

¹Reduction in production time, increase in material utilization and reduced energy consumption.

Table A.1: Milling Cutter Specifications

Parameter	Value
Milling Cutter Diameter (D)	100 mm
Number of Teeth (Z)	7
Feed/Insert (f_z)	1 mm
Depth of Cut (a)	3.5 mm
Cutting Speed (V_c)	50 m/min

A.1 Machining

The face milling operation was selected to manufacture the product as it is suitable for bulk machining operations. A typical roughing carbide milling cutter (AVANTOP KC1.1 Milling Cutter 2004) is selected. The cutter's specifications are presented in Table A.1 (the chosen cutting speed is the recommended cutting speed for cutting steel with carbide tools (Oberg et al. 2000)).

The corresponding rotational speed (N), table feed (F) and material removal rate (MRR) are:

$$N = \frac{V_c}{\pi D} = 160 \text{ rpm} \quad (\text{A.1})$$

$$F = f_z \times Z \times N = 1\,120 \text{ mm/min} \quad (\text{A.2})$$

$$MRR = F \times D \times a = 392\,000 \text{ mm}^3/\text{min} \quad (\text{A.3})$$

The calculation of the cutting time for the top surface is based on the following process plan (Fig. A.2):

- Cut the top surface with 3.5 mm increments of depth of cut.
- Paths are taken parallel to the width of the workpiece where the cut length is the width (200 mm) + cutter diameter (100 mm).

From which the top surface machining time is calculated as follows:

$$L = \text{width} + 2 \times D = 200 + 200 = 400 \text{ mm} \quad (\text{A.4})$$

$$t_p = \frac{L}{F} = \frac{400}{1\,120} = 0.36 \text{ min} \quad (\text{A.5})$$

$$n_a = \frac{100 - 60}{2 \times 3.5} = 5.7 \text{ (6 paths)} \quad (\text{A.6})$$

$$n_w = \frac{350 + 300}{100} = 6.5 \text{ (7 paths)} \quad (\text{A.7})$$

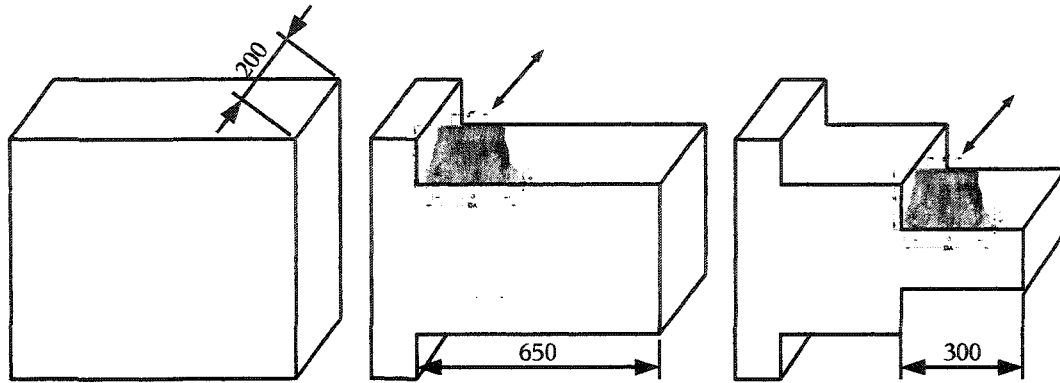


Figure A.2: Machining Operation Process Plan

$$P = n_a \times n_w = 6 \times 7 = 42 \text{ paths} \quad (\text{A.8})$$

$$T = P \times t_p = 0.36 \times 42 = 15.12 \text{ min} \quad (\text{A.9})$$

where,

L = Length to be cut in one path.

t_p = Machining time for one path of length L .

n_a = number of required paths in depth direction.

n_w = number of required paths in width direction.

P = Total number of required paths to cut the top surface.

T = Total machining time for the top surface.

Neglecting the time used to turn the workpiece so the tool can machine the bottom surface the total machining time is then = $15.12 \times 2 = 30.24$ min and the corresponding material utilization for the process is 50%.

A.2 Forging

The workpiece is simulated to be forged on a general open die forging cell with a forging bite of 100 mm. The average pressure required to forge the workpiece was computed based on the Hosford and Caddell (1993) formula for plain strain upsetting and the corresponding forging force was found to be 6.18 GN. A suitable 7 GN Schuler inc. hydraulic press was selected from the Hydraulic Press Buyers' Guide (2003). The press had the following specifications:

- Forging speed = 79 - 114 mm/s (187 - 270 ipm)
- Return speed = 698.5 mm/s (1650 ipm)

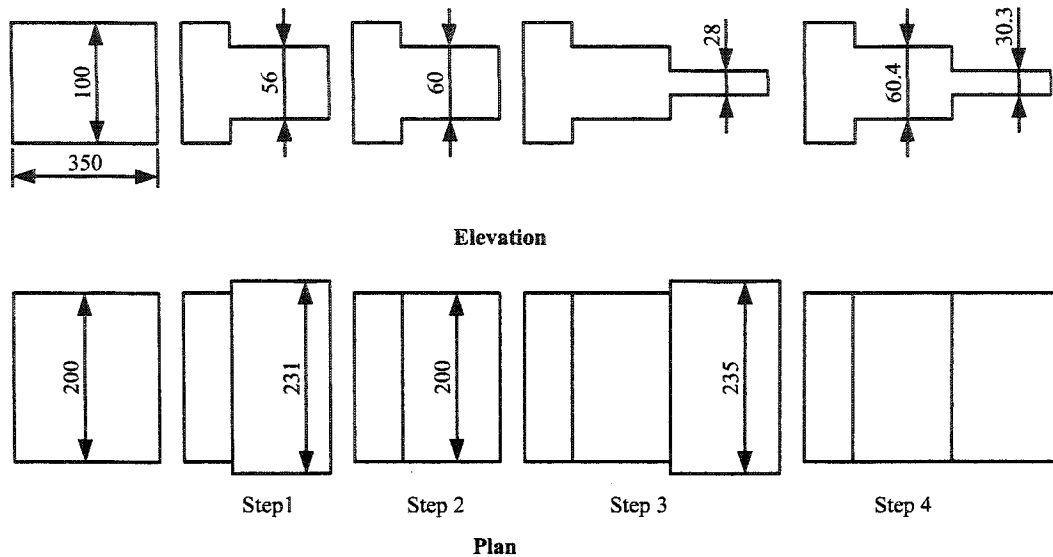


Figure A.3: Forging Schedule for Sample Product

A forging velocity of 84 mm/s was selected for operation. A forging plan based on the incrementally updated spread prediction formula (developed in Section 5.3.3) is shown in Fig. A.3.

The computed total forging time is 6.45 s. If the workpiece is measured after each forging step to collect feedback information, the modified total forging time will be 2 min and 6.45 s (assuming the measurement time is 30 s and that measurements are taken at the end of each forging step). The corresponding material utilization is 100% without considering the machining allowance² and 94.7% considering it.

The example shows that not only is the production time³ for forging is $\frac{1}{16}^{th}$ that of machining, but it demonstrates that forging is also characterized by higher material utilization and lower energy consumption⁴. A summary of the comparison is presented in Table A.3.

²The production of the workpiece was based on having a 1 mm machining allowance for finishing operations for both milling and forging.

³The production time computed is the time for roughing operation. Both products from milling and forging will be subsequently finished by another process.

⁴Typical energy consumption for machining is 74 MJ and for forging 47 MJ for each kg of material (European Powder Metallurgy Association 2004).

Table A.2: Forging Schedule for the Sample Product

Step	Forging Direction	Forge starting at x= (mm)	Width (mm)	Height (mm)	Length (mm)	Forging steps	Squeeze Value (mm)	Forging Time s
1	z	50	200	100	300	3	44	1.75
2	y	50	231	56	535.71	6	31	2.46
3	z	400	200	60.44	149	2	32	0.85
4	y	400	235	28	300	3	35	1.39
Final Dimensions			200	30.68			Total Time	6.45

Table A.3: Forging vs Machining of the Sample Product

Process	Production Time	Material Utilization	Energy Required MJ/kg
Milling	32 min 14 sec	50%	66-82
Incremental Forging	7 sec	94.7%	46-49
Incremental Forging with Feedback inspection	2 min 7 sec	94.7%	46-49

Appendix B

Ring Compression Test

Table B.4: Ring Initial Dimension

Outer Diameter	Inner Diameter	Height
$\frac{3}{4}$ in 19 mm	$\frac{3}{8}$ in 9.5 mm	$\frac{1}{4}$ in 6.3 mm

Table B.5: Deformed Ring Diameters, Height=2 mm

	Outer Diameter (mm)	Inner Diameter (mm)
Major axis	30	8.5
Minor axis	27	8

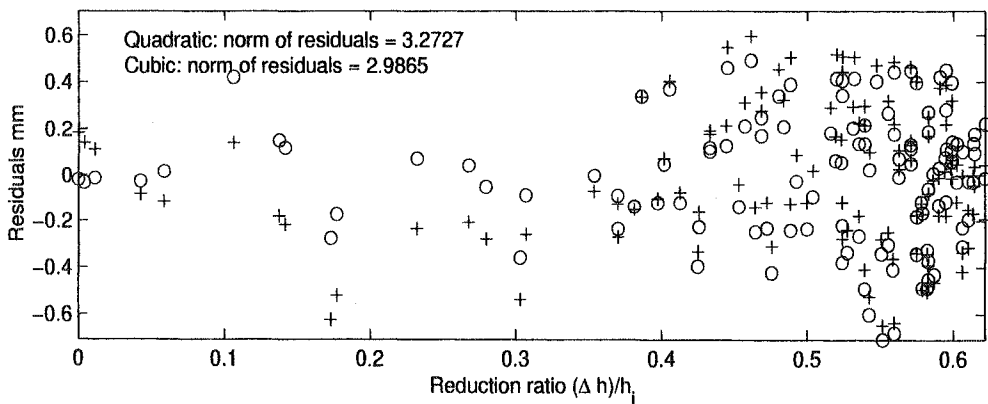
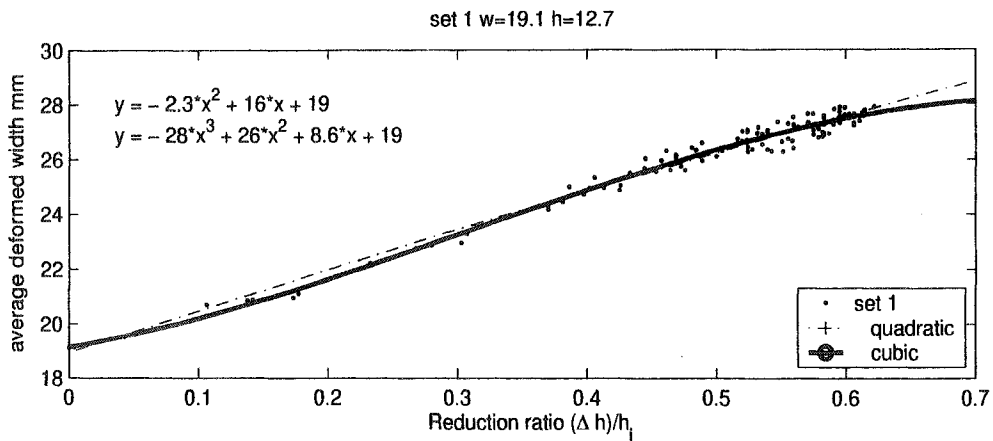
The corresponding reduction in height and decrease in internal diameter are, 68% and 13% respectively. The friction factor, m according to Lee and Altan (1972) calibration curves is

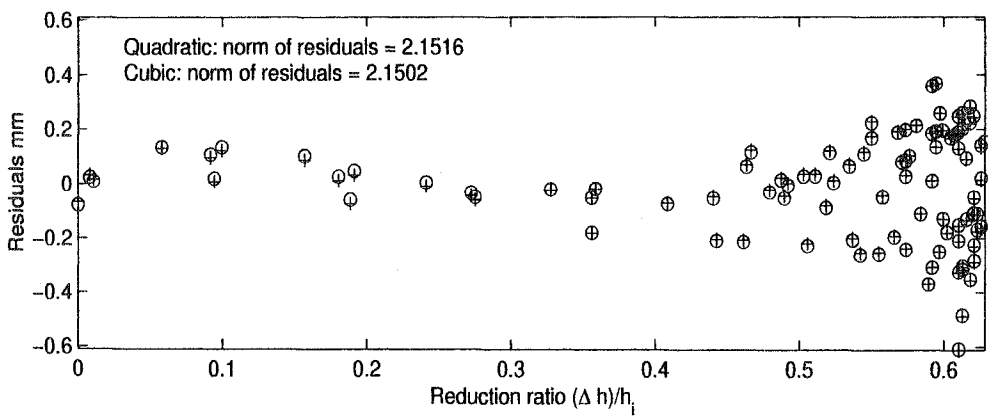
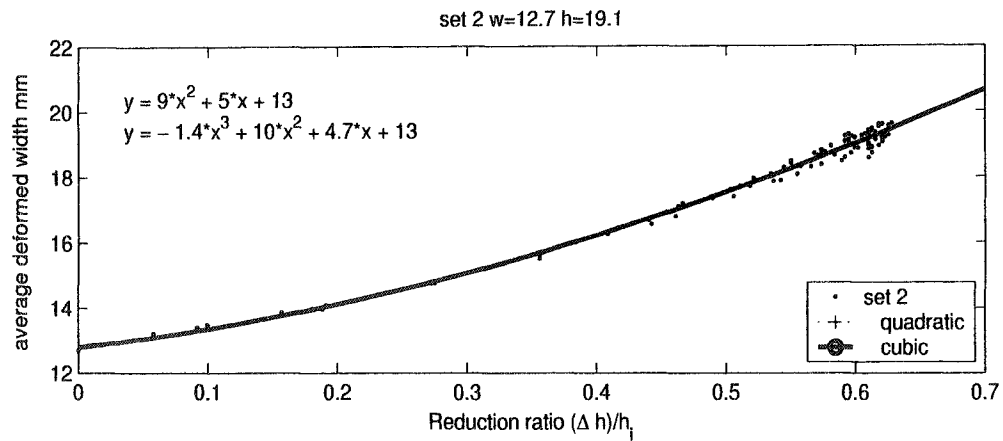
Table B.6: Friction Factor m

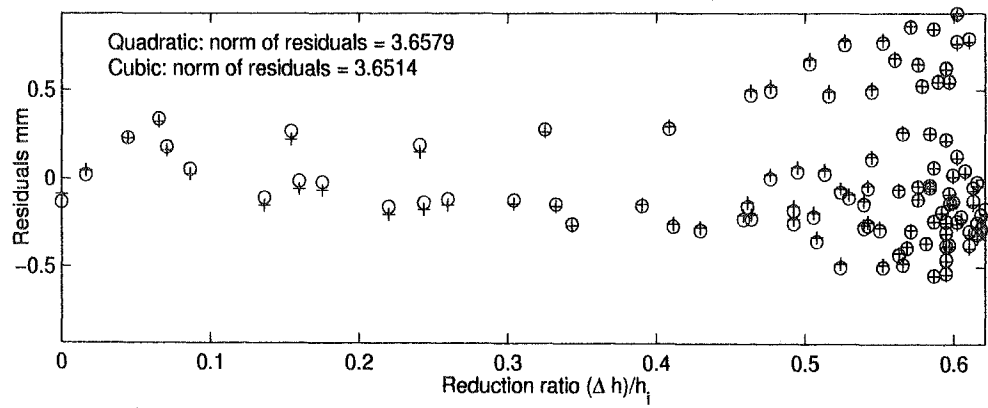
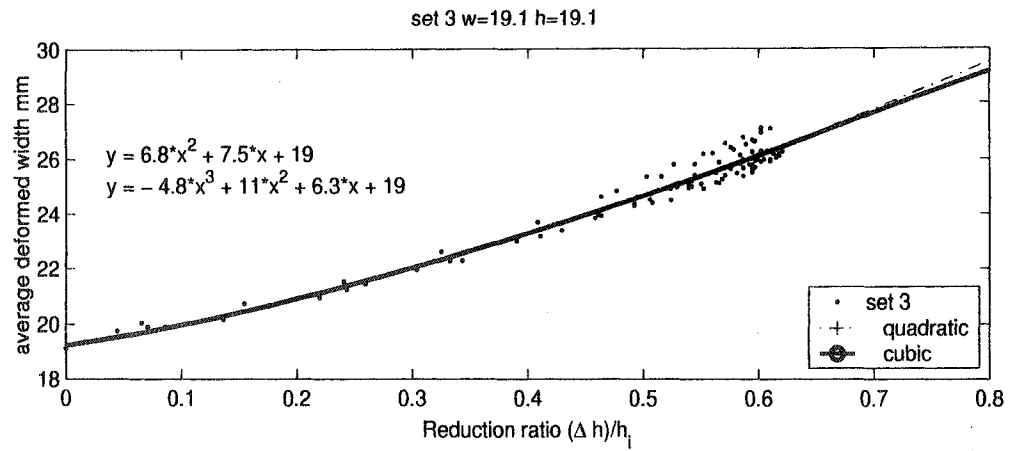
	Lee and Altan (1972)	Danckert (1988)
m	0.2	0.16

Appendix C

Regression Analysis of Spread Measurements







Appendix D

Analytical Proof for Tarnowski's (1950) Empirical Spread Prediction Formula

For the upper bound uniform pattern of deformation (Section 5.3.1) an interesting analysis is to study the material flow solely based on friction. Assuming the deformation zone is a rectangular block being upset. It can be argued that the deformation work acts to reduce the height of the workpiece and has rather small effect on longitudinal and side spread. Another way to put it is that the deformation work drives the material to spread evenly¹ side ways with no particular preference to the longitudinal or the width direction.

Studying friction on the top surface of the workpiece one notice that $\triangle OAB$ and $\triangle OBC$ are similar (Fig. 5.3) and as a result of this similarity one can deduce that the frictional work acting on, $\triangle OAB$, is equal to that acting on, $\triangle OBC$. In other words, regard the two triangles as if they are two separate identical triangles with different orientation being upset under the press. The frictional work for both of them should be equal given they have identical tribological characteristics. Thus one can conclude that:

$$E_u = E_v \quad (\text{D.10})$$

and substituting in Eq. (5.45) and Eq. (5.46):

$$v_{x0}^3 \ln (\sqrt{1 + \phi^2} + \phi) = -v_{y0}^3 \ln \left(\frac{\sqrt{1 + \phi^2} - 1}{\phi} \right) \quad (\text{D.11})$$

¹This holds for axisymmetric upsetting though for upsetting non-axisymmetric workpieces FE results indicated that the pressure distribution has its peaks at the corners of the workpiece preventing them from spreading.

Manipulating:

$$(\sqrt{1 + \phi^2} + \phi) = \left(\frac{\phi}{\sqrt{1 + \phi^2} - 1} \right)^{\phi^3} \quad (\text{D.12})$$

This equality is satisfied when $\phi = 1$. Thus:

$$\phi = \frac{v_{x0}}{v_{y0}} = \frac{s y_0}{(1 - s) x_0} = 1 \quad (\text{D.13})$$

From which the well known Tarnowski (1950) formula is reached

$$s = \frac{x_0}{x_0 + y_0} = \frac{\text{Bite}}{\text{Bite} + \text{width}} \quad (\text{D.14})$$